Dust Attenuation and Maintenance-Mode Feedback in the 6 Gyr old Universe and Now

Ivana Barišić

Dissertation
submitted to the
Combined Faculty of Natural Sciences and Mathematics
of Heidelberg University, Germany
for the degree of
Doctor of Natural Sciences

Put forward by
Ivana Barišić
Born in Zagreb, Croatia
Oral examination: June 19th, 2020

Dust Attenuation and Maintenance-Mode Feedback in the 6 Gyr old Universe and Now

Referees:

Prof. Dr. Arjen van der Wel

Prof. Dr. Hans-Walter Rix

All of the fun is contained in curiosity itself.

Abstract

This thesis addresses two distinct challenges in the galaxy formation and evolution theory. The first one is to accurately measure the dust attenuation. Understanding the global effects of dust on stellar light is crucial in deriving a number of galaxy physical properties. The second one is to explain how galaxies with the most massive halos remain passive. Models have implemented various feedback mechanisms to explain this phenomenon. Quiescence has been linked to the presence of radio-loud AGN through evidence gathered in the local universe. However, such observations were not feasible at high redshift up until recently.

The first part of the thesis presents a novel approach to measure the attenuation of individual star forming galaxies at $z \sim 0.8$ based on deep optical LEGA-C survey spectra and multi-band photometry. A new attenuation curve modeling technique, and a new prescription for a typical attenuation curve of $z \sim 0.8$ galaxies are introduced. Using this technique, a large diversity among the main attenuation curve features (slope and UV bump strength) is observed, and the variation of those features with global galaxy properties is inspected. The main finding is that geometric effects dominate observed variations in attenuation. The second part of the thesis explores maintenance-mode feedback in quiescent galaxies through the incidence of radio-loud AGN, both in the local and high redshift ($z \sim 1$) universe. A high incidence rate of radio-loud AGN among round quiescent galaxies is observed, based on a $z \sim 0.1$ sample drawn from the SDSS/FIRST/NVSS surveys. On the other hand, radio-loud AGN are not seen among flat quiescent galaxies. This finding brings the general validity of the maintenance-mode feedback picture into question, as a different mechanism must be responsible for keeping these galaxies quiescent. This work is extended to $z \sim 1$ for a radio-loud AGN sample drawn from LEGA-C/VLA. The finding is that radio-loud AGN preferentially reside in galaxies with large stellar velocity dispersions, old stellar populations and round shapes but a larger sample is required to explore the dependence on flattening.

Zusammenfassung

Diese Dissertation befasst sich mit zwei unterschiedlichen Herausforderungen in der Galaxienbildung und der Evolutionstheorie. Die erste besteht darin, die Staubdämpfung genau zu messen. Das Verständnis der globalen Auswirkungen von Staub auf das Sternenlicht ist entscheidend für die Ableitung einer Reihe physikalischer Eigenschaften der Galaxie. Die zweite ist zu erklären, wie Galaxien mit den massereichsten Halos passiv bleiben. Modelle haben verschiedene Rückkopplungsmechanismen implementiert, um dieses Phänomen zu erklären. Die Ruhe wurde durch im lokalen Universum gesammelte Beweise mit dem Vorhandensein von radio-laut AGN in Verbindung gebracht. Solche Beobachtungen waren jedoch bis vor kurzem bei hoher Rotverschiebung nicht möglich.

Der erste Teil der Dissertation präsentiert einen neuartigen Ansatz zur Messung der Abschwächung einzelner sternbildender Galaxien bei z $\sim$ 0.8 basierend auf tiefen optischen LEGA-C-Vermessungsspektren und Mehrbandphotometrie. Eine neue Dämpfungskurvenmodellierungstechnik und ein neues Rezept für eine typische Dämpfungskurve von z $\sim$ 0.8 Galaxien werden eingeführt. Unter Verwendung dieser Techniken wird eine große Vielfalt unter den Hauptmerkmalen der Dämpfungskurve (Steigung und UV-bump) beobachtet, und die Variation dieser Merkmale mit globalen Galaxieneigenschaften wird untersucht. Das wichtigste Ergebnis ist, dass geometrische Effekte die beobachteten Schwankungen der Dämpfung dominieren. Der zweite Teil der Dissertation untersucht die Rückkopplung im "maintenance-modus" in ruhenden Galaxien durch das Auftreten von radio-laut AGN sowohl in der lokalen als auch in der hohen Rotverschiebung (z $\sim$ 1). Eine hohe Präferenz für radio-laut AGN-Inzidenz bei runden ruhenden Galaxien wird beobachtet, basierend auf einer z $\sim$ 0.1 Stichprobe aus den SDSS / FIRST / NVSS-Untersuchungen. Auf der anderen Seite sind radio-laut AGN in flachen ruhenden Galaxien nicht zu sehen. Dieser Befund stellt die allgemeine Gültigkeit des Rückkopplungsbildes im "maintenance-modus" in Frage, da ein anderer Mechanismus dafür verantwortlich sein muss, dass diese Galaxien ruhig bleiben. Diese Arbeit wird für eine radioaktive AGN-Probe aus LEGA-C / VLA auf z $\sim$ 1 erweitert. Das Ergebnis ist, dass radio-laut AGN bevorzugt in Galaxien mit großen Sterngeschwindigkeitsdispersionen, alten Sternpopulationen und runden Formen vorliegt, aber eine größere Probe erforderlich ist, um die Abhängigkeit von der Abflachung zu untersuchen.

Contents

List of Figures iii

List of Tables iv

Acronyms vi

1 Introduction 1
- 1.1 Star-formation . . . 1
- 1.2 Interstellar medium properties . . . 4
- 1.3 Feedback in most massive galaxies . . . 8
- 1.4 Thesis outline . . . 10

2 Dust Attenuation Curves at z ∼ 0.8 from LEGA-C: Precise Constraints on the Slope and 2175Å Bump Strength 11
- 2.1 Introduction . . . 11
- 2.2 Data . . . 13
  - 2.2.1 The LEGA-C Survey . . . 13
  - 2.2.2 Attenuation-free stellar spectra . . . 14
  - 2.2.3 Attenuation curve . . . 17
- 2.3 Results . . . 19
  - 2.3.1 Attenuation curve prescription . . . 19
  - 2.3.2 Global Attenuation Properties . . . 20
  - 2.3.3 Unexplained Scatter in Attenuation Properties . . . 26
  - 2.3.4 Strong UV Bumps in Face-on Galaxies . . . 27
- 2.4 Conclusion . . . 28

3 An Absence of Radio-loud Active Galactic Nuclei in Geometrically Flat Quiescent Galaxies: Implications for Maintenance-mode Feedback Models 30
- 3.1 Introduction . . . 30
- 3.2 Data and sample selection . . . 31
  - 3.2.1 SDSS . . . 31
  - 3.2.2 NVSS and FIRST . . . 32
  - 3.2.3 Selection of Radio-Loud AGN Hosts . . . 32
- 3.3 Which Parameters Correlate the Radio-Loud AGN Fraction? . . . 34
  - 3.3.1 Radio-Loud AGN Fraction Increases with σ_* . . . 34
  - 3.3.2 Geometry Plays a Role in Radio-Loud Fraction . . . 35

3.3.3 Radio-Loud AGN Fraction of Intrinsically Round and Flat Galaxies . . . 36
3.3.4 Satellites, Centrals and Halo Mass . . . 37
3.4 Discussion . . . 38

4 Stellar Dynamics and Star Formation Histories of z ∼ 1 Radio-loud Galaxies 40
4.1 Introduction . . . 40
4.2 Data, Sample Selection and Classification . . . 42
4.2.1 LEGA-C . . . 42
4.2.2 VLA - COSMOS . . . 42
4.2.3 Selection of radio-loud AGN . . . 43
4.2.4 Classification of the radio-loud objects . . . 44
4.3 Properties of $z \sim 1$ jet-mode galaxies . . . 45
4.3.1 Fraction of jet-mode galaxies . . . 45
4.3.2 Stellar Populations of Galaxies with Radio-Loud AGN . . . 51
4.4 Conclusions . . . 51

5 Summary and Outlook 54
5.1 Summary . . . 54
5.2 Outlook . . . 55
5.2.1 Outline & Motivation . . . 55

6 First author publications 57

Bibliography 58

Acknowledgements 69

List of Figures

1.1 Bimodality in galaxy population 3
1.2 Illustration: extinction vs. attenuation 5
1.3 Schematic example of the extinction/attenuation curve 6
1.4 Direct and indirect evidence for maintenance-mode feedback 9

2.1 Star-formation rate vs stellar mass M_* of $0.61 < z < 0.94$ LEGA-C sample 15
2.2 An example of the observed and attenuation-free spectrum 16
2.3 Attenuation curve examples 17
2.4 Typical attenuation curve at $z \sim 0.8$ 21
2.5 Specific star-formation rate vs. stellar mass for star-forming galaxies . 23
2.6 Axis ratio vs. stellar mass (left) and specific star-formation rate (right) 24
2.7 Attenuation curve features plotted against each other 25
2.8 Expected vs. observed attenuation A(4500Å) 26
2.9 Attenuation A(4500Å) vs. axis ratio 27

3.1 1.4 GHz luminosity vs. SFR for SDSS/NVSS galaxies 33
3.2 Left: Radio-loud fraction vs. σ_*; Right: heatmap of the observed axis ratio distribution vs. σ_* 34
3.3 RL fraction among quiescent galaxies vs. projected axis ratio 35
3.4 Normalized histogram of the observed axis ratio distribution for quiescent (left) and RL quiescent (right) galaxies 36
3.5 The RL fraction among triaxial and oblate galaxies vs. σ_* for quiescent galaxies 38

4.1 3 GHz radio luminosity vs. SFR for LEGA-C/VLA $z \sim 0.8$ galaxies . 43
4.2 Venn diagram 44
4.3 Example images of RL sources 47
4.3 Continued 48
4.4 Fraction of jet-mode galaxies among all and quiescent galaxies in the LEGA-C vs. stellar mass 49
4.5 Left: Jet-mode fraction among the full LEGA-C sample and among the quiescent galaxies vs. σ_*; Right: σ_* vs. stellar mass 50
4.6 The 3 GHz luminosity vs. σ_* for the LEGA-C/VLA cross-matched sample of galaxies 51
4.7 SFR_{UV+IR} vs. rest-frame U-V color 52
4.8 Hδ vs. $D_n(4000)$ 52

List of Tables

2.1 Values for the attenuation curve prescription (A(λ)/A(4500Å)) 22

4.1 Physical properties of the observed sub-sample of radio-loud galaxies 45

Acronyms

ALMA Atacama Large Millimeter Array.

BH black hole.

CDM Cold Dark Matter.

EW equivalent width.

FIR far infrared.

FIRST Faint Images of the Radio Sky at Twenty-cm.

FRI Fanaroff-Riley I.

HERG high excitation radio galaxy.

HST Hubble Space Telescope.

IR infrared.

IRAC The Infrared Array Camera.

ISM interstellar medium.

LEGA-C Large Early Galaxy Astrophysics Census.

LERG low excitation radio galaxy.

LMC Large Magellanic Cloud.

MIPS The Multiband Imaging Photometer.

MW Milky Way.

NIR near infrared.

NVSS NRAO VLA Sky Survey.

PAH polycyclic aromatic hydrocarbons.

PSF point spread function.

RL radio loud.

SDSS Sloan Digital Sky Survey.

SED spectral energy distribution.

SF star formation.

SFR star formation rate.

SMBH supermassive black hole.

SMC Small Magellanic Cloud.

sSFR specific star formation rate.

UV ultraviolet.

VIMOS Visible Multi-Object Spectrograph.

VLA Very Large Array.

VLT Very Large Telesope.

WISE Wide-field Infrared Survey Explorer.

Chapter 1

Introduction

Over the years, photometric and spectroscopic surveys, involving ground- and space-based telescopes, have been employed to gather information which enables astronomers to examine and compare a large variety of physical properties of galaxies across cosmic time. This ultimately helps us on the path of learning about the processes involved in galaxy formation and evolution — an extremely complex subject with many open questions. With the great multitude of available and yet-to-come data sets comes the challenge of connecting the pieces of puzzle together, as well as determining and interpreting underlying physical processes that shape galaxies.

1.1 Star-formation

The process of star-formation is not yet entirely understood and is a subject of ongoing research within galaxy formation and evolution theory. From the research that has been conducted so far, it is evident that the presence of the cool gas is crucial in the formation of a new stellar body. The current theory suggests that the process of star formation occurs in the following way: with cooling of the dark matter halo gas, its inflow towards the center of the halo begins. This increases the density of the gas, ultimately leading to a collapse under its own gravity into a cloud. If cooling processes are efficient enough, the dense gas cloud becomes unstable, and can fragment into smaller clouds. Eventually, those critically dense clouds become birth places for new stars (e.g. Mo et al., 2010). This simplified picture is much more complex in reality, and we are yet to learn about many of the intricacies regarding the galaxy formation and evolution theory.

Through decades, astronomers relied on matching observational evidence and physical simulations in order to investigate properties of the universe. Stellar light offers a unique window into physical properties of galaxies. Ideally, determining the star formation activity of a galaxy would rely on observing unobscured and unprocessed light originating in young stars. Young and bright OB stars are considered to be the main providers of rest-frame ultraviolet photons that trace recent star formation activity. Simultaneously, the presence of young and bright stars excites and ionizes the gas within birth cloud regions, resulting in emission lines. For this

reason, emission lines originating from HII regions can be used as direct tracers of active star formation. The Hα emission line is an example of the most trusted star formation tracer (e.g. Moustakas et al., 2006). However, the reality is such that the interstellar medium, or more precisely one of its contents – dust grains, attenuate the stellar light coming from young, bright stars. This means that the ultraviolet light alone will not be sufficient to estimate the star formation activity (e.g. Madau & Dickinson, 2014). We need to take into account the effect that the dust grains have on the stellar light if we want to know the true star formation rate. A detailed picture of the influence of the dust grains on the stellar light will be presented in Section 1.2. In short, as the dust grains absorb the ultraviolet radiation, depending on the physical properties of the dust grains, they will re-radiate the energy in the form of infrared light. The amount of ultraviolet light attenuated by dust will likely be proportionate to the amount of infrared light radiated by the dust grains. Emission lines are also subjected to dust absorption and re-processing. On the other hand, radio emission is unaffected by dust absorption due to its long wavelengths and offers another window into measuring star formation. Most of the observed radio emission is due to free-free emission from ionized HII regions and synchrotron radiation from relativistic electrons (Condon, 1992). However, while free-free emission is a direct dust unbiased tracer of recent star formation, it is much fainter compared to the synchrotron emission, which is fueled by both supernovae (star formation) and accretion procesess (underlying active galactic nucleus).

Studies have proposed several different techniques that can be used to determine the star formation activity (e.g. Kennicutt Jr & Evans, 2012; Bell, 2003; Madau & Dickinson, 2014) from continuum light at different wavelengths (ultraviolet, optical, infrared, radio), and/or from the emission lines. Depending on which tracer is chosen to determine the star formation rate, there are established empirical relations calibrated on large local samples (e.g. Kennicutt Jr, 1998). The obvious and above stated drawback of using only ultraviolet or optical stellar light to estimate the star formation activity is that light at these wavelengths will be affected by dust and in reality will not reflect the true star formation rate. To reach a consensus regarding the true star formation activity of a galaxy, one benefits greatly from multiwavelength observations. Still however, a certain amount of caution is due when it comes to infrared light, as not all of the infrared light contribution is due to star formation: it can originate from active galactic nuclei (e.g. Huynh et al., 2010) or older stellar populations. Likewise, not all stellar light at radio wavelengths is due to star formation, and once the (agreed upon) limiting radio luminosity is reached ($> 10^{23}$ WHz^{-1} ; Condon, 1992), it is difficult to distinguish between the contribution due to star formation or due to an active galactic nucleus.

Local universe based studies were the first to show the dependence of star formation rate on stellar mass, and have pointed out the existence of bimodality in galaxy populations (e.g. Brinchmann et al., 2004; Salim et al., 2005). This bimodality refers to the blue and red sequence of galaxies (see Figure 1.1). Galaxies that belong to the blue sequence are active in star formation and are often referred to as 'normal' star forming galaxies. According to the Hubble classification scheme, the blue sequence is populated by late type galaxies. The galaxy evolution theory pre-

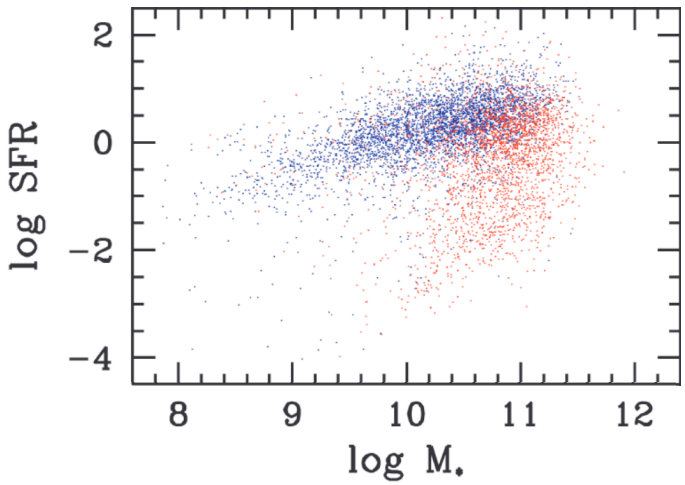

Figure 1.1 Star formation rate vs stellar mass adapted from Salim et al. (2005) based on the SDSS sample. Blue and red points represent star forming and passive galaxies respectively

dicts that the stellar mass growth of blue sequence galaxies occurs via gas accretion, and through merging processes. Once these galaxies reach a certain mass threshold, it is expected that they evolve towards the red sequence. As galaxies become less and less star forming – practically devoid of significant star formation, they move to the red sequence. These galaxies are often referred to as passive (quiescent) and belong to the early type in the Hubble classification scheme. The challenge here is that empirical star formation relations do not hold for quiescent galaxies, so caution is needed when determining their star formation rate.

Studies have found that galaxies that are active in forming stars and do so at a 'normal' rate follow a tight correlation in the star formation rate – stellar mass plane which is referred to as the main sequence. First such relation has been established by Noeske et al. (2007) based on a sample of galaxies at z $\sim$ 0.8 (see also e.g. Elbaz et al., 2007; Rodighiero et al., 2011). Studies at a large lookback time have shown that the slope of this relation evolves, however, the main sequence itself still remains tight (0.2 dex scatter; e.g. Speagle et al., 2014). However, this tight correlation holds for 'normal' star forming galaxies only – whereas galaxies from the red sequence fall below the main sequence.

Understanding physical properties of quiescent galaxy population is rather challenging and the relevant puzzle here can be presented as twofold. Firstly, active efforts are being put towards figuring out how to accurately measure star formation rate of passive galaxies. Secondly, ongoing studies are attempting to understand how red sequence galaxies maintain the state of passiveness.

In the following sections I will present the influence of interstellar medium properties on the observed stellar light (Section 1.2), together with an overview of valuable information we can gain about galaxies themselves by studying the interstellar medium components. Secondly, in section 1.3 we will look into properties of passive

galaxies, and the feedback mechanisms used thus far to explain the state of galaxies that are passive in star formation activity.

1.2 Interstellar medium properties

The evolution and properties of galaxies in the universe as a whole can only be fully understood by exploring all of the components that make up galaxies. An important building component is the matter that fills the space between the stars – the interstellar medium. The interstellar medium is thought to consist of small particles (dust grains) and clouds of gas. The importance of this medium is its way of influencing the radiation from stellar populations. Even though dust grains make up only about 1% of the total interstellar medium matter (e.g. Rémy-Ruyer et al., 2014), they are shown to have significant impact on galaxies. The presence of dust grains on the pathway of stellar light will absorb, scatter and re-emit the light. Understanding the properties of the interstellar medium is an important and open challenge, with active efforts being put towards adding more to the existing pool of information.

The formation and evolution of dust grains remains unsolved. Current theory predicts that dust grains form from several different sources: the atmospheres of evolved stellar populations known as the asymptotic giant branch, and from condensation of the material from the supernovae ejecta (Draine, 2010). It is also thought that dust grains could form in the interstellar medium through grain growth processes involving surrounding atoms and molecules (Galliano et al., 2018, and references therein). The way dust grains are being processed and destroyed is an important part of their evolution. Collisions between grains causes them to undergo fragmentation and shattering, dust grains may coagulate, or be affected by high energy photons, all of which ultimately affects the grain size distribution. Eventually, processes such as bombardment of dust grains by high energy particles, or desorption of atoms or molecules due to photons, causes grains to deteriorate or evaporate, leading to their destruction. Dust grains may also disappear with incorporation into stellar bodies. The effect of dust grains on the stellar light is driven by a range of grain properties. These properties include: grain size (typically $\sim$1-100 nanometer; Weingartner & Draine, 2001), chemical composition (the main building components of grains are thought to be carbonaceous and silicate material), grain shape, grain abundance, distribution (which will largely depend on galaxy inclination; Calzetti, 2001; Pierini et al., 2004), etc. All of these properties combined are specific to each galaxy, and add to the complexity of dust and therefore of the interstellar medium. Nonetheless, proper interpretation of the observations and star formation processes at various cosmic epochs requires good understanding of dust properties.

Most of our understanding of the interstellar medium currently comes from multiwavelength observations. Contributions of different processes, namely emission, absorption and scattering have their own signature in the spectral energy distribution (SED). Essentially, the presence of dust affects the stellar light across all wavelengths, mostly modifying the continuum light in the range from ultraviolet out to near infrared. Dust heated by the absorbed/scattered stellar light will pro-

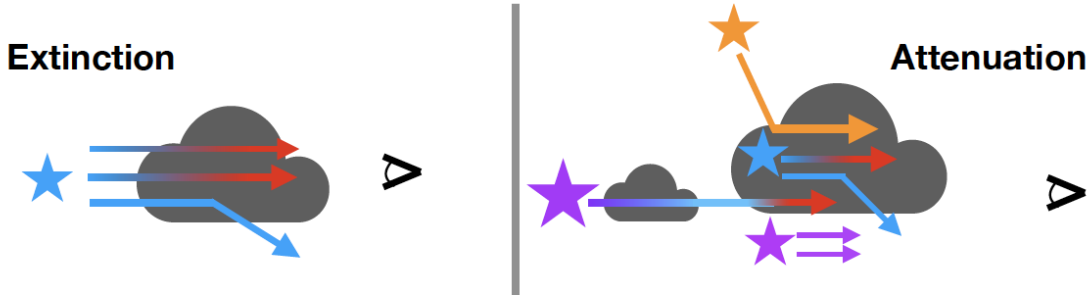

Figure 1.2 Illustration adapted from Salim & Narayanan (2020), showing a difference between extinction and attenuation. Extinction includes absorption and scattering of stellar light out of the sightline, whereas attenuation additionally includes scattering into the sightline.

duce emission at infrared wavelengths. In parallel to observations, a multitude of laboratory based experiments also try to provide valuable information about possible grain properties and reconstruct some of the main observational signatures of dust grains (Joblin et al., 1992; Steglich et al., 2010).

The preferred approach to examine the influence of dust grains on the stellar light is to explore its effects across a wide wavelength range. This can be done by exploring either extinction or attenuation curves. Extinction refers to the absorption and scattering away of the stellar light from the line of sight. Attenuation refers to the effect of the global dust distribution on the integrated stellar light – the attenuation thus includes absorption, and scattering of the stellar light out of, but also into the line of sight (Salim & Narayanan, 2020, shown in Figure 1.2). As first studies emerged, they attempted to characterise physical properties of galaxies based on extinction curve features. One of the features routinely used to characterise the galaxy includes the optical slope of the curve which indicates the 'greyness', meaning – shallower slopes usually point to larger optical depths. Another important, yet not fully understood feature is the strength of the 2175Å bump (ultraviolet bump; e.g. Stecher, 1965, see Figure 1.3 for an example).

Extinction Law

The extinction measurement greatly depends on the column density of the cloud of dust along the line of sight. This dependence therefore folds in various grain properties, such as size distribution of grains, their chemical composition and abundance.

Studying the effects of dust on the stellar light historically began with extinction curves. Assessment of the extinction curve has been done by comparing the spectra of stars affected by dust to those stars of similar properties (spectral type and luminosity) that are ideally dust free. This type of comparison can be achieved either through comparing pairs of stars (Stebbins et al., 1939; Fitzpatrick & Massa, 1986), or using dust free stellar atmosphere models. The challenge of the former lies in the fact of not knowing definitely whether the spectrum of the comparison star is entirely dust free (Salim & Narayanan, 2020, and references therein).

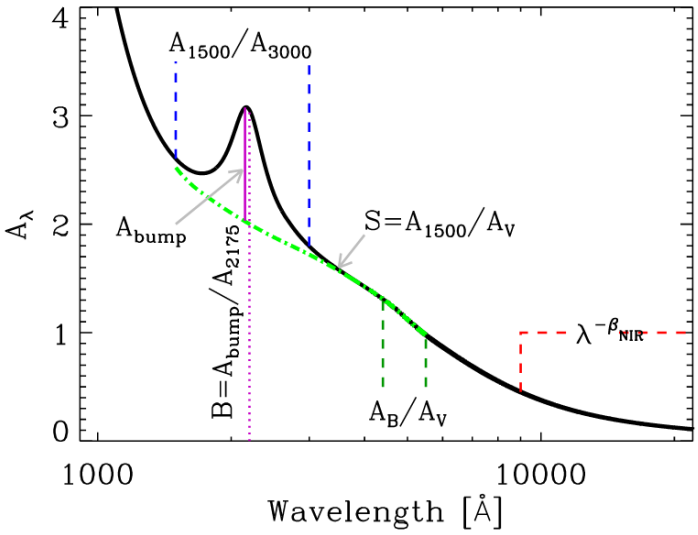

Figure 1.3 Schematic example of the extinction/attenuation curve from Salim & Narayanan (2020). Parameters used to describe the curve are shown as well (B ≡ UV bump strength, A_B/A_V ≡ optical slope).

The first observations that emerged were those of nearby stars, and consequently, the first extinction measurements were based on them. With the first extinction measurements also came the need to parametrize the extinction curve, in order to describe its shape and features. One of the first and most referred to parametrizations is that of the Milky Way stars by Cardelli et al. (1989), which uses a higher order polynomial with fixed curve coefficients. In this parametrization the ultraviolet (UV) bump also has a fixed amplitude. Other parametrizations (e.g. Fitzpatrick & Massa, 1986, 1990; Gordon et al., 2003) allowed flexibility in fitting the UV bump by implementing the Drude profile which included 3 flexible parameters: bump strength, bump width and its central wavelength. Nonetheless, these parametrization choices still relied on a higher order polynomial to describe the baseline of the curve – though with fewer fitting parameters. These first parametrizations of extinction curves provided a starting point for the attenuation curve studies that soon followed.

Attenuation Law

Examination of the attenuation curves aimes to gather the information about the global effects of dust on the stellar light. The main challenge of this is to accurately determine the unattenuated spectral energy distribution. So far, the search for a dust free spectral energy distribution to determine the attenuation curve relied on either empirical or model based methods.

The idea behind the empirical method is very similar to the pair-matching based technique used for extinction curves: attenuation curves determined for different galaxies are mutually compared and relative attenuation is found (e.g. Calzetti et al.,

1994, 2000; Wild et al., 2011). Model based methods rely on deriving spectral energy distribution based on the stellar population synthesis models. A popular approach to derive the spectral energy distribution is to use various SED fitting codes (e.g. *MAGPHYS, CIGALE, Prospector*; da Cunha & Charlot, 2011; Boquien et al., 2019, Johnson et al. in prep.). This technique is based on generating a library of dust-free SEDs with a wide range of physical properties (star formation histories, metallicity). These SEDs are then attenuated, and based on the comparison between the observed and model photometry returns the most likely dust-free spectral energy distribution.

Regardless of the method chosen to determine the dust-free spectral energy distribution, the ultimate description of the attenuation curve requires a choice of parametrization. The very first attenuation curve parametrizations in literature used those applied to recover the extinction curve shapes – an example being higher order polynomial (multi-parameter) parametrizations defined by Cardelli et al. (1989) and Fitzpatrick & Massa (1988). The former parametrization choice allowed flexibility in slope, but not in the bump strength, while the latter allowed the flexibility in both parameters. Studies that followed started using a modified version of the Calzetti et al. (2000) dust law to describe the attenuation curve (e.g. Noll et al., 2009). This parametrization allows variation in the slope of the attenuation curve, as well as its UV bump strength which is included as a free parameter in the Drude profile. After making a parametrization choice, several parameters which are considered sufficient to describe the curve features are then chosen – the most often used ones are the slope of the attenuation curve and the strength of the UV bump. Studies so far have shown a large diversity in attenuation curve features, namely the UV bump strength and the slope (e.g. Buat et al., 2012; Kriek & Conroy, 2013; Tress et al., 2018; Salim et al., 2018). This diversity holds for both galaxies in the local universe, and high redshift universe – even though high redshift attenuation curve studies face limitation in terms of the available data and its quality. Some studies claim a possible correlation between the slope and the UV bump strength (e.g. Kriek & Conroy, 2013), however, this is still a topic of active research. It has also been shown that the slope of the attenuation curve greatly depends on the opacity, and therefore, the measurement will also depend on the galaxy inclination (Conroy et al., 2010; Chevallard et al., 2013). One of the greatest challenges we face right now is the diversity in approaches used to measure the main attenuation curve features, unclear main feature definitions and different normalizations applied. All of this combined makes for a complicated comparison between results from different studies.

Exploring attenuation curves and its features enables us to learn about the influence of dust on stellar light. The main attenuation curve features can help us characterize the geometry of star-dust mixture and dust content of galaxies – which is ultimately important in understanding galaxy evolution processes. In addition, information gathered from observations and attenuation curve measurement can be helpful in radiative transfer models and galaxy simulations.

1.3 Feedback in most massive galaxies

In Λ – Cold Dark Matter (CDM) cosmology, structure formation follows a 'bottom-up' (hierarchical growth) scenario – small structural overdensities collapse first, providing sites for future star formation (Peebles, 1982; Blumenthal et al., 1984). During the evolution phase, galaxies grow in stellar mass via star formation processes and by merging into larger structures. It is thought that different types of galaxies follow different evolutionary paths. The most massive galaxies in centers of groups and clusters are observed to host the oldest stellar populations. The term describing this is called 'downsizing' – meaning that the most massive galaxies formed very early (e.g. Fontanot et al., 2009). The problem here is the absence of star formation in the most massive galaxies in massive haloes – the question is why does this happen?

In an attempt to understand this enigma, many galaxy formation and evolution models have implemented a range of feedback mechanisms in order to explain properties of the most massive galaxies and processes that govern regulation of star formation (e.g. Bower et al., 2006; Croton et al., 2006; Vogelsberger et al., 2014; Schaye et al., 2015). A very powerful mechanism is needed in high halo mass systems to prevent star formation activity. Such a process needs to be sufficiently efficient in order to keep the halo gas warm during its downfall towards the central part of the galaxy. A promising candidate is the feedback from the central engine – supermassive black hole. Depending on the rate at which halo gas falls onto the supermassive black hole, two different modes can occur: radiative-mode and jet-mode. This gas accretion rate is referred to in Eddington units (Narayan et al., 1998; Heckman et al., 2004).

Radiative-mode feedback is related to a high ($\sim$ Eddington) accretion rate, and is thought to manifest via strong outflows of the gas. This type of feedback is thus thought to strip the galaxy off of its star formation fuel, resulting in the absence of star formation (e.g. Di Matteo et al., 2005). However, this type of feedback is not considered sufficient to maintain the state of passiveness in galaxies over a longer period of time, therefore making it an improbable explanation for quiescence. Jet-mode feedback (also called maintenance-mode) is on the other hand related to the low (sub-Eddington) accretion rate of the gas onto the central engine. This type of feedback is thought to manifest itself in the form of jets which originate from an active galactic nucleus (e.g. Fabian, 2012). If present, the jets are likely to be observed at radio wavelengths, and the sources that host an active galactic nucleus are referred to as radio-loud. The term radio-loud in general refers to the luminosity of these galaxies at radio wavelengths that is larger than 10^{23} WHz^{-1} (Condon, 1992). Specifically, jet-mode feedback has been considered as a possibly powerful enough process to maintain the state of the absence of star formation in the most massive, early type galaxies. In this feedback picture, the powerful feedback by central engine acts as a heating mechanism for the surrounding halo gas, preventing its cooling and further star formation.

Even though this feedback mechanism is considered enough to prevent star formation – so far, no direct evidence has been observed to confirm this scenario, except

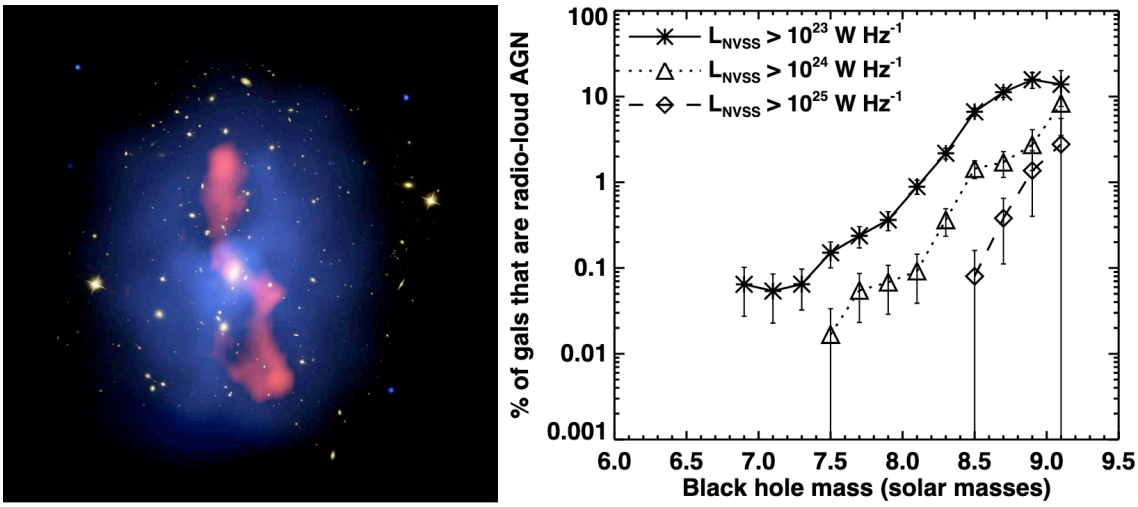

Figure 1.4 **Left:** An example of direct evidence for maintenance mode feedback picture – Figure adapted from McNamara & Nulsen (2007) of the MS0735.6+7421 cluster. Figure contains visual, radio (red) and X-ray (blue) image. Cavities are evident in the X-ray. Within the cavities one can see radio emission. **Right:** Indirect evidence for the maintenance mode feedback picture as presented by Best et al. (2005). This work shows that galaxies which host supermassive black holes have large radio-loud AGN fraction.

in the local universe. The direct evidence detected for passive galaxies in the local universe is in the form of cavities in the X-ray emitting gas (e.g. McNamara & Nulsen, 2007, see left panel in Figure 1.4). The existence of those cavities could be explained by the powerful jets exerted by the central engine which then inflate bubbles and form said cavities in the halo gas. The gathering of such direct evidence at larger lookback time is so far limited by insufficient X-ray sensitivity. For this reason, at larger lookback time we can only rely on the indirect evidence – through a link between quiescence and the presence of radio-loud AGN. This connection has been established in the local universe where Best et al. (2005) have shown that galaxy black hole mass sets the probability for the occurrence of radio-loud AGN (right panel in Figure 1.4). Nonetheless, even though presence of jet-mode feedback goes in support of the picture of maintaining the state of quiescence, it does not explain how galaxies quench in the first place. This question remains an open challenge.

Only high quality observations of both stellar kinematics and stellar populations, together with high sensitivity radio observations can serve to provide an insight into the existence of a jet-mode feedback mechanism in high-redshift systems. It is also essential that this evidence is gathered for a large number of galaxies. The Large Early Galaxy Astrophysics Census (LEGA-C) spectroscopic survey in combination with the recent Very Large Array (VLA) 3GHz survey offers the first ever ability to conduct a statistically significant investigation of maintenance-mode feedback at a larger lookback time.

1.4 Thesis outline

The aim of this thesis is to present the results obtained by examining various physical properties of galaxies. The main focus is on the interstellar medium properties of high redshift ($z \sim 0.8$) galaxies, and properties of quiescent galaxies in both the local and high redshift ($z \sim 1$) universe.

Chapter 2 focuses on the interstellar medium properties, where the new approach to measure the attenuation in $z \sim 0.8$ galaxies is presented. A new attenuation curve modeling technique is introduced, together with a new prescription for a typical attenuation curve for $z \sim 0.8$ galaxies. Attenuation curve modeling uncovers a diversity among attenuation curves and their main features (slope and the UV bump strength). The examination of the dependence of attenuation curve features on global galaxy properties yields an important result: galaxy geometry influences observed variations in attenuation. Subsequent chapters focus on the properties of quiescent galaxies as follows: Chapter 3 investigates the rate at which radio-loud AGN occur in round (spheroidal) as compared to flat (disk-like) quiescent galaxies. This research is conducted for a large sample of galaxies in the local universe and it shows that radio-loud AGN preferably occur in round galaxies. Given that radio-loud AGN are not observed among flat galaxies, this finding challenges the picture in which the maintenance-mode feedback is a sufficient explanation for maintaining passiveness. Chapter 4 shifts the focus to high redshift where the combination of recently conducted surveys (LEGA-C spectroscopic and VLA radio surveys) provide evidence in support of the maintenance-mode feedback picture for galaxies at $z \sim 1$.

Chapter 2

Dust Attenuation Curves at z ∼ 0.8 from LEGA-C: Precise Constraints on the Slope and 2175Å Bump Strength*

The challenge of studying the attenuation in galaxies is that it requires reliable information about the attenuation-free spectral energy distribution. This chapter introduces a novel approach to measure the attenuation for individual star-forming galaxies at z ∼ 0.8 based on deep optical LEGA-C survey spectra and multi-band photometry. A new attenuation curve modeling technique is presented as well, and the new prescription for typical z ∼ 0.8 attenuation curve is given. I further analyse correlation between main attenuation curve features and global galaxy properties.

2.1 Introduction

Examining dust properties of galaxies improves our understanding of the evolution of galaxies through cosmic time. Yet, properly addressing and interpreting properties of dust presents a very challenging task. One of the techniques applied to tackle this challenge is to investigate the effect of dust on stellar light at different wavelengths, which was done first through examination of extinction curves (e.g. Savage, 1975; Fitzpatrick & Massa, 1986, 1988, 1990). Extinction curves describe line of sight effects of the influence of dust on stellar light, but in order to understand the global effect of dust in a galaxy it is necessary to measure attenuation (absorption and scattering) of the integrated light. The first step toward understanding attenuation is to determine the wavelength dependence of the attenuation curve. Thus far, dust attenuation studies faced limitations due to the inability to directly measure the intrinsic stellar spectrum. This precludes the determination of the attenuation

*The contents of this chapter are adapted from the article Barišić et al. 2020, submitted to the Astrophysical Journal. I am the lead author of this paper, for which I have conducted research and analysis.

curve without strong degeneracies with stellar population properties such as age and metallicity.

Before discussing how we address this issue, let us first summarize how the description of extinction and attenuation curves have evolved over time: from e.g. Savage (1975) who applied a linear (λ^{-1}) extinction curve baseline term, to those involving higher order polynomial applied by studies that followed (e.g. Fitzpatrick & Massa, 1986). Independently of the extinction curve baseline choice, Milky Way studies included an additional term (i.e. Drude profile) to describe the profile and strength of the prominent UV bump feature. As more observations of other local and low-redshift galaxies emerged, some studies proceeded to only examine the attenuation curve baseline, not accounting for the possible contribution by the UV bump (e.g. Calzetti et al., 2000). Later on, dust attenuation curves of local and high-redshift galaxies have often been described by a high-order polynomial (e.g. Cardelli et al., 1989; Buat et al., 2012; Battisti et al., 2017) or a modified power-law version of Calzetti dust law (e.g. Noll et al., 2009), in combination with a Drude profile to account for a possible presence of the UV bump feature. Understanding the origin of the UV bump (Stecher, 1965; Savage, 1975) and its properties is important to interpret the physical properties of those galaxies that demonstrate this feature, and to explore the evolution of these properties through cosmic time. A number of theoretical and laboratory based studies have been conducted over the last few decades in attempt to explain the origin of the UV bump feature, and more recent findings suggest PAH molecules as a promissing carrier candidate of the 2175Å feature (Joblin et al., 1992; Beegle et al., 1997; Steglich et al., 2010). The UV bump, together with the attenuation curve slope, which describes the reddening of the attenuation curve, have been used to characterize properties of the attenuation by dust (e.g. Burgarella et al., 2005; Buat et al., 2012; Kriek & Conroy, 2013; Battisti et al., 2017; Tress et al., 2018; Narayanan et al., 2018; Salim et al., 2018).

Up until now, dust attenuation studies in both the local and high redshift universe have mostly relied on deriving spectral energy distribution (SED) fits based on the observed multi-band photometry to recover the information about the attenuation in galaxies (e.g. Buat et al., 2012; Battisti et al., 2016; Gordon et al., 2016; Battisti et al., 2017; Salim et al., 2018). For example, Reddy et al. (2015) found a steep attenuation law for a sample of z ∼ 2 galaxies compared to Calzetti et al. (2000). In addition, Kriek & Conroy (2013) sampled the SED by combining narrow- and medium- band photometry of galaxies at similar redshifts, producing stacked high-resolution pseudo-spectra, providing significant evidence for the existence of the UV bump at z ∼ 2. Scoville et al. (2015) find evidence for the presence of the UV bump in their sample of high redshift z = 2 – 6 galaxies. Tress et al. (2018) is the only high-redshift study, so far, of attenuation properties in individual galaxies, based on low-resolution spectra and they do not find strong correlations between the slope of the attenuation curve and the strength of the UV bump with global galaxy properties including stellar mass M_*, specific star-formation rate, and inclination. Finally, at very high redshifts constraints on attenuation are inferred from the relation between the UV slope and the infrared excess (e.g. Reddy et al., 2006; Capak et al., 2015; Bouwens et al., 2016; Barisic et al., 2017a; Bourne et al.,

2017; Faisst et al., 2017; Fudamoto et al., 2017; Reddy et al., 2018; Wang et al., 2018).

It is important to note that the choice of the attenuation curve parametrization and of the UV bump profile will dictate the measurement of the UV bump strength and of the slope of the attenuation curve. The variety of attenuation curve parametrization choices in the literature makes the comparison between studies rather difficult. Additionally, a wide variety in procedures involved in obtaining the attenuation information makes for a challenging comparison as well. Taking this into account, diversity in prescriptions among studies and techniques applied to derive the attenuation may explain inconsistencies in terms of the trends between the slope of the attenuation curve, strength of the bump feature and general attenuation with other galaxy properties.

Ideally, absorption line strength information and stellar population models should be used in tandem to obtain high quality information on the effects of dust on stellar light. Absorption lines are far less sensitive to dust effects and thus can provide information about the underlying stellar populations, while the stellar population models can serve for the comparison of the calibrated continuum flux to the observed spectrum. Even though high quality stellar population models have been developed, deep absorption line strength information was unavailable this far. The deep and high-resolution Large Early Galaxy Astrophysics Census (LEGA-C, van der Wel et al., 2016) continuum spectra enables studying intrinsic stellar spectra of individual galaxies, yielding an independent attenuation curve measurement. In this study we present, for the first time, an approach to measure dust attenuation using continuum based intrinsic stellar spectra combined with the observed multi-band photometry, on an individual galaxy basis. The main goal of this work is to provide a more accurate description of the attenuation curve for the integrated light of galaxies. This will help efforts to interpret the attenuation of distant galaxies in terms of both schematic dust distribution models and full radiative transfer-based mock observations (see Salim & Narayanan (2020) for an excellent review of the current state of the art). We examine the diversity in dust attenuation properties among our galaxies, with the main focus on the strength of the UV bump feature and the slope of the attenuation curve. Furthermore, we explore the dependence of these properties on galaxy orientation, specific star-formation rate (sSFR) and stellar mass M_*.

The outline of this paper is as follows: in the following section 2 we introduce the data set used in this study, and the choice of attenuation curve parametrization. In section 3 we present a new attenuation curve prescription and discuss the results. A summary of this work is given in section 4.

2.2 Data

2.2.1 The LEGA-C Survey

The Large Early Galaxy Astrophysics Census (LEGA-C; van der Wel et al., 2016), an ESO public spectroscopic survey, conducted between 2014 and 2018 with the VI-

MOS spectrograph at the Very Large Telescope, was devised to obtain high signal-to-noise (S/N $\sim$ 20Å^{-1}) and high resolution (R = 3500; Straatman et al., 2018) optical continuum spectra of high redshift galaxies (van der Wel et al., 2016). The survey gathered continuum spectra of $>$ 3000 K-band selected galaxies from the UltraVISTA survey (Muzzin et al., 2013) within the 1.62 square degree region of the COSMOS field at a redshift range between 0.6 $<$ z $<$ 1, covering the wavelength range between 6300Å $\lesssim \lambda \lesssim$ 8800Å . This study utilizes the most recent Data Release II sample (Straatman et al., 2018), comprised of a total of 1989 galaxies.

We make use of spectroscopic redshifts and axis ratio. Additionally, we also make use of the observed multi-band photometry from the UltraVISTA photometric catalog (Muzzin et al., 2013). SFR values are derived from UV and 24μm photometry, following Whitaker et al. (2012a) relation, while stellar mass M$_*$ estimates are obtained following Pacifici et al. (2012) (Pacifici et al. 2020, in prep). For further details on data reduction and the most recent data release we refer to Straatman et al. (2018).

We select UVJ color based star-forming galaxies in the redshift range 0.61 $<$ z $<$ 0.94, with 'use' flag = 1 (see Straatman et al., 2018) and available intrinsic stellar spectra measurement. We target this redshift range to achieve coverage in the UV bump region with at least one ($u-$ band) measurement. As the typical width of UV bump is 350Å (Noll et al., 2009), in the chosen redshift range the $u-$ band measurement probes the UV bump over a wavelength range of 2175Å $\pm$ 200Å. These criteria secure good observed continuum stellar spectra quality and enable us to consistently model the strength of the UV bump feature with available photometric coverage. The combination of this criteria yields a sample of 524 star-forming galaxies shown with pink and teal colored symbols in Figure 2.1. A small fraction of star-forming galaxies in our selected sample has low SFR based on their infrared luminosity, however, this does not affect our results.

2.2.2 Attenuation-free stellar spectra

The advantage of deep and high resolution LEGA-C optical continuum spectra (e.g. top panel in Figure 2.2) lies in the ability to estimate the intrinsic stellar spectra free of dust attenuation effects, and to do so for a large number of galaxies.

We follow the methodology developed by Pacifici et al. (2012, 2016). A library of model spectra is created by combining physically motivated star formation histories from cosmological simulations with stellar and nebular emission models (Charlot & Longhetti, 2001; Bruzual & Charlot, 2003) and the effect of dust attenuation on the emission lines only (following Charlot & Fall, 2000). Both the observed and the model spectra are convolved with a Gaussian kernel to mimic a velocity dispersion of 250km/s, to avoid discrepancies in the widths of the emission and absorption lines when fitting the spectra pixel by pixel. The continuum is then calculated for each galaxy with a running median in windows of 180Å. This is optimized to remove all emission and absorption lines in the wavelength range of interest, preserving the

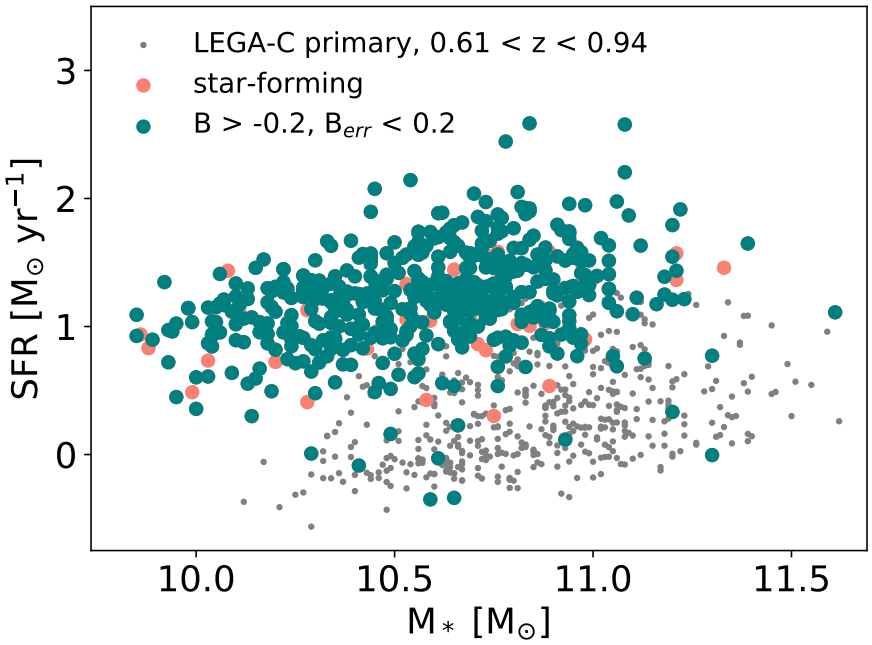

Figure 2.1 Star-formation rate vs stellar mass M_* of $0.61 < z < 0.94$ LEGA-C Data Release II sample shown with grey symbols, together with the selected sample of star-forming galaxies (pink). Teal circles represent galaxies with UV bump strength $B > -0.2$ and small uncertainty on the bump strength $B_{err} < 0.2$ (introduced in Section 2.2.3)

color of the spectrum. The continuum is then subtracted from the spectrum and the result is divided by the same continuum to produce a normalized, flat spectrum. The same procedure to subtract the continuum is applied to the observed and the model spectra (middle panel in Figure 2.2). After removing the shape of the continuum and thus the effect of dust attenuation on the global shape of the continuum, the model spectra are fitted pixel by pixel to the observed LEGA-C spectra. The output is an intrinsic, attenuation-free spectrum per observed galaxy covering the full UV to NIR rest-frame wavelength range (1200Å$\sim$ 45000Å; bottom panel in Figure 2.2). Since the attenuation slope measurement sensitively depends on where the attenuation reaches 0, we normalize the intrinsic, dust-free model spectra so that attenuation is forced to be zero at 3.3μm by linearly extrapolating from the UltraVISTA $J-$ and $Ks-$ band photometry in inverse wavelength space $1/\lambda$. In principle, IRAC photometry should be more suitable for this normalization, as it is closer in wavelength, but the difficulty in matching photometry due to the large IRAC PSF precludes us from doing so with sufficient accuracy. Several examples of the intrinsic stellar spectra, together with the intrinsic and observed flux density values at corresponding UltraVISTA bands can be seen in the left panels of Figure 2.3. The difference between the attenuation-free model and the observed broad-band photometry provides us with the attenuation (as shown in right panels of Figure 2.3).

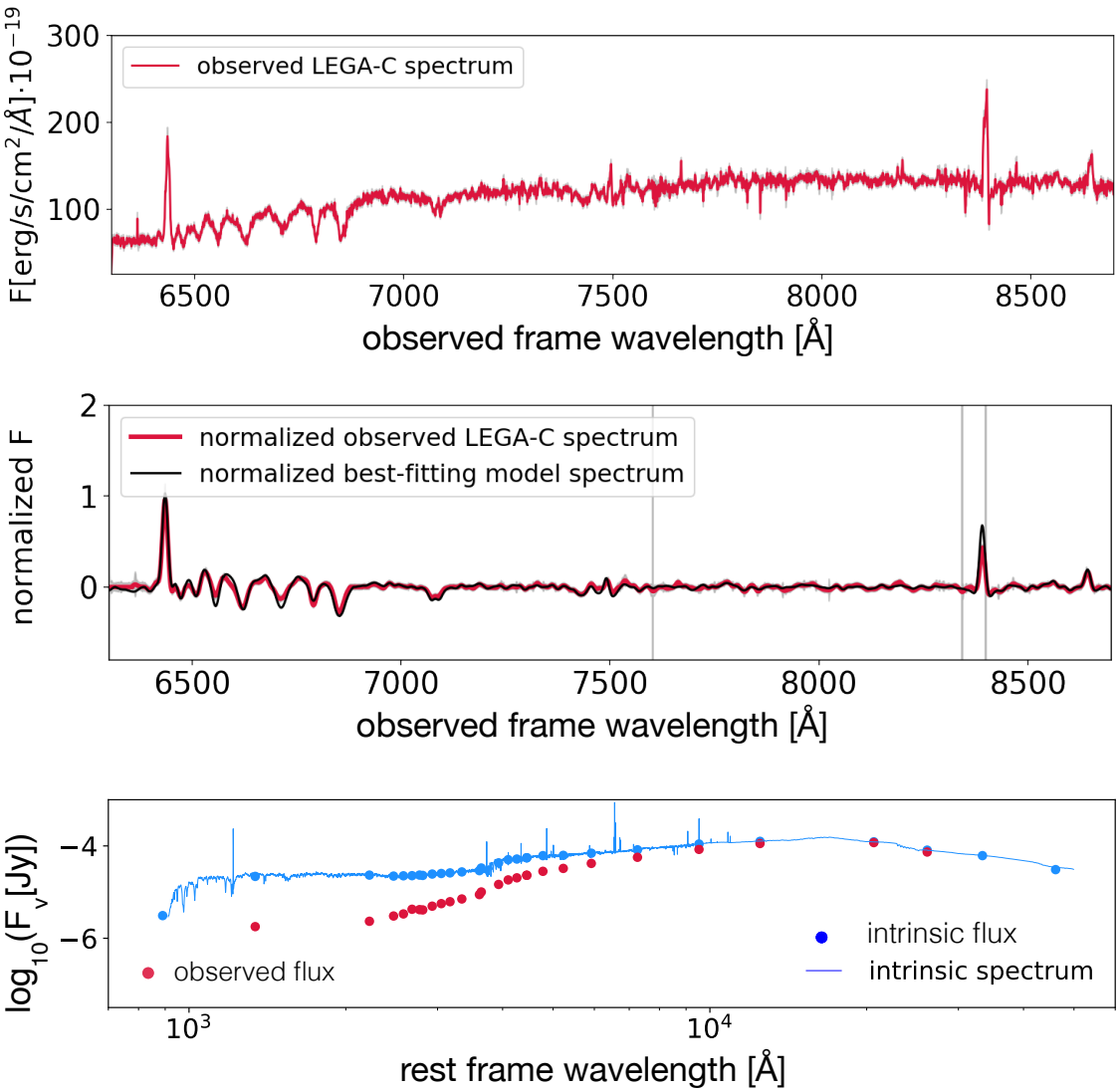

Figure 2.2 **Top:** An example of the observed LEGA-C spectrum (galaxy ID: 131198); **Middle:** Normalized and continuum subtracted observed spectrum (red curve) together with the best-fitting model spectrum (blue curve); **Bottom:** Intrinsic, attenuation free spectrum (blue curve) with photometric data-points in the corresponding observed bands, and the observed photometry (red circles)

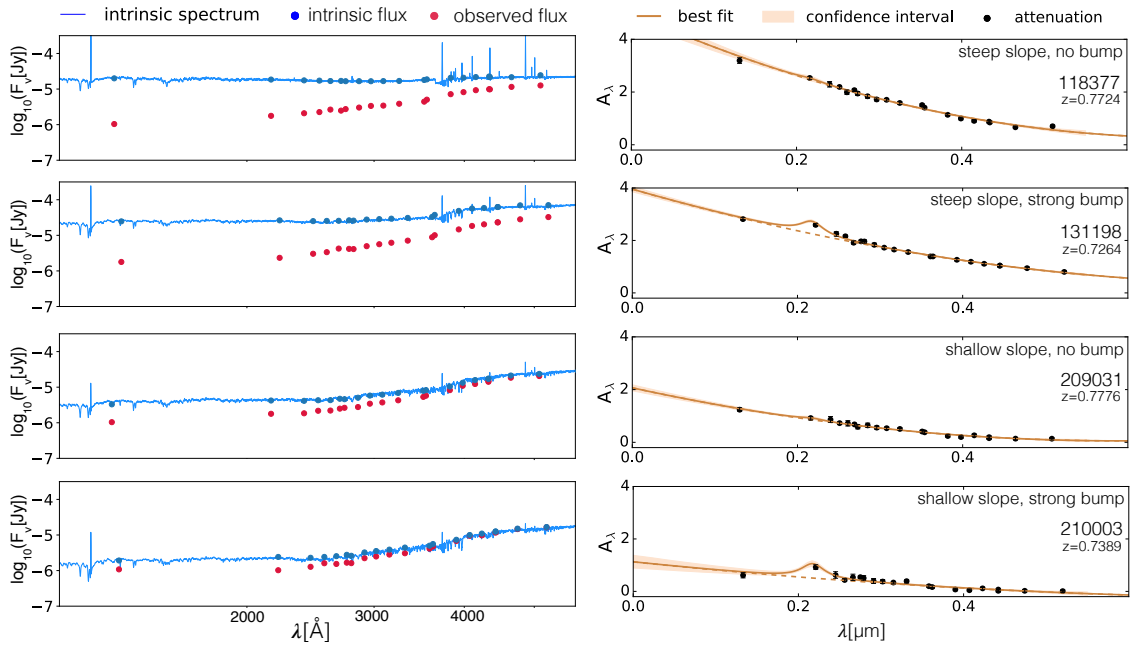

Figure 2.3 **Left:** Observed (red circles) and attenuation-free model (blue circles) flux density values, together with attenuation-free model spectra (blue curve). **Right:** Attenuation data points together with best fit attenuation curves using a combination of the second order polynomial and the Lorentzian function to describe the bump feature, with 68% confidence range. Error bars are smaller than the symbols. We show examples of steep/shallow attenuation curve with no bump detected (118377 and 209031) and prominent bump feature (131198 and 210003) respectively.

2.2.3 Attenuation curve

The UltraVISTA catalog contains flux density values in 30 photometric bands, and our attenuation curve determination is based on a subset of those. GALEX $FUV-$ band is excluded as it covers rest-frame Lyman-α forest in the selected redshift range ($0.61 < z < 0.94$). We choose to fit the attenuation curve in 20 photometric bands including: GALEX $NUV-$, CFHT Megaprime $u-$, SUBARU Suprime-Cam intermediate and broad ($B-$, $V-$, g^+-, r^+-, i^+-, z^+-) band filters – included in Figure 2.3. The observed attenuation is obtained via:

$$A = -2.5 \cdot \log_{10}\left(\frac{f_{obs}}{f_{int}}\right)$$

where f_{obs} and f_{int} are the observed and intrinsic flux density values. Attenuation in the GALEX $NUV-$ band puts a constraint on the blue part of the attenuation curve as it is the only data point at shorter wavelength than the UV bump (covered by the $u-$ band).

Given the diversity in the literature when it comes to the choice of the attenuation curve parametrization to be fitted to the observed attenuation (e.g. Noll et al., 2009; Battisti et al., 2017), we opt for the second order polynomial to describe the baseline

of the attenuation curve, in a linear combination with the Lorentzian function[1] to describe the UV bump feature:

$$A(\lambda) = a\lambda^2 + b\lambda + c + \frac{\alpha}{\pi}\frac{0.5\Gamma}{(\lambda - \lambda_0)^2 + (0.5\Gamma)^2} \tag{2.1}$$

Here λ is wavelength in μm, Γ is the width of the bump feature (0.035μm, Noll et al., 2009), λ_0 is the central wavelength of the bump (0.2175 μm), and B is the amplitude parameter to scale the Lorentzian function. The parameters a, b, c are free fitting parameters of the second order polynomial, as is the amplitude α of the Lorentzian function. We define the strength of the UV bump feature in the following way:

$$B = \frac{A(2175\mathring{A}) - A_{base}(2175\mathring{A})}{A_{base}(2175\mathring{A})} \tag{2.2}$$

where $A_{base}(\lambda)$ is the baseline value of the second order polynomial. Additionally, we define the slope of the attenuation curve as a non traditional R(4500Å):

$$R(4500\mathring{A}) = \frac{A(4500\mathring{A})}{A(3000\mathring{A}) - A(4500\mathring{A})} \tag{2.3}$$

We choose this attenuation curve slope definition over the typical R_V[2] since the second order polynomial in our parametrization $A(\lambda)$ often shows an inflection at ≈ 5500Å, leading to non-informative R_V values. The physical origin of this inflection is discussed below, when we make a comparison with the results from standard attenuation law prescriptions (e.g. modified Calzetti law).

Since our parametrization differs from the standard prescriptions, it is useful to calculate UV bump strength B and slope of the attenuation curve R(4500Å) for the widely used attenuation/extinction laws. Applying our parametrization to the Cardelli et al. (1989) prescription for the Milky Way (MW) extinction curve we find B ∼ 0.48, and a slope R(4500Å) ∼ 2.2, whereas for the Calzetti et al. (2000) attenuation law we find R(4500Å) ∼ 2.4. Extrapolating from the data given in Table A4 in Gordon et al. (2003) we find R(4500Å) ∼ 2.1 and 2.5 for the Small Magellanic Cloud (SMC) and Large Magellanic Cloud (LMC), respectively.

We fit our $A(\lambda)$ parametrization (see Equation 2.1) to the observed attenuation in several steps. If any observed attenuation data point is >3σ from the best-fit parametrization curve, it is excluded and the fit is performed again. As a next step, we make sure an optimal fit to the observed attenuation around the UV bump region is achieved. This is done by integrating the $u-$ band (together with $IB427-$ band at z > 0.8) transmission curve (Muzzin et al., 2013) with the most-recent best-fit to obtain the predicted attenuation data point. The difference between the predicted and the observed attenuation data point is then added to the observed data point, and the fit is performed again. We find two iterations leads to convergence. We prefer this approach of fitting data points to the attenuation curve over the much

[1] http://mathworld.wolfram.com/LorentzianFunction.html

[2] $R_V \equiv A_V/E(B-V) \equiv A_V/(A_B - A_V)$

computationally slower approach of convolving the attenuation curve with all filter transmission curves to find the best fit. A variety of examples of the attenuation data points and the resulting attenuation curves is shown in the right panels of Figure 2.3. Applying this fitting procedure, we reject[3] galaxies with highly negative UV bump strength measurement (B < - 0.2), and those with large uncertainties on the bump measurement ($B_{err} > 0.2$) as an indicator of the good fit, which gives us a sample of 485 galaxies (teal colored symbols in Figure 2.1). Out of 485 galaxies, 260 have the UV bump measured with 99% confidence.

Apart from the second order polynomial, we also explored several other parametrizations, including the most often applied – the modified Calzetti dust law combined with the Drude profile, as given in e.g. Salim et al. (2018). However, the issue we encountered while applying this particular parametrization is that the power-law fit provided poor fits for the majority of galaxies in our sample[4]. For this reason we adopted the second order polynomial as our default parametrization. The main reason for this is that the galaxies in our sample generally have a broad age range in their stellar populations, and the dust attenuation is likely strongly age dependent. Old stellar populations with little dust attenuation dominate at longer wavelengths, while young stellar populations with more dust attenuation can dominate at shorter wavelengths, leading to curvature in the attenuation that cannot be captured with a power law – for this reason studies often make use of two-component dust models. This phenomenon also strongly affects the inferred slope, which will be discussed further in Section 2.3.

2.3 Results

2.3.1 Attenuation curve prescription

As the existing parametrization prescriptions in the literature do not provide good quality fits for the observed attenuation of star-forming galaxies in our sample, we provide our own prescription. The following prescription is meant to reproduce the median slope R(4500Å) and UV bump values of star-forming galaxies in the selected sample ($R_{median}(4500Å) \sim 1.2$, $B_{median} \sim 0.12$). To achieve this we select a subset of attenuation curves in a narrow slope range $1 < R_{median}(4500Å) < 1.4$, and simultaneously fit all of the attenuation data points, achieving a mean attenuation curve. This prescription, represents a typical curve for star-forming galaxies at z ∼ 0.8, normalized at 4500Å, and is defined in the wavelength range $0.13\mu m < \lambda < 0.5\mu m$:

$$\frac{A(\lambda)}{A(0.45\mu m)} = \begin{cases} (14.780\lambda^2 - 16.654\lambda + 5.498 + D_\lambda), \\ D_\lambda = \frac{0.017}{\pi}\frac{0.5\Gamma}{(\lambda-\lambda_0)^2+(0.5\Gamma)^2}, \\ 0.13\mu m < \lambda < 0.5\mu m \end{cases} \tag{2.4}$$

Reproduced slope and UV bump values following this prescription are 1.18 and

[3] 7% of the total sample of 524 galaxies

[4] $\chi^2 > 1.5$ for >60% of star-forming galaxies when using power-law, as opposed to ∼30% when using a second order polynomial

0.12 respectively. At wavelengths longer than 0.5μm we recommend the standard Calzetti et al. (2000) prescription, scaled by factor N to match our prescription:

$$A(\lambda) = \begin{cases} N \cdot (2.659(-2.156 + \frac{1.509}{\lambda} - \frac{0.198}{\lambda^2} + \frac{0.011}{\lambda^3}) + R_V), \\ N = 0.194; 0.5\mu m < \lambda < 0.63\mu m \\ \\ N \cdot (2.659(-1.857 + \frac{1.040}{\lambda}) + R_V), \\ N = 0.194; 0.63\mu m < \lambda < 2.2\mu m \end{cases}$$

Wavelength λ used in both equations is in μm. In order to account for the variation in the slope of the attenuation curve, we offer a modified version of Equation 2.4:

$$A'(\lambda) = \frac{A(\lambda)}{A(0.45\mu m)} \cdot \left(\frac{\lambda}{0.45}\right)^{\delta} \tag{2.5}$$

$$\delta = \frac{log_{10}(R(4500\mathring{A})/1.18)}{log_{10}(0.45/0.3)}$$

Upper panel in Figure 2.4 presents all of the attenuation curves in the selected narrow slope range (gray) together with the typical curve following from the fit (teal) together with its confidence interval. Teal solid curve in Figure 2.4 shows our parametrization prescription up to 5000Å, combined at longer wavelengths with re-scaled Calzetti et al. (2000) curve. For comparison we also show MW extinction curve (Cardelli et al., 1989) which we have normalized to 4500Å (dotted grey curve). The standard Calzetti et al. (2000) attenuation curve (dashed grey curve), and Small Magellanic Cloud as given by (Gordon et al., 2003) (solid grey curve) are also shown, both of which have been re-scaled by the same factor as MW curve in order to preserve their mutual R_V ratios. It is worth noting that the steepness of the slope of the Calzetti attenuation curve in the region below 0.2μm is very similar to the slope of the curve given by our prescription, as compared to the SMC curve slope which is considerably steeper. This justifies our Calzetti prescription recommendation at wavelengths longer than 0.5μm. In the table below we provide normalized attenuation A(λ)/A(4500Å) values for our prescription:

2.3.2 Global Attenuation Properties

In Figures 2.5 and 2.6 we present the variation of the dust attenuation properties of galaxies – namely attenuation A(4500Å), slope of the attenuation curve R(4500Å) and UV bump strength B with several global galaxy properties: specific star-formation rate (sSFR = SFR/M_*), stellar mass M_* and projected axis ratio (as an inclination proxy).

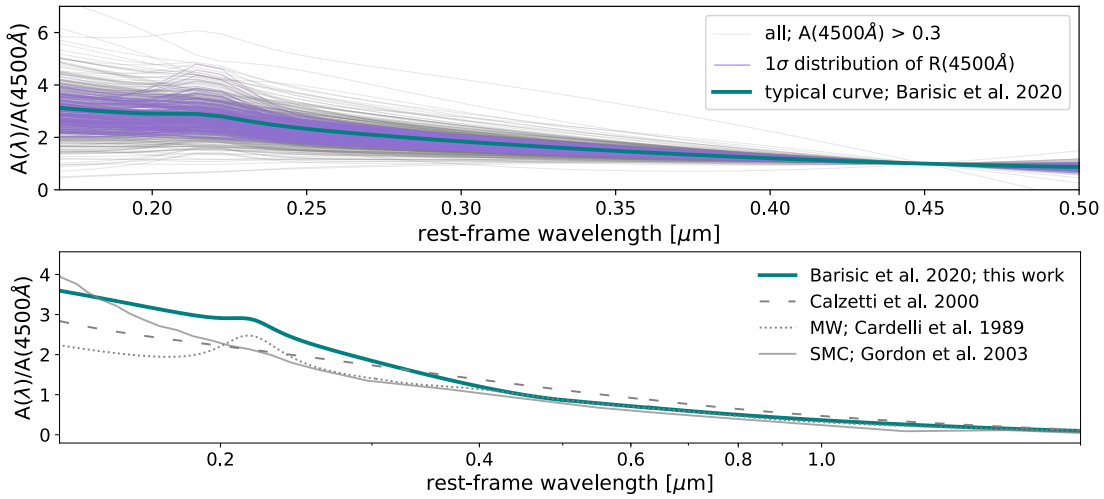

Figure 2.4 **Top:** All of the attenuation curves (gray) from a subset of the selected sample (A(4500Å) > 0.3); representing the scatter – we highlight attenuation curves (purple) of those galaxies within 1σ of the slope R(4500Å) distribution. The typical attenuation curve (teal) is also shown. **Bottom:** A typical attenuation curve for z ∼ 0.8 star-forming galaxies (solid curve) out to 0.5μm. At wavelengths longer than 0.5μm we show re-scaled Calzetti et al. (2000) attenuation curve (0.5μm – 2.2μm). For comparison we also show Milky Way Cardelli et al. (1989) extinction curve re-normalized to 4500Å. We also show the standard Calzetti et al. (2000) attenuation curve and Small Magellanic Cloud (Gordon et al., 2003) extinction curve re-scaled by the same factor as Milky Way.

We observe an increase in A(4500Å) with stellar mass M_*, and sSFR. This trend can be explained by the larger dust content in more star-forming and more massive galaxies – a trend also seen in present day universe (e.g. Cortese et al., 2012), which can be attributed to the combination of large gas fraction and high metallicity. However, the strongest correlation is between A(4500Å) and axis ratio (see top panels in Figure 2.6), which immediately tells us that geometry to a large extent shapes observed attenuation curves, both for present day galaxies (e.g. Salim et al., 2018) and for galaxies at large lookback time (see also Patel et al., 2012; Wang et al., 2018)

The slope R(4500Å) does not exhibit a clear correlation with stellar mass M_* or sSFR (Figure 2.5), but it is interesting to note that the typical attenuation curve slope value (median: R(4500Å) ∼ 1.2) is much steeper than the MW (R(4500Å) ∼ 2.2), Calzetti (R(4500Å) ∼ 2.4), LMC (R(4500Å) ∼ 2.5) and SMC (R(4500Å) ∼ 2.1) extinction curve (see Figure 2.7). The UV bump is typically much weaker than the MW UV bump (0.12, compared to 0.48 for MW bump), and only a few galaxies (7%) have B > 0.4, comparable to the MW.

We do not observe a clear trend in the sSFR - M_* plane with the UV bump strength (see Figure 2.5), but we see variations from B = 0 to B = 0.4, indicating a large intrinsic scatter (typical uncertainty on the UV bump strength ∼ 0.04). However, we see an indication that more (less) massive galaxies[5] on average have

[5] $\log_{10}(M_*/M_\odot) > 10.7$

Table 2.1: Values for the attenuation curve prescription (A(λ)/A(4500Å)) shown with teal solid curve in Figure 2.4

$\lambda[\mu m]$	A(λ)/A(4500Å)	$\lambda[\mu m]$	A(λ)/A(4500Å)
0.13	3.595	0.5	0.867
0.145	3.411	0.57	0.754
0.16	3.238	0.64	0.664
0.175	3.081	0.71	0.581
0.19	2.956	0.78	0.513
0.205	2.908	0.85	0.456
0.22	2.85	0.92	0.408
0.235	2.554	0.99	0.366
0.25	2.327	1.06	0.331
0.265	2.159	1.13	0.299
0.28	2.016	1.20	0.272
0.295	1.886	1.27	0.247
0.31	1.766	1.35	0.225
0.325	1.655	1.42	0.205
0.34	1.551	1.49	0.187
0.355	1.454	1.56	0.171
0.37	1.364	1.63	0.156
0.385	1.281	1.70	0.142
0.4	1.204	1.77	0.13
0.415	1.135	1.84	0.118
0.43	1.072	1.91	0.107
0.45	1.	1.98	0.097
0.46	0.966	2.05	0.088
0.475	0.924	2.12	0.079
0.49	0.888	2.2	0.071

shallower (steeper) attenuation curve slope and weaker (stronger) UV bump values. Our results are therefore consistent with Salim et al. (2018) who find shallower slope values and a general decrease in the UV bump strength at higher stellar mass M_* for present-day galaxies. In addition they find a general increase in the bump strength on both sides of the main sequence, which we do not observe. This is perhaps not surprising, given the limited sample size and a large scatter in the UV bump strength values.

Secondly, we observe steeper attenuation curve slope values for face-on galaxies, as compared to edge-on galaxies (see Figure 2.6), which is in agreement with the results from Wild et al. (2011) for present-day galaxies. Similarly, even though Salim et al. (2018) find a weak trend in the slope of the attenuation curve with galaxy orientation, they see on average a steeper slope for face-on galaxies. This trend is consistent with predictions by Chevallard et al. (2013), who show that scattering at low optical depth (face-on orientation) would result in the steep observed attenuation curve. However, the differences in spatial distribution and dust obscuration

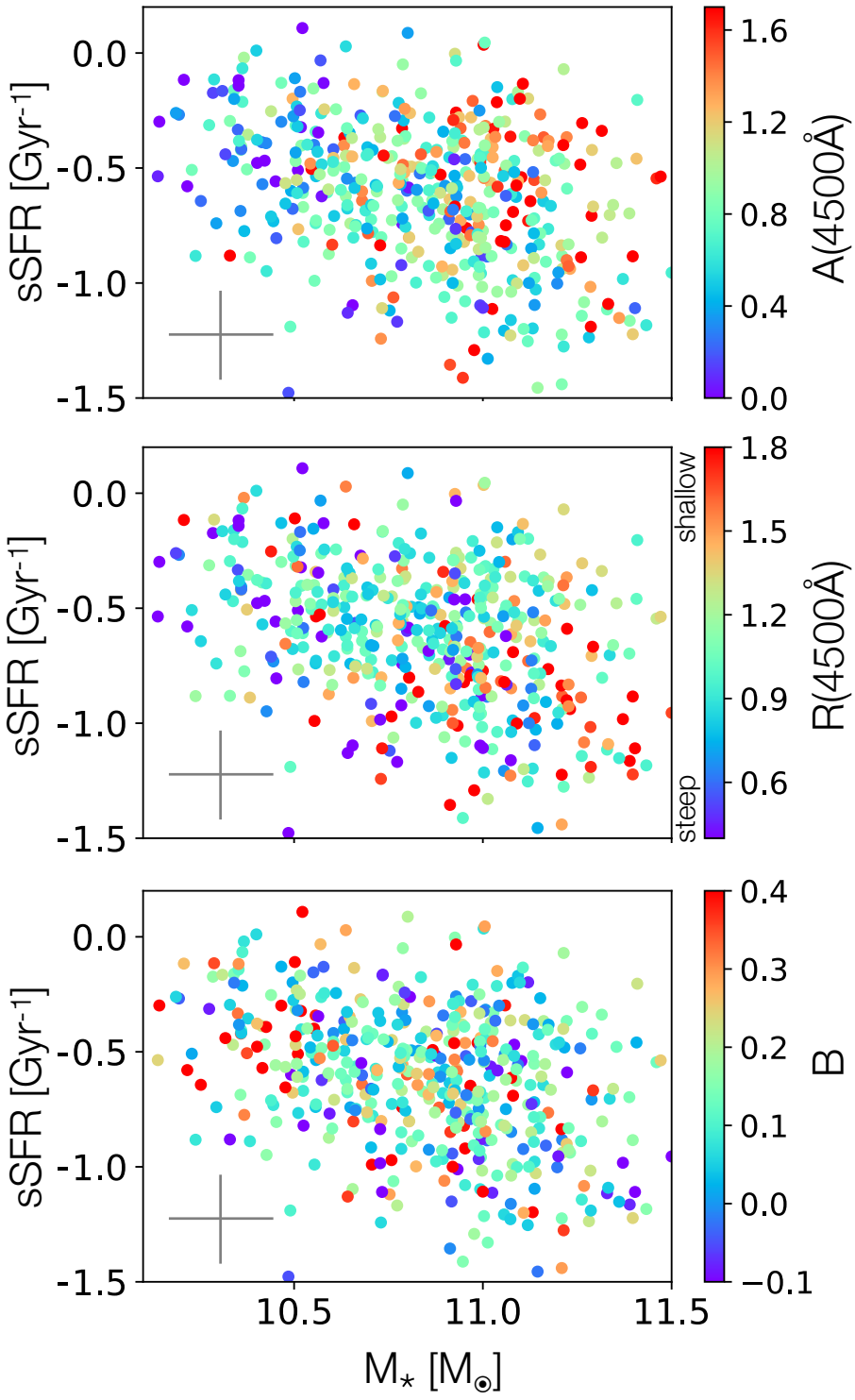

Figure 2.5 Specific star-formation rate (sSFR) vs. stellar mass M_* for star-forming galaxies color-coded by A(4500Å) (top panel), slope R(4500Å) (see Eq. 2.3; middle panel) and the UV bump strength B (see Eq. 2.2 bottom panel).

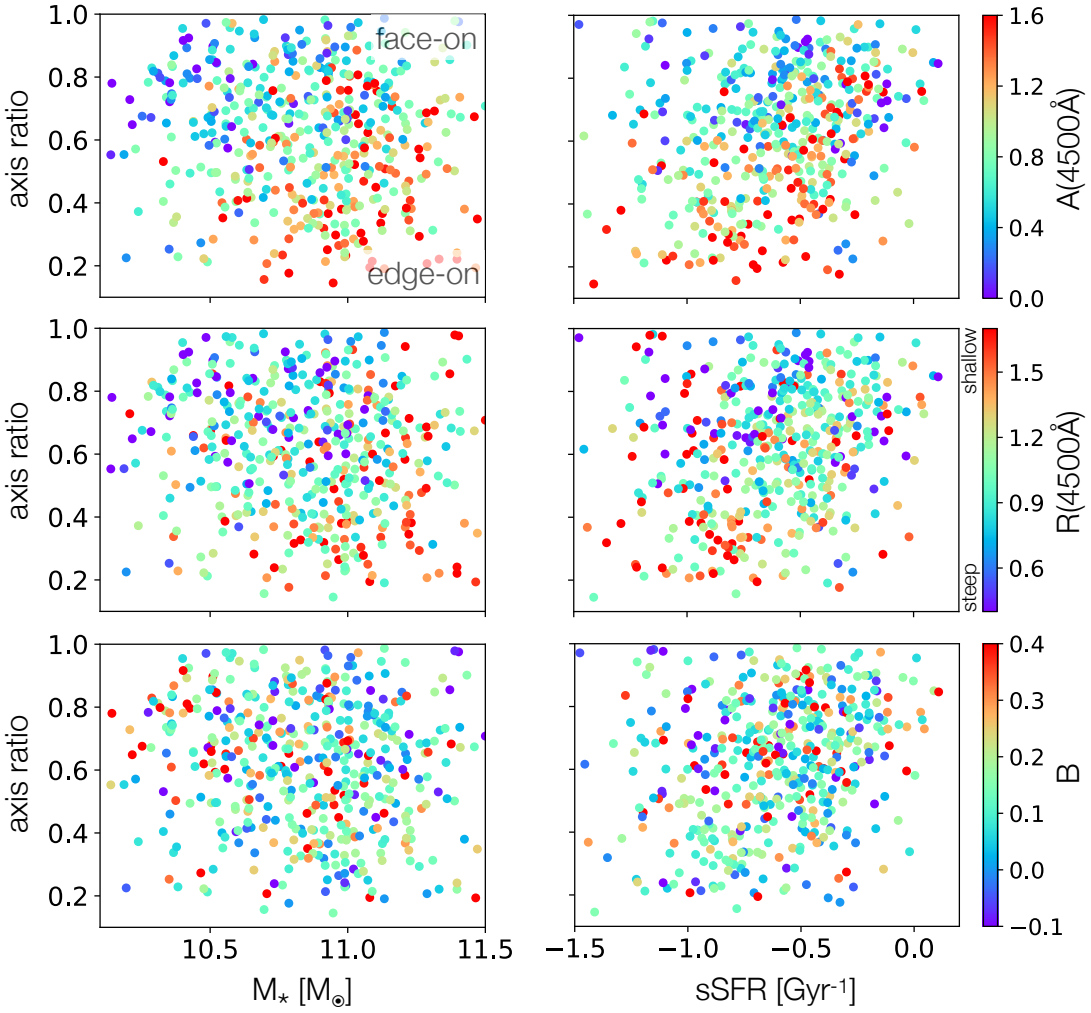

Figure 2.6 Axis ratio vs. stellar mass M_* (left panels) and specific star-formation rate (sSFR, right panels), color-coded by the attenuation at 4500Å (top panels), slope of the attenuation curve R(4500Å) (middle panels), and strength of the UV bump feature (bottom panels). Face-on galaxies are less attenuated compared to edge-on galaxies, and also tend to have steeper slopes than edge-on galaxies.

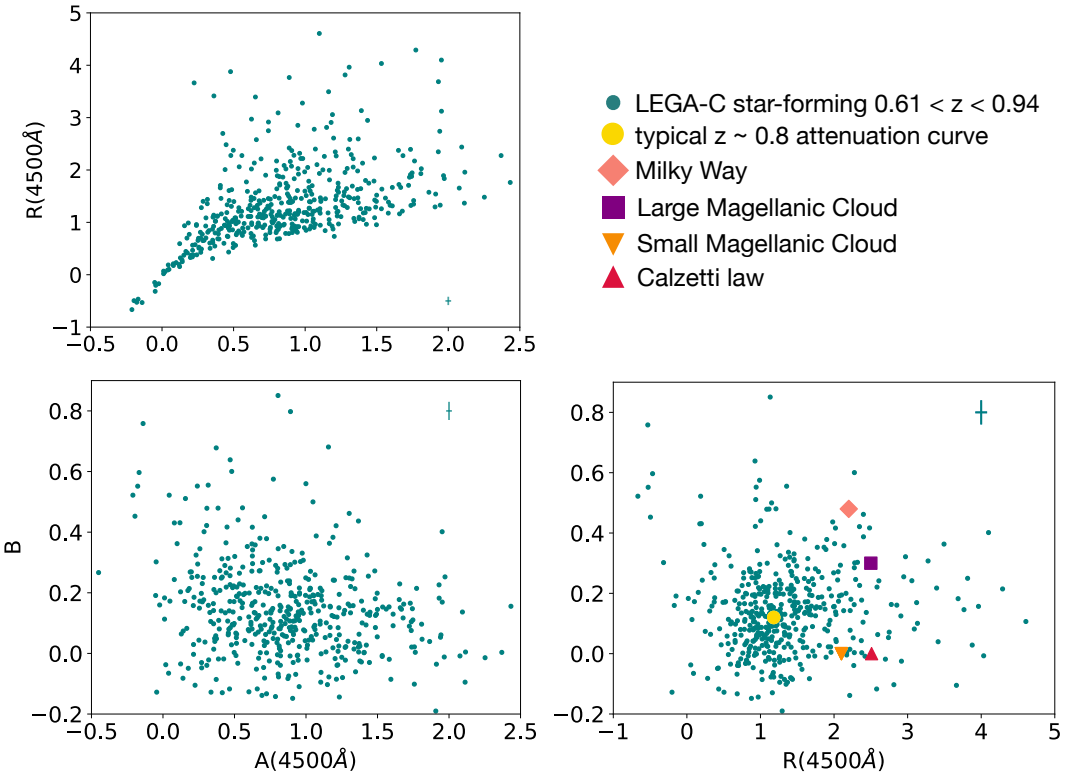

Figure 2.7 Attenuation curve features – attenuation A(4500Å), slope R(4500Å) and UV bump strength B, plotted against each other. Additionally, for comparison we also show slope and bump strength values for Milky Way, Large and Small Magellanic Clouds, translated to our parametrization. Even though left panels imply shallower slopes and weaker bump strengths with increased attenuation, there is no clear correlation between bump strength and the slope.

of young and old stellar population will also play a role. If embedded, young stars are always attenuated, including face-on viewing angle, while older stars only see increased attenuation when galaxies are viewed more edge-on. Thus, edge-on galaxies will have flatter global attenuation curves than face-on galaxies. Additionally, we also observe a possible indication of stronger UV bumps for low-mass galaxies, in qualitative agreement with Salim et al. (2018), which will be explored further in Section 2.3.4.

It is interesting to examine mutual dependence of the attenuation curve parameters A(4500Å), R(4500Å) and B (see Figure 2.7). Upper and bottom left panels imply possible flattening of the attenuation curve and, on average, weakening of the bump strength, as the attenuation increases. However, a possible correlation between the slope and the bump strength remains very challenging to recognize. It is worth noting that the linear-like behaviour (lower left corner in top left panel in Figure 2.7) is dominated by random error.

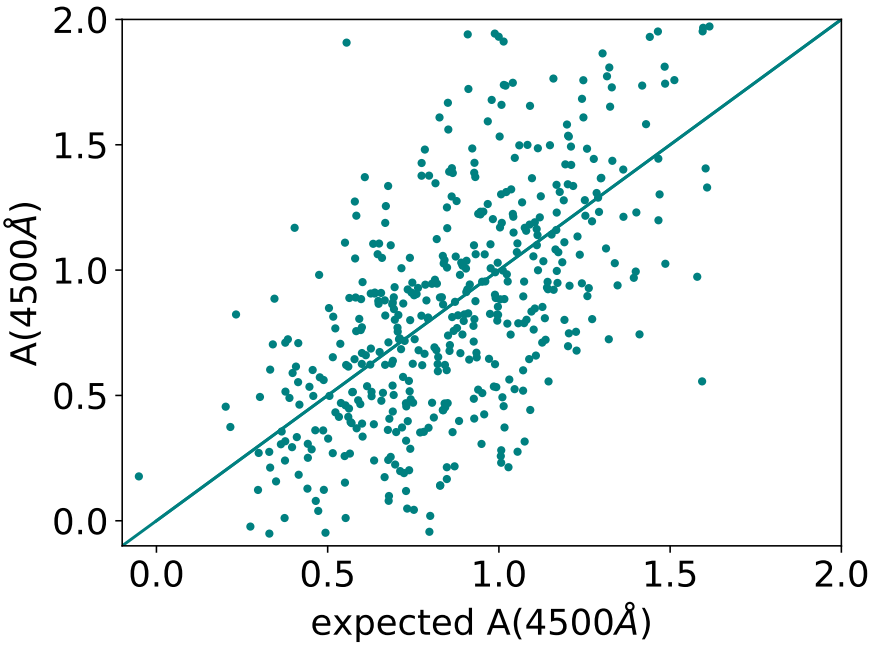

Figure 2.8 Expected attenuation A(4500Å) based on the prescription given in Section 2.3.3 as a function of the observed attenuation A(4500Å). The diagonal line presents just a one-to-one relation. A large residual scatter still remains.

2.3.3 Unexplained Scatter in Attenuation Properties

So far we explored the correlation between dust attenuation curve properties and global physical properties of galaxies. Here we explore how these correlations explain the observed variety in attenuation properties: do they account for most of the variation, or are there additional variables? To quantify this we perform a multiple linear regression to predict the attenuation at 4500$\mathring{A}$ using the following prescription:

$$A(4500\mathring{A}) = c_0 + c_1 \cdot \frac{b}{a} + c_2 \cdot \log_{10}(SFR) + c_3 \cdot \log_{10}(M_*)$$

and we find best fitting parameters: $\{c_0, c_1, c_2, c_3\}$ = {-2.963, -1.101, 0.315, 0.379}. In Figure 2.8 we show the expected attenuation as a function of the observed attenuation A(4500$\mathring{A}$). The standard deviation for the observed A(4500Å) is $\sigma = 0.5$. The standard deviation of the residual scatter after applying the prescription above is $\sigma = 0.4$, only somewhat reduced with respect to the observed scatter. This means that most of the variation in A(4500Å) is not accounted for by the known correlations with global galaxy properties. In terms of variance, 36% of the variation is produced by these correlations, while 64% is not accounted for.

It is worth noting that no significant contribution from other global physical properties was found – including redshift, galaxy age, size and other structural parameters. We note that the formal uncertainties on A(4500Å) are typically only $\sim$ 0.02, so the inferred intrinsic scatter is similar to the observed scatter of 0.28. The reason that the scatter remains relatively large might be due to underestimated measurement uncertainties as they are dependent on the spectral models and the

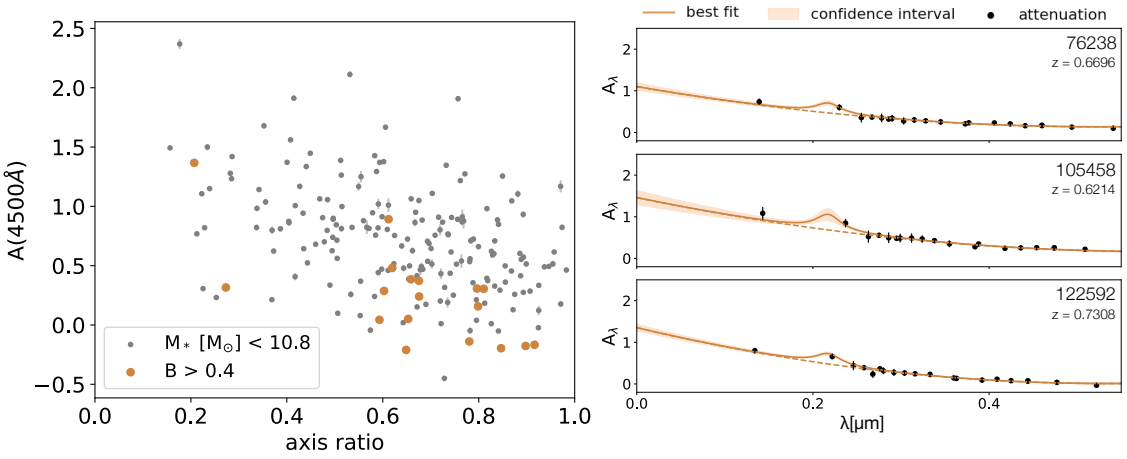

Figure 2.9 **Left**: Attenuation A(4500Å) as a function of axis ratio for a sub-sample of low stellar mass galaxies ($M_* < 10.5\ M_\odot$) (grey circles) with indicated galaxies with strong UV bump (orange circles). **Right:** Example attenuation curves for low stellar mass face-on galaxies with strong UV bump. A large residual scatter still remains.

possible existence of unknown systematics in the photometry. However, it is also clear that we do not have a complete understanding of which physical mechanisms drive the variation in attenuation. We speculate that short-term processes ($\sim 10^8$ yr) can randomize dust geometry and the distribution of young stars, which could play an important role.

2.3.4 Strong UV Bumps in Face-on Galaxies

At lower stellar mass values ($\log_{10}(M_*/M_\odot) < 10.8$) we see an increased number of low-attenuation, face-on galaxies with very strong UV bump values (see Fig 2.9); this is consistent with the idea that the UV bump is associated with small dust grains which mostly reside immediately around star-forming regions[6]. Why some galaxies show strong bumps and others do not – even if similar in all other properties – remains unclear.

Salim et al. (2018) found that a weaker UV bump feature is in general associated with shallower attenuation curve slope values. Moreover, even high redshift studies come to similar conclusions: specifically Kriek & Conroy (2013) find that their attenuated sub-sample of $A_V > 0.5$ galaxies shows stronger UV bump feature when the slope of the attenuation curve is steeper. We can not draw this conclusion directly from Figure 2.5 as a strong UV bump feature is in general not associated with particularly steep or shallow slope values. In general we do not see a clear trend between the UV bump strength and the slope. Given the uncertainties on the UV bump and slope measurement which are approximately the size of the scatter, it is difficult to draw conclusions regarding the existence of an underlying trend.

[6]One of the suggested carriers of the UV bump itself is due to the presence of amorphous hydrocarbon materials (e.g. Jones et al., 2013)

Even though the above mentioned studies have found evidence for a correlation between the slope of the attenuation curve and the bump strength, the most precise measurements (this work) do not find such a trend. It is unlikely that we can attribute the difference to the parametrization choice, given the agreement between some local based (e.g. Salim et al., 2018) and high-redshift based (e.g. Kriek & Conroy, 2013) studies in terms of trends between the slope of the attenuation curve and the strength of the UV bump – regardless of them applying mutually distinct modified Calzetti dust law parametrization. Even the high redshift low-resolution study based on individual galaxies by Tress et al. (2018) following higher order polynomial based parametrization (Conroy et al., 2010) find an indication of a similar dependence between the slope of the attenuation curve and the UV bump strength. On the other hand, a high redshift study by Buat et al. (2012), who apply the same modified Calzetti dust law parametrization as Noll et al. (2009) do not find any correlation between the slope of the attenuation curve and the UV bump strength. Similarly, Burgarella et al. (2005) finds no particular underlying trend between the slope of the attenuation curve and UV bump strength for their local galaxy samples.

Possible differences between our and other studies may emerge from the methods applied in deriving the attenuation. Determination of the attenuation at high redshift in past studies have originated from the SED fits based on the observed multi-band photometry (e.g. Buat et al., 2012) and often rely on stacks of the derived SEDs in order to achieve the equivalent-to low-resolution observed spectra (e.g. Kriek & Conroy, 2013). We note that these previous studies do not use high signal-to-noise spectroscopy to infer the underlying stellar continuum, which is a clear advantage of this study. The main caveat of our study is that we do not take into account any systematic uncertainties in the stellar population model used to model our spectra. Future work will include a systematic exploration of several stellar population models and the effect of that choice on the inferred attenuation.

2.4 Conclusion

We explore the attenuation curve diversity of individual star-forming galaxies at $0.61 < z < 0.94$. Our results are based, for the first time, on deep and high-resolution optical spectra. Using this unique information we provide a new attenuation curve prescription for $z \sim 0.8$ star-forming galaxies. Based on the broad agreement of our results with the results from Salim et al. (2018) on present-day galaxies we suggest that our new prescription (Equations 2.4 and 2.5) is generally more accurate than commonly adopted prescriptions (e.g. Calzetti et al., 2000; Cardelli et al., 1989) to model the integrated SEDs of galaxies. We show that these galaxies exhibit a wide variety of properties in terms of the slope of the attenuation curve R(4500Å) and strength of the UV bump feature. Since the significant amount of scatter in measured attenuation parameters (e.g. A(4500Å)) is not accounted for, we argue that we can not provide the attenuation curve prescription based on global galaxy parameters (M_*, SFR, and b/a).

We explore the dependence of the attenuation curve features on the galaxy orientation, stellar mass M_* and sSFR. In general, we observe steeper attenuation curve

slopes as compared to the MW, SMC and LMC, and even the Calzetti attenuation curve. We observe that the UV bump strength is weaker as compared to the MW bump strength value ($\sim$ 0.5). We see an increase in overall attenuation A(4500Å) with sSFR and stellar mass M_*, however, any underlying trend with the slope of the attenuation curve and the UV bump strength is very challenging to recognize. The strongest correlation we find is between the galaxy orientation and the overall attenuation and slope. We find that face-on galaxies are less attenuated and have a steeper slope – suggesting the geometry has a significant influence on the observed attenuation. Secondary correlations with stellar mass and star-formation rate can be attributed to the higher metallicities and dust masses of higher-mass, gas-rich galaxies. Additionally, we also observe an indication of a stronger bump feature in face-on low stellar mass M_* galaxies. Despite the systematic changes of dust attenuation with global galaxy properties and viewing angle, most of variations in attenuation are not accounted for. This implies that more subtle geometric effects and/or random factors such as patchiness of the young stellar populations and dust patterns dominate the attenuation.

Chapter 3

An Absence of Radio-loud Active Galactic Nuclei in Geometrically Flat Quiescent Galaxies: Implications for Maintenance-mode Feedback Models*

Maintenance-mode feedback, manifesting itself via radio-loud AGN, is thought to prevent star formation in passive galaxies. In this chapter, I explore the incidence of radio-loud AGN in geometrically round and flat quiescent galaxies, for a sample drawn from SDSS, FIRST and NVSS. I show that radio-loud AGN preferably occur in round quiescent galaxies. Since the majority of quiescent galaxies are relatively flat this result challenges the maintenance-mode feedback picture as a generally valid explanation for quiescence.

3.1 Introduction

To explain the mismatch between the theoretical dark matter halo mass function and the observed galaxy stellar mass function, semi-analytical and hydrodynamical simulations of galaxy formation and evolution have implemented a set of feedback mechanisms to reduce the efficiency of star-formation; they rely on supernova feedback in low halo mass systems, and super-massive black-hole (SMBH) feedback in systems with high mass halos (Croton et al., 2006; Bower et al., 2006; Fabian, 2012; Vogelsberger et al., 2014; Pillepich et al., 2017). The most common picture states that the SMBH feedback generally manifests through radio-loudness in active galactic nuclei (AGN) in the form of the jets ("radio-mode") or gas outflows ("quasar-mode") as a consequence of a low- or high-accretion rate (respectively) of

*The contents of this chapter are adapted from the refereed article Barišić et al. (2019) published in the Astrophysical Journal. I am the lead author of this paper, for which I have conducted research and analysis.

the gas onto the SMBH. This feedback picture states that powerful jets transfer their energy to the surrounding gas, heating it up and therefore preventing it from cooling and forming new stars. "Radio-mode" feedback has thus been introduced as the leading mechanism in explaining the mass growth deficiency in the most massive early type galaxies with SMBH.

Direct observational evidence for this picture in local galaxies comes from observations of cavities in the X-ray emitting gas caused by jets, connecting the presence of radio-loud (RL) AGN with the absence of star-formation (McNamara & Nulsen, 2007; Heckman & Best, 2014a). Indirect evidence in the local universe has also provided additional support to this radio-mode feedback picture (Matthews et al., 1964; Kauffmann et al., 2003b), including studies that show a strong, increasing trend in the RL fraction with M_* and stellar velocity dispersion σ_* (Best et al., 2005). According to the van den Bosch (2016) BH mass $-$ σ_* relation (see also Gebhardt et al., 2003; Beifiori et al., 2012), this implies an increasing trend of the RL fraction with the BH mass, suggesting the importance of the BH mass as a parameter in setting the probability for a galaxy to become RL (see also Häring & Rix, 2004; Terrazas et al., 2017).

In this Letter we explore how the incidence rate of RL AGN varies with geometric shape (flat or disk-like vs. round). We test this by examining the correlation of the RL fraction with σ_* and the projected axis ratio for a sample of galaxies drawn from the Sloan Digital Sky Survey (SDSS; York et al., 2000), NRAO VLA Sky Survey (NVSS; Condon et al., 1998) and Faint Images of the Radio Sky at Twenty centimeter (FIRST; Becker et al., 1995) survey, and we present evidence that round galaxies host RL AGN much more frequently than disk-like galaxies at any fixed σ_* and M_*. According to the 'radio-mode' feedback picture, and the association of the presence of RL AGN with quiescence, this raises a question to why are these galaxies not forming new stars in the absence of a visible heating source.

In Section 2 we give an overview of the data-set we use in this study, and in Section 3 we present or results and discuss the implications. In section 4 we give a brief summary of our main results. We use standard cosmology: $H_0 = 70$(km/s)/Mpc, $\Omega_M = 0.3$, $\Omega_\Lambda = 0.7$.

3.2 Data and sample selection

3.2.1 SDSS

The SDSS survey (York et al., 2000) provides unique and high quality information on various physical properties of a large number of present-day galaxies. Physical properties of those galaxies are measured and derived using photometry and spectroscopy, and include σ_*[1], star-formation rate (SFR), M_*, redshift and the projected axis ratio. The resolution of the spectroscopic data-set is $R = 1850 - 2200$, covering the wavelength range between 3800 Å to 9200 Å, with a minimum signal-to-noise

[1] http://classic.sdss.org/dr7/algorithms/veldisp.html

S/N $\sim$ 14 Å^{-1}.

In this Letter we make use of the SFRs and M_* obtained from modelling galaxy spectral energy distributions (SED; Chang et al., 2015) based on SDSS Data Release 7 (DR7; Abazajian et al., 2009) and WISE (Cutri et al., 2013).

In order to create a volume-selected sample (303,785[2]) complete in M_* we apply a redshift-dependent mass-cut: $\log(M_*) > 10.6 + 2.28\times\log(z/0.1))$ (Chang et al., 2015), consequently spanning a redshift range from $0.02 < z < 0.14$. For sample classification between star-forming and quiescent galaxies, we apply a color-based criteria following Chang et al. (2015) (u - $r > 1.6 \times (r$ - $z) + 1.1$) for quiescent galaxies. Star-forming galaxies are considered to be all other galaxies that fall outside of this color-based criteria.

3.2.2 NVSS and FIRST

The NVSS (Condon et al., 1998) 1.4 GHz sky survey north of $\delta = -40^o$ has been conducted in the period between 1993 and 1996. The angular resolution of the observed data-set is 45, with the noise level rms of 0.45 mJy beam^{-1} and the point source flux density 50% completeness level at 2.5 mJy. For more details see Condon et al. (1998). The FIRST (Becker et al., 1995) 1.4 GHz survey of the northern Galactic cap has been conducted in the period between 1993 and 2004. The average rms of the images is 0.15 mJy, with an angular resolution of 5 and the flux density limit of 1 mJy. Both surveys have been conducted using the Very Large Array (VLA) radio interferometer.

Taking advantage of the high resolution FIRST data-set, Best & Heckman (2012) cross-match sources with galaxies in the SDSS DR7. Flux density measurements are subsequently performed on the NVSS data-set. The resulting cross-matched catalog, with a limiting NVSS flux density value of 5 mJy, is complete for radio-loud AGN down to $L_{1.4GHz} \sim 10^{23}$ WHz^{-1} at $z = 0.1$. Since the sample is incomplete below $L_{1.4GHz} < 2.5 \times 10^{23}$ WHz^{-1} at highest redshifts, we apply a volume-correction that reaches at most a factor 4 for $L_{1.4GHz} \sim 10^{23}$ WHz^{-1} at z = 0.14.

3.2.3 Selection of Radio-Loud AGN Hosts

To select a radio-loud sub-sample we consider galaxies with detected radio emission at 1.4 GHz by the NVSS and FIRST. From the total number of galaxies in the selected galaxy sample, the number of those detected with $F_{1.4GHz} > 5$ mJy is 4,571, and they are shown with red and blue symbols in Figure 3.1.

We use Condon (1992) luminosity relation (α = - 0.8), to convert the NVSS measured flux density values $F_{1.4GHz}$ into luminosities. Derived luminosities at 1.4 GHz are then converted to radio-based SFRs using the Bell (2003) radio−far-infrared

[2]We removed 11058 galaxies (3.5%) that lack rest-frame u-, r-, and z-band photometry and a measurement of the axis ratio.

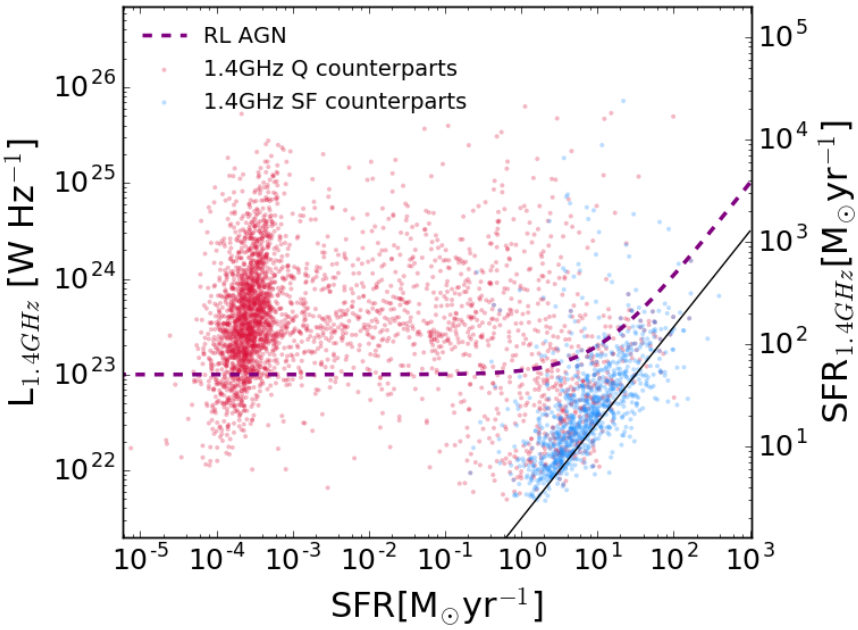

Figure 3.1 1.4 GHz luminosity vs. mid-IR SFR estimates (Chang et al., 2015) for quiescent (red) and star-forming (blue symbols) galaxies. Right-hand side y-axis converts the 1.4 GHz luminosity into SFR. All data points have a radio counterpart in the NVSS, and the purple line indicates selected radio-loud (RL) AGN. The selection reflects the minimum required AGN luminosity of 10^{23} WHz^{-1} and accounts for a contribution of star-formation (see text for details). The clump of galaxies at low SFR reflects the minimum SFR allowed in the SED model used by Chang et al. (2013) and has no physical meaning.

calibration.

We follow Best et al. (2005) 1.4 GHz luminosity limit $L_{1.4GHz} > 10^{23}$ WHz^{-1} to select radio-loud galaxies. We subtract the contribution of star-formation as follows: $L_{1.4GHz}$ - ($3 \times L_{1.4GHz,SFR}$) $> 10^{23}$, where $L_{1.4GHz}$ is the luminosity based on the 1.4 GHz flux density value, and $L_{1.4GHz,SFR}$ is the expected $L_{1.4GHz}$ luminosity based on the SFR (taken from Chang et al. (2015)). In order to select RL AGN with high confidence we multiply $L_{1.4GHz,SF}$ by a factor 3 to account for uncertainties in radio- and mid-IR based SFR estimates.

We keep the color-based classification from Chang et al. (2015) to separate the radio-detected sample between quiescent (red) and star-forming (blue symbols) galaxies. The selected radio-loud AGN sub-sample is indicated with the purple dashed line in Figure 3.1.

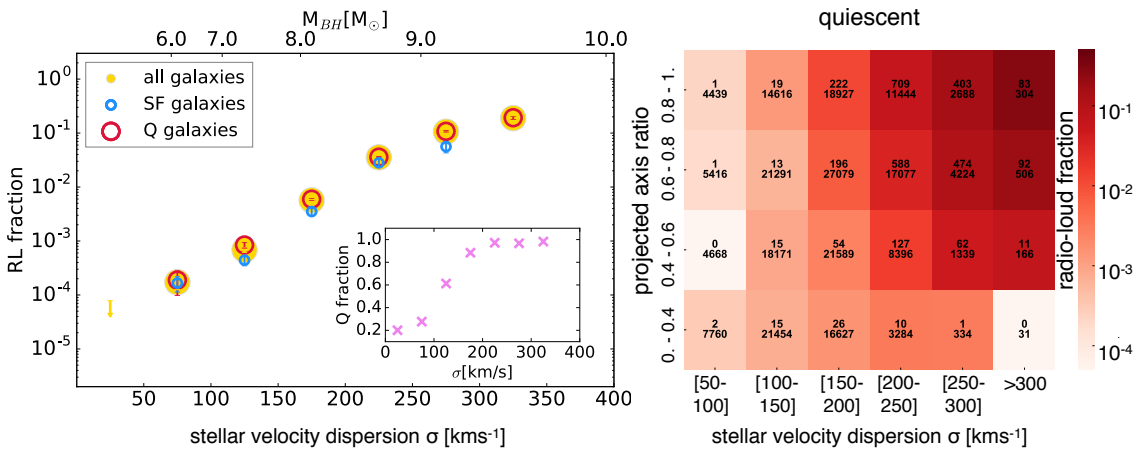

Figure 3.2 Left: RL fraction among all (yellow), quiescent (red empty) and star-forming (blue empty circles) galaxies as a function of the σ_*, (including Poissonian error bars) and derived BH masses van den Bosch (2016) on top. Yellow arrow centered at 25 kms^{-1} represents RL fraction upper limit. The RL fraction increases with the σ_* for both quiescent and star-forming galaxies. Violet crosses represent the fraction of quiescent galaxies among the total sample. Right: The heat-map of the observed axis ratio distribution as a function of the σ_* for quiescent galaxies, color-coded by the RL fraction. We see an increasing trend in the RL fraction with σ_* and with the projected axis ratio.

3.3 Which Parameters Correlate the Radio-Loud AGN Fraction?

In the following subsections we explore the RL fraction trend with the σ_* (or equivalently BH mass; van den Bosch, 2016) for all, quiescent and star-forming galaxies. We also explore the aspect of radio-loudness having a preference to occur more frequently among galaxies of a specific shape.

3.3.1 Radio-Loud AGN Fraction Increases with σ_*

It has been shown in the local universe that the RL fraction of massive elliptical galaxies exhibits a strong increasing trend with σ_* (Best et al., 2005). According to the BH mass$-\sigma_*$ relation (van den Bosch, 2016) this implies a strong dependence of the RL fraction on the BH mass. In Figure 3.2 (left panel) we show the fraction of quiescent galaxies in the selected sample (violet crosses), and the RL fraction among all (yellow circles), quiescent (red empty circles) and star-forming (blue empty circles) galaxies as a function of σ_* and the corresponding BH mass (van den Bosch, 2016). It is evident that the RL fraction exhibits an increasing trend with σ_*, which reproduces the result from Best et al. (2005).

Evidently, the RL fraction is increasing among star-forming galaxies as well, and these galaxies appear to host RL AGN as frequently as quiescent galaxies at fixed σ_* (i.e. Janssen et al., 2012). Since the star-forming galaxies host RL AGN at a comparable rate as the quiescent galaxies, then the radio-loudness is not a sufficient

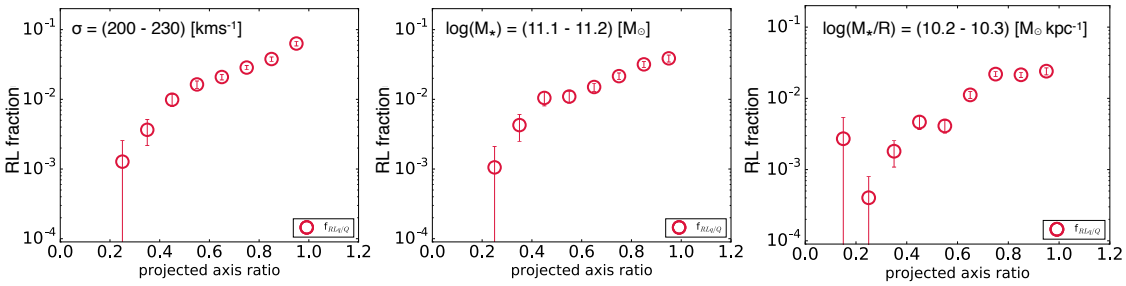

Figure 3.3 RL fraction among quiescent galaxies as a function of the projected axis ratio in the narrow bins of the σ_* (left), M_* (middle) and M_*/R as a σ_*^2 proxy (right panel). Radio-loud fraction exhibits and increasing trend with the observed axis ratio in all three panels.

condition for a galaxy to become quiescent.

3.3.2 Geometry Plays a Role in Radio-Loud Fraction

For the remainder of this Letter we only consider quiescent galaxies, as we are interested in constraining maintenance-mode feedback. We divide the sample into six evenly spaced bins of σ_* and four in the projected axis ratio. In each bin we determine the fraction of RL galaxies. The right panel of Figure 3.2 presents the heat-map of the projected axis ratio distribution as a function of σ_* for quiescent galaxies, color-coded by the fraction of RL galaxies. The top number inside of each bin corresponds to the number of RL galaxies, while the bottom number corresponds to the total number of galaxies. We observe that RL fraction among quiescent galaxies exhibits an increasing trend with both parameters – σ_* and the projected axis ratio.

This result illustrates that the important parameters in determining the probability for a galaxy to "switch on" as a RL AGN is not only its σ_* but also the geometry of the galaxy.

We note that the σ_* measurement for all but face-on galaxies is to a certain degree affected by contribution of the rotational velocity. Due to this effect, the actual σ_* should be lower for inclined galaxies, further suggesting lower RL fractions. Assuming that the M_* roughly corresponds to the virial mass, then the ratio between the galaxy M_* and its inclination-independent semi-major axis (half-light) radius R, can serve as a proxy for the intrinsic σ_* free of the rotational velocity effects, and independent on the inclination. Figure 3.3 shows the RL fraction trend with the projected axis ratio for quiescent galaxies, in narrow bins of the σ_* (left hand), M_* (middle) and the σ_* proxy $\log(M_*/R)$ (right panel). These trends are representative of the sample as a whole. The increasing trend in all three panels is likely dominated by a dependence of the RL fraction on the intrinsic shape of the galaxy, rather then its inclination. We note that replacing the semi-major axis radius with the inclination-independent circularized radius in estimating the σ_* proxy $\log(M_*/R)$ results in an even stronger trend than seen in the right panel of Figure 3.3. Therefore,

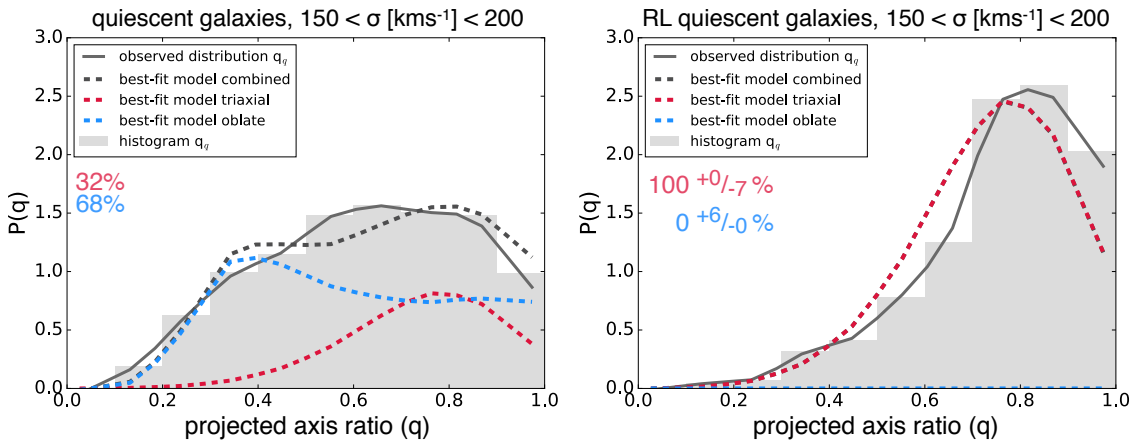

Figure 3.4 Normalized histogram of the observed axis ratio distribution (grey bins) for quiescent (left) and RL quiescent (right panel) galaxies and the function describing the observed axis ratio distribution (grey curve) in the σ_* bin $150 - 200$ kms^{-1}. We also show the best-fit two-component model probability distribution (black dashed curve), and the underlying triaxial (red dashed curve) and oblate (blue dashed curve) best-fit fractions.

correcting σ_* measurement of inclined galaxies for the rotational velocity effects would not significantly alter the increasing trend we see, which implies the preference for RL AGN to occur in round galaxies.

3.3.3 Radio-Loud AGN Fraction of Intrinsically Round and Flat Galaxies

Chang et al. (2013) developed a two-population model to reproduce the observed axis ratio distribution of quiescent galaxies up to $z = 2.5$, combining round (triaxial) and flat (oblate) populations of galaxies. They perform their modelling in three different mass bins, and to simplify the analysis we only use the fit parameters of the highest stellar mass bin ($M_* > 10.8$) [3] where the intrinsic axis ratio of the oblate component is b[4] = 0.29±0.07. The best-fit triaxility (T[5] = 0.64±0.06) and ellipticity (E[6] = 0.41±0.02) parameter values, and their standard deviations (σ_T, σ_E = 0.08±0.05, 0.19±0.02) are used to generate distributions of intrinsic intermediate-to-long axis ratio β and short-to-long axis ratio γ. Combining these distributions with random viewing angles provide us with model triaxial and oblate intrinsic axis ratio distributions.

We split the sample of quiescent galaxies into six equally spaced σ_* bins, and in each bin we find the best-fit linear combination of model triaxial and oblate shape distributions which reproduce the observed axis ratio distribution. This gives us the triaxial and oblate fraction of galaxies in the specific σ_* bin. As an example, in

[3] This mass limit corresponds to a σ_* limit of $\sim$ 120km s^{-1}, but even below this limit the shape parameters are not very different and our analysis would not be affected.

[4] b = intermediate axis of the triaxial ellipsoid

[5] T = [1 - β^2]/[1 - γ^2]

[6] E = 1 - γ

Figure 3.4 we show a normalized histogram (gray bins) of the observed axis ratio (q) distribution, and a corresponding function describing the distribution obtained after binning, for quiescent (left panel) and for RL quiescent (right panel) galaxies in the range of σ_* values from 150 - 200 km s^{-1}. For illustration, we choose the σ_* bin in which the total population is similarly populated by both triaxial and oblate galaxies according to the two-population model. Blue and red dashed curves represent best-fit oblate and triaxial fractions, respectively. We see that the triaxial fraction ($100 \pm ^{0}_{7}\%$) of RL AGN in the observed quiescent population in this σ_* bin completely dominates over the oblate fraction, implying a more frequent occurrence of RL AGN among round galaxies.

The best-fit model triaxial and oblate fraction for the observed axis ratio distribution of quiescent galaxies can be rescaled to fit the observed axis ratio distribution of RL quiescent galaxies. Multiplying these rescaling factors by the RL fraction gives the RL fraction among triaxial and oblate galaxies.

Figure 3.5 shows the RL fraction among triaxial (red filled squares) and oblate (red open squares) galaxies for quiescent population as a function of the σ_*. The overall triaxial fraction (black crosses) increases with the σ_*. The increase in RL fraction with σ_* is entirely due to its increase among the triaxial population. In fact, the inferred RL fraction among oblate population is essentially zero. This analysis, by accounting for round (face-on) disk-like galaxies, further strengthens our result that RL AGN preferentially reside in intrinsically round galaxies. We note that we do not claim that the RL fraction among disk-like quiescent galaxies is, in fact, zero; the triaxial population is defined to consist of objects with a wide range in intrinsic β and γ values (see above), including a subset with $\beta \sim 1$ and small γ, that is, disk-like geometries.

3.3.4 Satellites, Centrals and Halo Mass

We now investigate whether the correlation between the shape and RL fraction is driven by an underlying connection between dark matter halo properties and RL AGN. This may be expected in case disk-like galaxies live in less massive halos than round galaxies, or if satellite galaxies, which are more often disk-like than centrals (Van der Wel et al., 2010), are less likely to be RL AGN.

We cross-match our sample with the SDSS DR7 based "petroC"[7] group catalog created by Yang et al. (2007). For this halo catalog, centrals are chosen based on stellar mass, and halo masses are assigned to groups based on their total stellar mass. We focus on quiescent galaxies with $200 < \sigma_*/(\text{km s}^{-1}) < 230$, which shows a strong correlation between the shape and RL AGN incidence, and for which the satellite fraction is non-neglible ($\sim 20\%$, Van Den Bosch et al., 2008). We find that RL fractions are similar: 2.3% for the satellites, and 2.8% for the centrals, and their trends with galaxy shape are consistent with each other. There is no substantial difference (<0.15 dex) between the halo masses of round central galaxies and flat central galaxies, and selecting galaxies by halo mass still contains a strong correla-

[7] http://gax.sjtu.edu.cn/data/Group.html

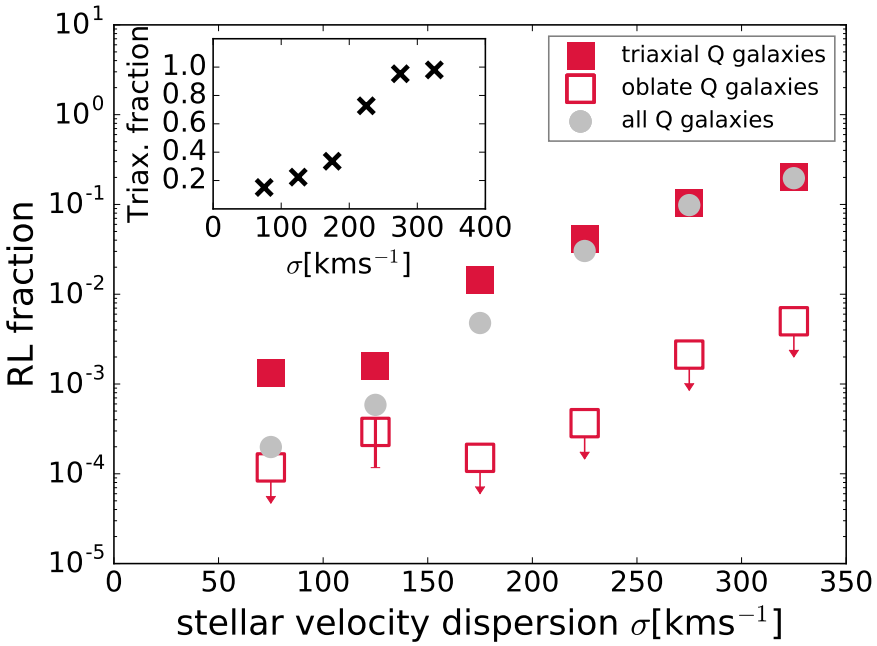

Figure 3.5 The RL fraction among triaxial (red squares) and oblate (open red squares) galaxies as a function of the σ_* for quiescent galaxies. The RL fraction is higher among triaxial galaxies. The plot also shows the RL fraction among quiescent galaxies (grey circles), and the best-fit triaxial fraction (black crosses).

tion between RL AGN fraction and galaxy shape.

We conclude that the strong dependence of RL AGN incidence on galaxy shape is intrinsic and cannot be explained by differences between RL AGN fractions in satellite and central galaxies, nor to differences in halo mass.

3.4 Discussion

In this Letter we demonstrate that RL AGN occur more frequently in round than in flat quiescent galaxies at any M_* or σ_*. The analysis of the projected axis ratio distribution of RL AGN hosted by quiescent galaxies shows that the increased RL fraction at higher σ_* values is entirely driven by intrinsically round (triaxial) galaxies. The RL fraction reaches $\sim$20% for the most massive, round quiescent galaxies (σ_* $\sim$300 km s^{-1}), whereas geometrically flat (disk-like) quiescent galaxies have an extremely low RL AGN fraction ($< \sim 10^{-3}$), even at high σ_* (>200 km s^{-1}).

This result is consistent with the common notion that luminous radio AGN reside in massive, elliptical galaxies. However, thus far, the correlation between the RL AGN occurrence in quiescent galaxies and a second global property, besides its σ_* (BH mass), has not been explicitly demonstrated. The roundness of a galaxy likely reflects its merger history, and the connection between an active merger history and the occurrence of low-accretion rate radio AGN has been made by many authors (De Ruiter et al., 2005; Capetti & Balmaverde, 2006; Sikora et al., 2007;

Fanidakis et al., 2010). The physical basis for this connection has been referred to as the "spin paradigm" (Blandford & Znajek, 1977; Wilson & Colbert, 1995; Hughes & Blandford, 2003; McKinney & Gammie, 2004) in which only BHs with large spin parameters can launch radio jets. In turn, a large spin parameter is the result of BH-BH mergers that reflect the merger history of the host galaxy.

Regardless of the physical explanation, the lack of RL AGN in disk-like quiescent galaxies raises important questions. In galaxy formation and evolution models, low-accretion rate AGN are universally assumed to play a crucial role in preventing excessive SF in massive galaxies, independent of their structure. Our findings suggest that, if this model is generally valid, the AGN feedback does not manifest itself at radio wavelengths for galaxies with disk-like structures. We conclude that there is compelling evidence for maintenance-mode feedback for intrinsically round galaxies, but that further study is needed to bolster the evidence for such feedback as a general explanation for the lack of star-formation activity in massive galaxies.

Chapter 4

Stellar Dynamics and Star Formation Histories of z ∼ 1 Radio-loud Galaxies*

The exploration of the maintenance-mode feedback picture is extended to z ∼ 1 and is based on a sample of radio-loud AGN constructed from the combination of the spectroscopic LEGA-C survey and the VLA-COSMOS 3 GHz data-sets. In this chapter I show that, at this lookback time, radio-loud AGN preferentially reside in round galaxies with old stellar populations and large stellar velocity dispersion values, which goes in support of the maintenance mode feedback picture.

4.1 Introduction

To match the stellar and dark matter halo mass functions and reproduce their evolution through cosmic time, semi-analytical and hydrodynamical galaxy formation models rely on two primary feedback channels to decrease the efficiency of star-formation. These models implement heating by supernovae that lead to a low star-formation efficiency in low-mass dark matter halos (White & Rees, 1978; White & Frenk, 1991; Hopkins et al., 2012). Feedback from super-massive black holes (SMBHs) is implemented to prevent excessive star-formation in high-mass halos (De Lucia & Blaizot, 2007; Croton et al., 2006; Bower et al., 2006; Vogelsberger et al., 2014; Schaye et al., 2015). The physical prescriptions differentiate between radiative-mode feedback and jet-mode feedback. Radiative-mode feedback ('quasar mode') is associated with the high accretion rate of the cold gas onto the SMBH and is related to the gas outflows (Shakura & Sunyaev, 1973; Di Matteo et al., 2005). Jet-mode ('radio mode') feedback is associated with a low accretion rate of hot ('coronal') gas onto the SMBH. The feedback loop is thought to exist between the cooling of hot gas that feeds the SMBH (e.g., Blanton et al., 2001) to trigger

*The contents of this chapter are adapted from the refereed article Barišić et al. (2017b) published in the Astrophysical Journal. I am the lead author of this paper, for which I have conducted research and analysis.

an active galactic nuclei (AGN) phase that subsequently provides a heating source, counter-acting cooling and preventing further growth in stellar mass.

Direct observational evidence for a link between AGN and the heating of halo gas is found in massive clusters, where radio jets are seen to produce cavities in the X-ray emitting gas (see McNamara & Nulsen, 2007; Heckman & Best, 2014b, and references therein) and also in early-type galaxies in lower-mass groups where the presence of cold gas and radio jets is linked to the thermodynamical state of the warm/hot gas (Werner et al., 2012, 2014). Furthermore, indirect evidence in the form of a strong correlation between a lack of star formation (quiescence) and the presence of radio AGN has been gathered for galaxies in the local universe (e.g., Matthews et al., 1964; Kauffmann et al., 2003b; Best et al., 2005). This correlation suggests that massive galaxies spend extended periods in a radio-loud AGN phase, which provides sufficient energy to keep the halo gas from cooling.

Until recently, radio observations of high-redshift galaxies were limited to the very highest luminosities ($L > 10^{24}\,W\,Hz^{-1}$), where radio AGN hosts are the most extreme galaxies: brightest cluster galaxies, but also star-bursting galaxies (De Breuck et al., 2002; Willott et al., 2003). Deep surveys with the Karl G. Jansky Very Large Array (VLA) are now probing lower luminosities ($L \gtrsim 10^{22}\,W\,Hz^{-1}$), enabling us to explore the link between radio AGN and quiescence at large look-back time. Donoso et al. (2009) showed that the fraction of radio-loud galaxies increases out to $z \sim 1$, and that its power-law dependence on stellar mass ($f_{radio-loud} \propto M_*^{2.5}$) is consistent with what is seen for present-day galaxies (Best et al., 2005). Simpson et al. (2013) demonstrate that up to $z \sim 1$ radio AGN preferentially reside in galaxies with evolved stellar populations as traced by the $D_n(4000)$ index. Rees et al. (2016) confirm these results, but show that at $z > 1$ radio AGN are hosted more frequently by star-forming galaxies. Finally, Williams & Röttgering (2015) demonstrate that the fraction of radio-loud AGN of luminosities $> 10^{24}\,W\,Hz^{-1}$ increases out to $z = 2$, that the power-law mass dependence becomes flatter with the increasing mass, and that the slope of mass dependence becomes shallower with the increasing redshift.

In this study we use deep, rest-frame optical spectra from the Large Early Galaxy Astrophysics Census (LEGA-C) survey of galaxies in the redshift range $0.6 < z < 1$ (van der Wel et al., 2016). The LEGA-C optical spectra provide us for the first time with direct constraints on recent and long-term star-formation histories and stellar dynamical properties of a large sample of galaxies at large look-back time. Cross-matching the LEGA-C sample with the recently completed 3 GHz VLA survey (Smolcic et al., 2017) allows us to examine for the first time stellar populations and velocity dispersions of intermediate luminosity radio-loud AGN at these redshifts. The aim of this paper is to test the hypothesis that radio-loud AGN preferably occur in quiescent galaxies with large velocity dispersions (black hole masses) over a broad range in cosmic time. The confirmation of this hitherto poorly constrained assumption is crucial for the radio-mode feedback picture.

This paper is organized as follows. In Section 2 we give an overview of LEGA-C and VLA datasets, and introduce the selection criteria and classification scheme for

the radio-loud sub-sample. We present our main results and describe stellar content and star-formation activity of radio-loud AGN in Section 3. A summary of our work is then given in Section 4.

4.2 Data, Sample Selection and Classification

In this section we give an overview of the data sets analysed in this work. We present the criteria adopted for the selection of the radio-loud sub-sample among the whole LEGA-C sample, and we describe the method used to classify the radio-loud galaxies into quiescent and star-forming galaxies. By comparing with local benchmark samples we also measure the evolution of the fraction of radio-loud galaxies out to z ∼ 1.

4.2.1 LEGA-C

The LEGA-C survey (van der Wel et al., 2016) is an ESO public spectroscopic survey with VLT/VIMOS (LeFevre et al., 2003) with the aim of obtaining high signal-to-noise ratio (S/N ∼ 20 Å^{-1}) continuum spectra of $0.6 < z < 1$ galaxies. The full LEGA-C sample will consist of more than 3000 galaxies, K-band selected from the Muzzin et al. (2013) UltraVISTA survey in the 1.62 square degree region within the COSMOS field (Scoville et al., 2007). The spectral resolution is $R = 2500$, spanning the wavelength range from 6300 Å to 8800 Å. The current paper uses the Data Release II [1] sample of 1989 galaxies observed during the first two years of LEGA-C observations. This sample is representative of the final sample, which is, in turn, representative of the galaxy population at a given K-band flux density. That is, our sample selection is independent of galaxy color and morphology.

In this study we use redshifts, stellar velocity dispersions, $D_n(4000)$ break and Hδ absorption indices, nebular emission line equivalent widths, as well as physical parameters estimated from broad-band photometry (UV+IR star formation rates (SFR) and stellar masses). UV and IR luminosity based SFRs are estimated following Whitaker et al. (2012b). Stellar masses are derived using a Chabrier (2003) Initial Mass Function, Calzetti et al. (2000) dust extinction, and using Bruzual & Charlot (2003) stellar population libraries and exponentially declining SFR. For further details on the data reduction steps and the method used to derive the physical parameters we refer to van der Wel et al. (2016).

4.2.2 VLA - COSMOS

We use the observations at 3 GHz (10 cm) (PI: Vernesa Smolčić) covering the 2 square degree COSMOS field, obtained by the VLA radio interferometer. The observations were conducted between 2012 and 2014, with a total observation time of 384 hours, yielding a final mosaic with the angular resolution of 0.75" and a median rms of 2.3 μJy beam^{-1}. For further details we refer to Smolcic et al. (2017).

[1] http://www.eso.org/qi/

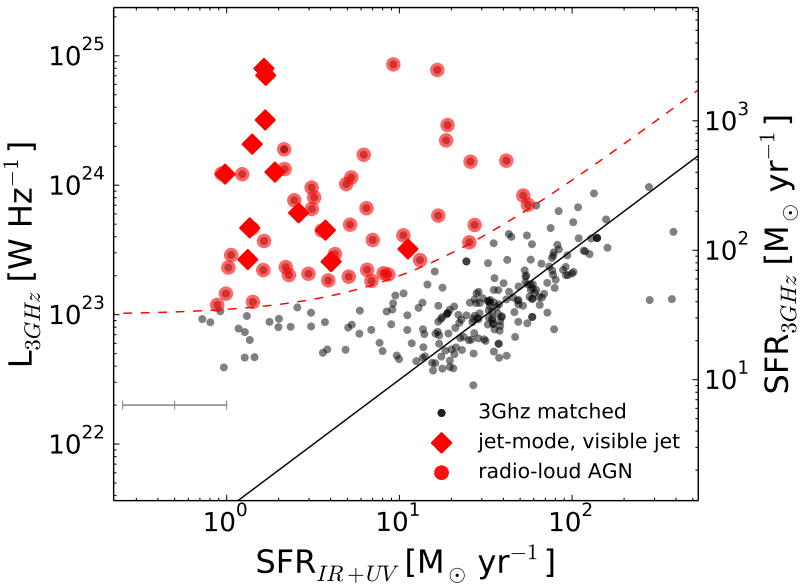

Figure 4.1 The 3 GHz radio luminosity (left-hand y-axis) and implied SFR (right-hand y-axis) versus SFR_{UV+IR} for the LEGA-C + VLA cross-matched sample. Red points meet our luminosity criteria for radio-loud AGN, red diamonds have visible jets in the radio image. Grey error bar represents the typical uncertainty of the SFR_{UV+IR}. The y-axis uncertainties for radio-loud AGN are smaller than the size of the data points.

4.2.3 Selection of radio-loud AGN

The current LEGA-C dataset contains 1989 galaxies, out of which 322 are found to have a radio counterpart after cross-matching the LEGA-C survey catalog and the VLA 3 GHz 5.5 σ catalog (Smolcic et al., 2017). The matching radius between LEGA-C and VLA coordinates is 0.7". The systematic offset in right ascension and declination is 0.1" and 0.03" respectively, while the random offset is 0.1". We convert radio continuum fluxes for cross-matched sources to luminosities, using VLA 3 GHz flux densities and LEGA-C spectroscopic redshifts, following the Condon (1992) luminosity relation. Implied radio-based star formation rates are then found from luminosities using Bell (2003) calibration of the radio-FIR correlation.

Figure 4.1 compares the radio luminosity, L_{3GHz} (and the corresponding star-formation rate) with the UV+IR-based SFR for this cross-matched sample. The good correspondence between the star-formation rate indicators is by construction, as the radio-based SFR is calibrated with the SFR derived from the IR luminosity. We see no evidence for a change in the far-infrared to radio luminosity ratio q, but this is not inconsistent with the evidence for such evolution (Magnelli et al., 2015; Delhaize et al., 2017) obtained from larger samples across a much larger redshift range than $z = 0$ to $z = 1$.

Of interest for this study are the sources that are outliers from the one-to-one relation (black line), that is, the sources with excessive radio luminosities. We

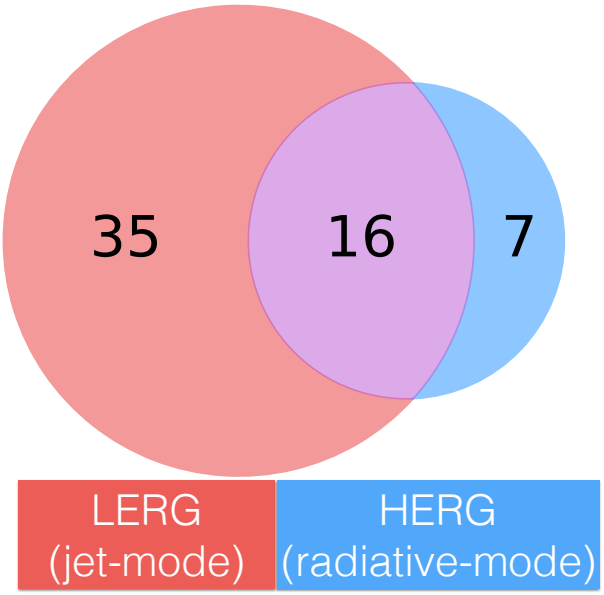

Figure 4.2 Classification of galaxies on jet-mode / radiative-mode based on the ratio of optical emission lines [OIII]/Hβ and [OII]/Hβ (see Section 4.2.4 for details).

estimate the radio AGN luminosity by subtracting 3× the radio luminosity expected on the basis of the UV+IR-based SFR from the observed radio luminosity. That is, we allow for a factor 3 scatter in the radio-SFR relation. Adopting the radio luminosity limit from Best et al. (2005), we select those 58 galaxies with radio AGN luminosities $> 10^{23}\,\mathrm{W\,Hz^{-1}}$ as our radio-loud AGN sample (see Figure 4.1, red dashed curve).

4.2.4 Classification of the radio-loud objects

We examine the optical spectra of the 58 radio-loud AGN in order to distinguish between jet-mode (low-excitation radio galaxy, LERG) and radiative-mode (high-excitation radio galaxy, HERG) based on the presence or absence of strong high-excitation emission lines (Hine & Longair, 1979; Laing, 1994). We classify a radio galaxy as a LERG if there are no or only low-excitation (Balmer) emission lines (EW([OIII], [OII], [Hβ]) > -5 Å). For systems with strong emission lines we classify those with high [OIII]λ5007/Hβ and/or [OII]λ3727/Hβ ratios (> 1) as HERGs. In our sample of 58 radio-loud AGN, 35 are classified as LERGs and 7 as HERG with high confidence. The classification of 16 objects remains undetermined, as we were not able to discriminate with high confidence between jet/radiative-mode. For the remainder of this paper we consider these objects as LERG with 50% probability for the purpose of statistical calculations. In Figure 4.2 we summarize the results of our classification, which illustrates that almost 60% of our sample are LERGs. We list the properties of the 58 radio AGN in Table 4.1.

We examine the VLA 3 GHz images of our sample for visual confirmation of radio jets. Forty six radio-loud galaxies are consistent with point sources, but in 12 cases we identify extended morphologies. We show the VLA 3 GHz and HST F814W images as well as the LEGA-C spectra of these 12 objects in Figure 4.3.

4.3 Properties of $z \sim 1$ jet-mode galaxies

4.3.1 Fraction of jet-mode galaxies

Using the selection criteria defined in Section 4.2.4, we determine the fraction of jet-mode radio galaxies in the LEGA-C sample, considering both star-forming and quiescent galaxies (see Figure 4.4). Since we adopt the radio-loud AGN selection criteria from Best et al. (2005), we compare our fraction of jet-mode galaxies at a redshift range $0.6 < z < 1$ to their fraction of jet-mode galaxies for present-day galaxies. At fixed mass the fraction of jet-mode galaxies is on average 5 - 10 times higher at $0.6 < z < 1$ compared to the present-day universe. Furthermore, we notice the flattening of the power-law mass dependence for the highest mass bin. These findings are consistent with the measurements from Donoso et al. (2009).

Table 4.1: Physical properties of the observed sub-sample of radio-loud galaxies

ID	R.A.	Dec.	z_{spec}	L[10^{23}WHz^{-1}]	$\alpha_3^{1.4}$ [a]	d [kpc] [b]	flag [c]
126578	150.09805	2.281367	0.750	2.89 ± 0.18	-0.46 ± 0.14		1
140050	150.14168	2.446062	0.899	8.04 ± 0.42	-0.03 ± 0.11		0.5
209637	150.10378	2.507702	0.608	3.21 ± 0.17	-0.93 ± 0.19	17.69 ± 5.10	0
131063	150.35016	2.334642	0.667	12.27 ± 0.63	-0.41 ± 0.09		1
182797	150.39577	2.481532	0.903	2.22 ± 0.17	< -0.42		1
184916	150.42589	2.513884	0.679	6.11 ± 0.33	< 1.77	50.00 ± 5.36	1
185625	150.42506	2.524558	0.984	1.83 ± 0.18	< -0.89		0.5
210716	150.17261	2.523343	0.69	12.21 ± 0.60	-0.80 ± 0.08		1
106926	150.29488	2.034494	0.955	77.68 ± 3.91	1.02 ± 0.09		0.5
108227	150.26643	2.049850	0.960	7.07 ± 0.39	-0.41 ± 0.31		0.5
109352	150.10892	2.063952	0.724	4.96 ± 0.28	$-0.49^{+0.16}_{-0.17}$		1
110509	150.26849	2.077003	0.667	6.64 ± 0.34	-0.06 ± 0.14		1
110805	150.17149	2.084074	0.729	3.77 ± 0.20	$-0.82^{+0.16}_{-0.17}$		0.5
113394	150.35657	2.117532	0.875	2.02 ± 0.16	< -0.48		1
128311	150.05669	2.301382	0.730	4.49 ± 0.24	-0.50 ± 0.28	19.12 ± 5.52	1
129746	150.02608	2.318864	0.941	3.40 ± 0.24	< 0.13		0.5
205180	150.00731	2.453467	0.730	18.94 ± 0.96	$-0.43^{+0.07}_{-0.08}$		1
209377	150.02267	2.508070	0.746	85.76 ± 4.47	-0.79 ± 0.07		0
210031	150.02242	2.516584	0.679	5.82 ± 0.29	-0.93 ± 0.13		0
210739	150.00941	2.526713	0.733	4.09 ± 0.24	-0.49 ± 0.25		1
234067	149.85017	2.452237	0.714	29.15 ± 1.48	-0.35 ± 0.07		1
236682	149.87180	2.479084	0.734	20.77 ± 1.04	-0.78 ± 0.07	95.81 ± 5.53	1
236994	149.86151	2.484360	0.730	2.57 ± 0.16	-0.65 ± 0.29	109.57 ± 5.52	1
129631	149.98328	2.317157	0.934	9.60 ± 0.49	-0.61 ± 0.16		0.5
131657	149.95264	2.341849	0.945	2.33 ± 0.19	-1.06 ± 0.20		1
169076	149.78040	2.318275	0.677	1.96 ± 0.12	-0.43 ± 0.17		1
169901	149.79379	2.327209	0.893	2.64 ± 0.19	< -0.23		0
210564	149.91573	2.521326	0.729	6.55 ± 0.35	-0.47 ± 0.14		1
235394	149.76112	2.460729	0.671	4.92 ± 0.25	$0.09^{+0.28}_{-0.29}$		1
235431	149.78880	2.466439	0.732	1.19 ± 0.11	< -0.61		0.5
237437	149.79221	2.489063	0.734	1.25 ± 0.11	< -0.56		1
111543	149.91492	2.094372	0.884	2.09 ± 0.17	<-0.54		0.5
113852	150.01424	2.123182	0.675	31.92 ± 1.59	-0.47 ± 0.07	35.63 ± 5.34	1
125257	150.06847	2.265479	0.979	3.62 ± 0.25	< -0.04		0.5
147270	149.87502	2.062635	0.847	12.63 ± 0.65	-1.28 ± 0.07	51.16 ± 5.81	1

151161	149.89481	2.109374	0.666	7.65 ± 0.43	-0.004 ± 0.14		1
161004	149.83919	2.226176	0.943	4.68 ± 0.28	-0.82 ± 0.32	24.00 ± 6.00	0.5
105328	149.90935	2.013062	0.848	1.84 ± 0.15	< -0.45		1
117992	149.94199	2.173145	0.688	2.31 ± 0.14	-0.28 ± 0.32		1
120120	149.99265	2.202235	0.629	2.21 ± 0.13	$-0.59^{+0.27}_{-0.25}$		1
157229	149.74300	2.179562	0.631	15.21 ± 0.75	-0.64 ± 0.08		0.5
212718	150.07712	2.548955	0.890	70.58 ± 0.62	< -1.03	247.90 ± 5.84	1
203666	150.39935	2.794159	0.822	8.33 ± 0.43	-0.95 ± 0.19		0.5
215835	150.24612	2.585822	0.675	10.21 ± 0.53	0.34 ± 0.15		0.5
217020	150.16193	2.601267	0.893	2.07 ± 0.18	< -0.55		1
218725	150.04684	2.620396	0.736	2.94 ± 0.18	-1.03 ± 0.11		0
232020	150.01646	2.784381	0.983	15.48 ± 0.78	-0.69 ± 0.17		0.5
232196	149.98419	2.787762	0.853	4.63 ± 0.28	-0.96 ± 0.33		0.5
245325	149.88518	2.581121	0.694	4.47 ± 0.24	-0.13 ± 0.11		1
94215	150.68156	2.324819	0.978	2.04 ± 0.20	< -0.81		0
94982	150.63631	2.333361	0.609	11.47 ± 0.63	-0.32 ± 0.09		1
96860	150.66121	2.364529	0.826	79.72 ± 0.52	< -1.03	150.99 ± 5.77	1
182890	150.61380	2.484840	0.744	1.45 ± 0.11	< -0.41		1
183927	150.61508	2.500369	0.796	2.66 ± 0.17	< 0.26	458.54 ± 5.69	1
225672	149.91795	2.701692	0.892	17.19 ± 0.85	-0.75 ± 0.1		0
233281	149.94615	2.801806	0.611	12.19 ± 0.61	-1.20 ± 0.23	59.58 ± 5.11	1
250117	149.77776	2.645909	0.737	22.20 ± 1.12	-0.52 ± 0.08		0.5
27265	150.14487	1.776603	0.733	13.33 ± 0.39	< 2.21		1

[a]Radio spectral slope α inferred using S $\propto \nu^{\alpha}$ at 1.4 GHz and 3 GHz

[b]Linear size (diameter) of the jet, with the errors estimated from the beam size (0.75")

[c]Classification of galaxies onto LERG (1) or HERG (0). For conflicting indicators, we classify galaxies as 50% LERG (0.5)

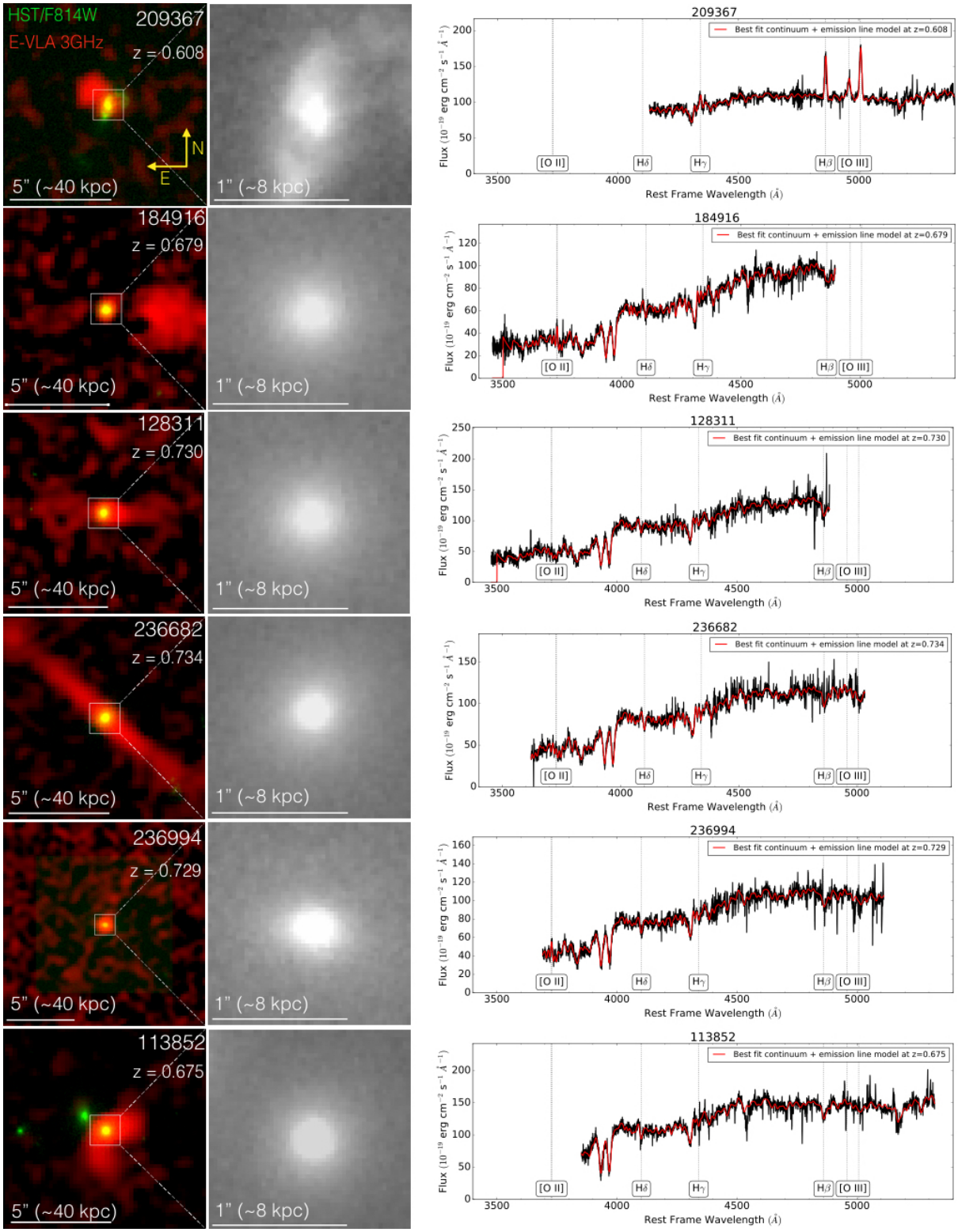

Figure 4.3 False-color HST/ACS/F814W+VLA/3 GHz images of radio sources with visible jets in the 3 GHz data, along with the corresponding LEGA-C optical spectra (black) with the best-fitting stellar continuum model (red).

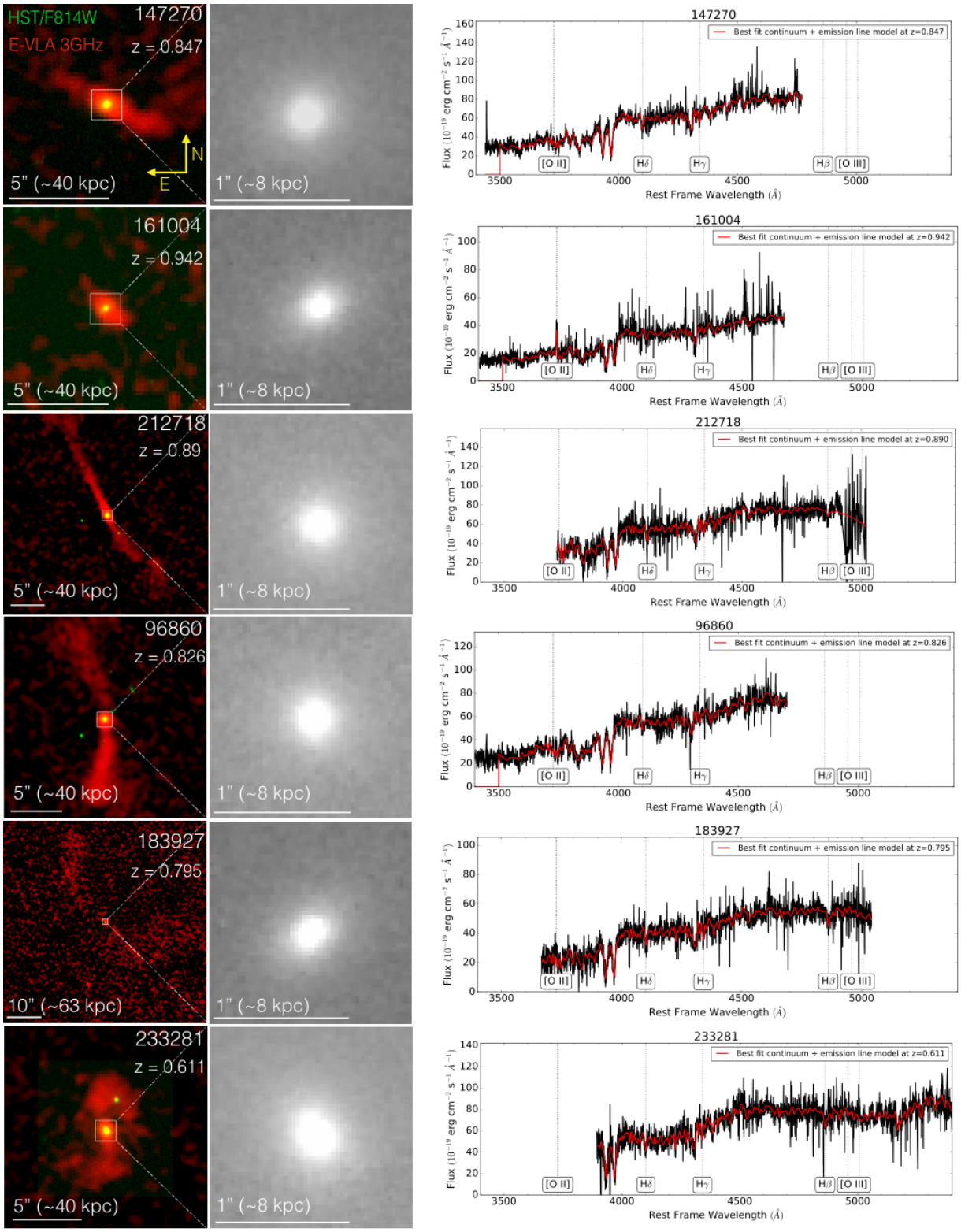

Figure 4.3 (Cont.) False-color HST/ACS/F814W+VLA/3 GHz images of radio sources with visible jets in the 3 GHz data, along with the corresponding LEGA-C optical spectra (black) with the best-fitting stellar continuum model (red).

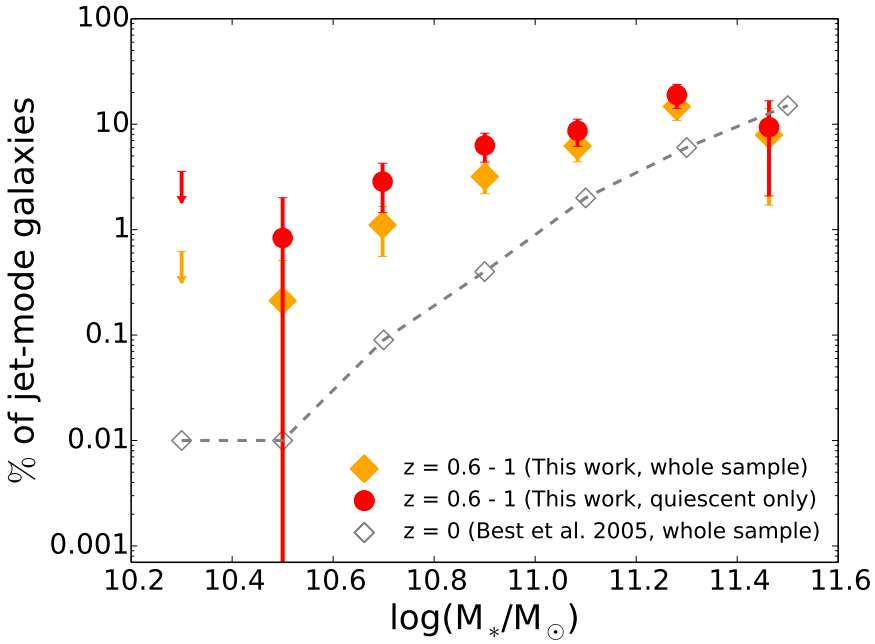

Figure 4.4 Fraction of jet-mode galaxies among all and quiescent galaxies in the LEGA-C as a function of the stellar mass (orange diamonds and red circles respectively). Open orange diamonds show the fraction of jet-mode galaxies for the sample of present-day galaxies.

One possible evolutionary scenario is that galaxies grow in stellar mass by a factor of two from z ∼ 1 to the present while conserving the fraction of jet-mode galaxies. This would imply that growth in stellar mass exceeds growth in black hole mass if we assume that the black hole mass is the only factor that sets the probability or frequency of becoming a radio galaxy. Alternatively, if BHs and stellar mass grow in lockstep (e.g., Calhau et al., 2017), then more frequent (or longer) radio-loud AGN phases at fixed BH mass could be understood by shorter cooling times at earlier cosmic times. The evolution in the fraction of jet-mode AGN in quiescent galaxies must be even faster than that for the general population, given that the fraction of quiescent galaxies is lower at $z \sim 1$ than at the present day (e.g. Bell et al., 2004; Faber et al., 2007). We show the fraction of jet-mode AGN in quiescent galaxies in Figure 4.4, and see that above $10^{11}\,M_\odot$ the fraction of jet-mode galaxies reaches 20 %.

The fraction of jet-mode AGN also strongly depends on stellar velocity dispersion σ_*, which can be seen as a proxy for black hole mass: in Figure 4.5 we show that more than ∼10% of galaxies with $\sigma_* \gtrsim 200\,\mathrm{km\,s^{-1}}$ have jet-mode AGN, reaching 20-30% at $\sigma_* \sim 300\,\mathrm{km\,s^{-1}}$. This behavior is only weakly dependent on star-formation activity if at all, which suggests that jet-mode AGN are not associated with quiescence but with high σ_*. Below $\sigma_* = 175\,\mathrm{km\,s^{-1}}$ we find three jet-mode AGN (one 100% and two 50% objects), whereas if the power-law trend seen at high σ_* were to continue to low σ_* we would expect a total of ten jet-mode AGN in the three low-σ_* bins. The detection of only three jet-mode AGN may suggest a threshold black-hole mass of $\sim 10^8\,M_\odot$ for jet-mode AGN, as inferred from the local black-hole

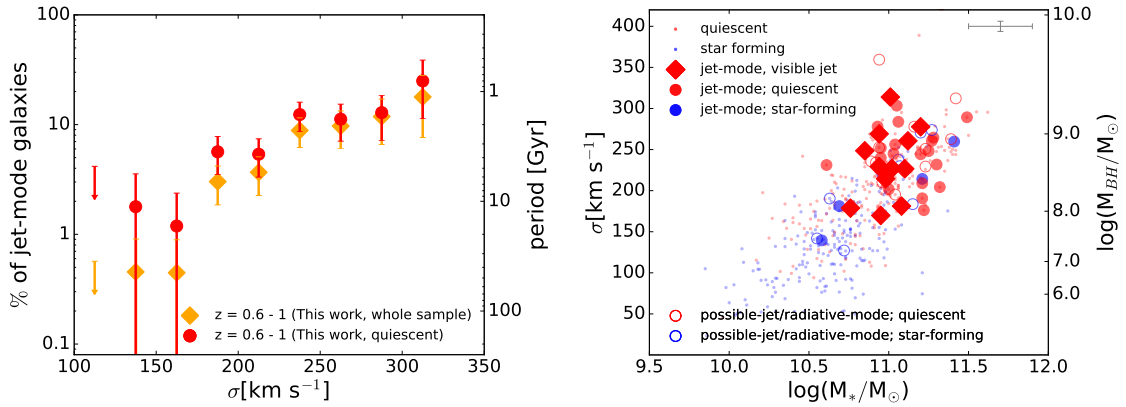

Figure 4.5 **Left**: Fraction of jet-mode galaxies among the full LEGA-C sample (orange diamonds) and among the quiescent galaxies the LEGA-C sample (red diamonds) as a function of the stellar velocity dispersion σ_*, **Right**: Stellar velocity dispersion σ_* as a function of the stellar mass. Blue and red points mark star-forming and quiescent galaxies, respectively. Large symbols represent radio AGN, with filled symbols showing those that are securely classified as jet-mode / low-excitation AGN (see Section 2.4). Large diamonds represent those with visible jets in the radio image (see Figure 3). Jet-mode AGN occur in massive galaxies with high stellar velocity dispersions, and old stellar populations. Typical error bars are indicated in the corners.

mass - σ_* relation (Gebhardt et al., 2003; Beifiori et al., 2012; van den Bosch, 2016). We argue that this threshold is not artificially introduced by our radio luminosity limit, as there is virtually no correlation between σ_* and radio luminosity, as shown in Figure 4.6.

Assuming that the jet-mode fraction of $10-30\%$ at high σ_* can be interpreted as a duty cycle, we convert these fractions into the period (or frequency) at which galaxies turn on a jet-mode AGN. In order to make the conversion of the fraction of jet-mode AGN into the period, we need a life time of an AGN jet. Examination of the jet structure morphology of the 12 objects in Figure 4.3 reveals that they are reminiscent of the classical Fanaroff-Riley I (FRI) type radio galaxy (Fanaroff & Riley, 1974; Ledlow & Owen, 1996). It has been argued that life times evolve with redshift (Athreya & Kapahi, 1998), but, among our radio galaxies that are detected in the pre-existing 1.4 GHz VLA data (Schinnerer et al., 2010) we find that the spectral slopes, and therefore presumably the ages, are similar to local counterparts (see Table 4.1). The typical spectral slopes of local counterparts range between -1.3 $< \alpha <$ -0.5 with the average spectral slope being -0.8 (Condon, 1992). Parma et al. (1998) find a correlation for FRI radio galaxies between the linear size of the jet and the synchrotron age of the jet as traced by the spectral slope, implying typical jet ages of about 100 Myr with an uncertainty of at most a factor 2. We therefore assume a lifetime of 2×100 Myr and show the resulting periods in Figure 4.5 on the left. We conclude that galaxies turn on a jet-mode AGN about once every Gyr provided that it has a stellar velocity dispersion in excess of $\sigma_* = 175\,\mathrm{km\,s^{-1}}$, corresponding with a black hole mass of $10^8\,\mathrm{M}_\odot$. Remarkably, this is the same black-hole mass

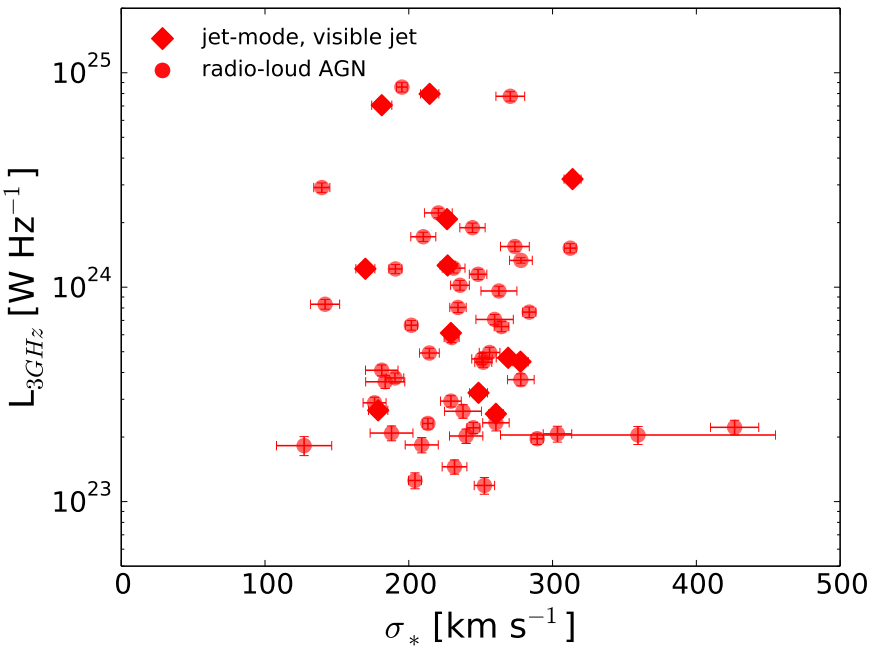

Figure 4.6 The 3 GHz luminosity as a function of the stellar velocity dispersion σ_* for the LEGA-C + VLA cross-matched sample of galaxies.

threshold that has been shown to separate quiescent and star-forming galaxies in the local universe (Terrazas et al., 2016).

4.3.2 Stellar Populations of Galaxies with Radio-Loud AGN

Our $z \sim 1$ radio AGN typically live in red, quiescent galaxies (Figure 4.7) as was shown before by Smolčić et al. (2009), Simpson et al. (2013), and Rees et al. (2016).

With the LEGA-C spectra we can examine, for the first time, the detailed stellar population properties of $z \sim 1$ radio galaxies. Figure 4.8 shows the Balmer absorption line index Hδ as a function of the 4000Å break $D_n(4000)$ (Bruzual et al., 1983; Balogh et al., 1999; Kauffmann et al., 2003a; Wu et al., 2018). Both of these parameters trace the recent star-formation activity within the galaxy. This shows that the jet-mode AGN have a strong $D_n(4000)$ and weak Balmer absorption, which implies that these galaxies have been quiescent for more than a Gyr (Bruzual & Charlot, 2003). That is, the observed AGN with a lifetime of ~ 100 Myr are not immediately responsible for the quenching of recent star formation. However, they may play a crucial role in maintaining quiescence, at least over the past 7 Gyr.

4.4 Conclusions

Maintenance-mode feedback from central BHs is a key element of all galaxy formation models in a cosmological context. Jet-mode AGN are the physical manifestation of this concept and a minimum requirement for the model in general is that jet-mode AGN frequently occur in galaxies devoid of significant levels of star formation. This

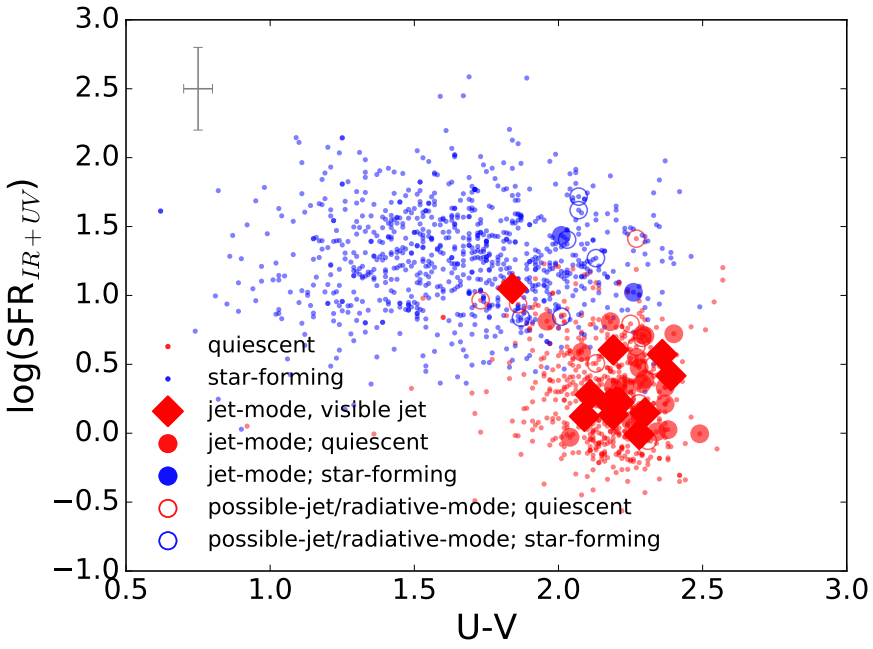

Figure 4.7 SFR$_{UV+IR}$ as a function of the rest-frame U-V color. The symbols are described in Figure 5. Jet-mode AGN reside in red, quiescent galaxies as had been demonstrated before.

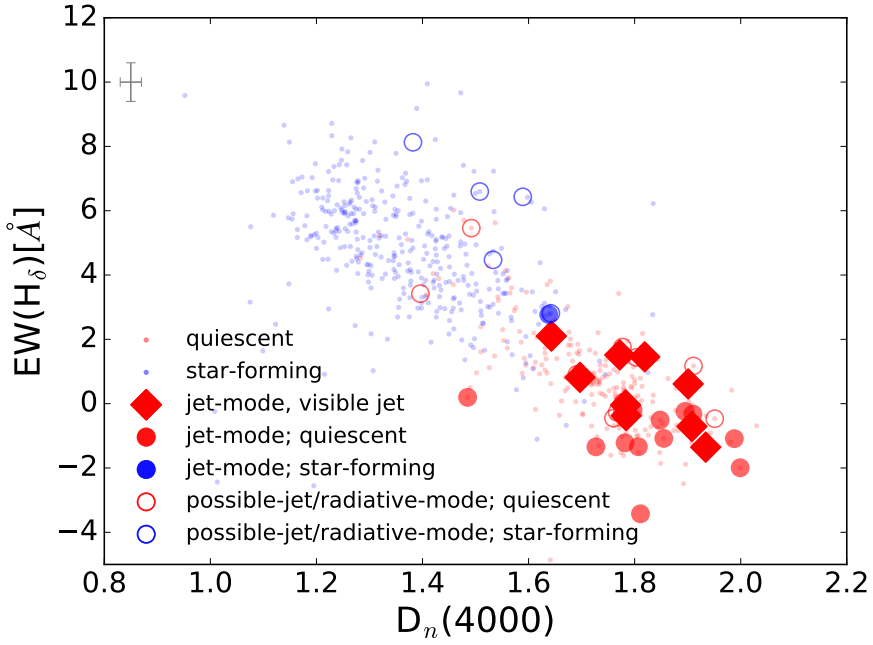

Figure 4.8 Balmer absorption line index Hδ as a function of the 4000Å break D$_n$(4000). The symbols are explained in Figure 5. Jet-mode AGN occur in galaxies with old stellar populations, with little star-formation activity for at least a Gyr.

hypothesis has thus far only been tested directly in the present-day universe but in this paper we investigate whether jet-mode galaxies at z $\sim$ 1 have been quiescent for an extended period of time.

We select the radio-loud subset of galaxies in the LEGA-C spectroscopic survey sample by matching against the newly acquired VLA 3 GHz dataset (Smolcic et al., 2017). We identify 58 radio-loud galaxies, most of which ($\sim$ 60%) are confirmed to be low-excitation radio AGN. Most radio sources appear point-like, but 12 sources show clear jet-like morphologies and are classified as FRI types.

The galaxies that host these jet-mode AGN have high stellar velocity dispersions of $\sigma_* > 175\,\mathrm{km\,s^{-1}}$, translating into a black-hole mass threshold of $\sim 10^8\,\mathrm{M_\odot}$ for jet-mode AGN, low specific star-formation rates ($< 10^{-1}\,\mathrm{Gyr^{-1}}$) and high stellar masses ($> 10^{11}\,\mathrm{M_\odot}$). The fraction of jet-mode AGN is $\sim$ 30% among galaxies with the highest stellar masses $\gtrsim 10^{11}\,\mathrm{M_\odot}$. Furthermore, strong 4000Å breaks and weak Balmer absorption lines imply that these galaxies have been devoid of significant star-formation activity for more than $\sim 1\,\mathrm{Gyr}$. Assuming the jet-mode AGN share similar physical properties in a certain mass bin, and considering their life time we infer that every massive, quiescent galaxy at $z \sim 1$ will switch on a jet-mode AGN about once every Gyr.

Our findings put the conclusions by Best et al. (2014) on firmer footing, who statistically link the quiescent and radio-loud populations by comparing the evolution of their respective luminosity functions out to $z \sim 1$. It therefore seems increasingly plausible that radio AGN play a crucial role across cosmic time in keeping the halo gas around massive galaxies hot, preventing further star formation.

Chapter 5

Summary and Outlook

The main focus of my thesis has been studying maintenance-mode feedback in the local and high-redshift (z $\sim$ 1) universe, and interstellar medium properties of z $\sim$ 0.8 galaxies.

5.1 Summary

The development of our understanding of processes that govern galaxy formation and evolution requires, among other aspects, exploring interstellar medium properties. Attenuation measurement across a range of wavelengths allows us to study the global effect of dust on stellar light. So far, attenuation studies mostly relied on spectral energy distribution fits derived from multi-band photometry to recover the information about the attenuation. A novel approach to measure attenuation for z $\sim$ 0.8 galaxies was presented in Chapter 2. This approach uses attenuation-free stellar spectra reconstructed using LEGA-C survey deep optical spectra (Pacifici et al., 2016, Pacifici et al. 2020, in prep.), in combination with the observed multi-band photometry. Furthermore, to describe the attenuation curve – a new modeling technique was introduced, and a new typical attenuation curve prescription for z $\sim$ 0.8 galaxies was given. A large diversity in the attenuation curve slope and UV bump (2175Å excess) characteristic has been observed, and the main finding is that the galaxy geometry plays a significant role in the attenuation measurement (Barišić et al. 2020, subm.).

Quiescence in galaxies with the most massive halos is generally attributed to the jet-mode feedback. This feedback is thought to manifest itself via radio-loud AGN, which keeps the halo gas hot, preventing it from forming new stellar content. Chapter 3 demonstrates that incidence of radio-loud AGN is not a sufficient condition to generally explain quiescence (Barišić et al., 2019). We examine the occurring frequency of radio-loud AGN in round and flat local quiescent galaxies by conducting a statistical analysis of combined spectroscopic SDSS (York et al., 2000), radio NVSS (Condon et al., 1998) and FIRST (Becker et al., 1995) data-sets. The finding is that radio-loud AGN almost exclusively occur in round, as compared to flat disk-like quiescent galaxies. This result suggests a possible existence of a

different mechanism involved in keeping geometrically flat quiescent galaxies from forming new stellar content.

High-redshift exploration of jet-mode feedback was limited in the past due to insufficient sensitivity of radio observations. This, however, changed recently. Chapter 4 shows that by combining the deep and high resolution LEGA-C spectroscopic data-set (van der Wel et al., 2016; Straatman et al., 2018), and high quality VLA 3GHz data-set (Smolcic et al., 2017), one can put constraints on the jet-mode feedback in z ∼ 1 galaxies. This chapter provides first evidence at this lookback time, that radio-loud AGN are preferably hosted by galaxies with highest black-hole masses (Barišić et al., 2017b). This result implies that the host black-hole mass sets the probability for radio-loud AGN presence, and provides crucial evidence in support of jet-mode feedback picture in high-redshift galaxies.

5.2 Outlook

In the future I intend to explore the interstellar medium properties of high-redshift quiescent galaxies and interpret rich, unexplored observational data-sets with the aim to better understand the absence of star-formation in massive galaxies.

5.2.1 Outline & Motivation

Thus far, exploration of the stellar content has been the main approach to study quiescence in galaxies. Observations suggest that quiescent galaxies, especially those at higher redshift, have rich dust and gas reservoir (e.g. Gobat et al., 2018). Studying the interstellar medium of quiescent galaxies is necessary to understand maintenance and quenching mechanisms from a previously unexplored perspective.

Using rich COSMOS field data-set together with the LEGA-C survey (van der Wel et al., 2016; Straatman et al., 2018) – containing high quality information on stellar population and kinematics, enables exploration of properties of quiescent galaxies. Recent Karl G. Jansky VLA 3GHz survey (Smolcic et al., 2017) allows tracing radio-loud AGN at higher redshift at luminosities down to 10^{22} WHz^{-1}. My future plans include exploring interstellar medium properties in z∼1 quiescent galaxies based on following diagnostics:

(i) emission lines: weak/absent Balmer emission lines hint to SF inefficiency, yet, strong forbidden OII, OIII lines are present (Straatman et al., 2018)
(ii) attenuation curve features: unusually strong UV (2175Å) bumps suggest presence of PAH molecules (Barišić et al. 2020, in prep.)
(iii) radio luminosity: indirect SF tracer if the source is non-thermal emission from electrons accelerated by supernova explosions (L < 10^{23} WHz^{-1}), else, radio-loud AGN tracer
(iv) 24μm luminosity (Sanders et al., 2007): corresponds to thermal emission from dust heated up by ultraviolet radiation from young stars, and can be used as a SF tracer — quiescent galaxies are surprisingly bright in dust continuum

Using this available data-set I intend to determine true star-formation rate of quiescent galaxies based on VLA 3GHz and 24μm luminosities. In the context of jet-mode feedback picture I will explore the connection between the presence of forbidden emission lines, 24μm emission and attenuation curve characteristics for radio-loud AGN, and determine their difference to non-AGN quiescent galaxies. This will provide unprecedented information about the interstellar medium characteristics of z∼1 quiescent galaxies.

True SFR in quiescent galaxies

Infrared and radio emission follow a very tight correlation at least out to z∼3 (e.g. Delhaize et al., 2017). Using the sensitivity and depth of the VLA 3GHz survey, together with MIPS 24μm observations (Rieke et al., 2004), I will determine true SFR of z∼1 quiescent galaxies. I will do so by exploring their position in the 24μm-radio plane and through the emission lines diagnostics (via LEGA-C), and ultimately compare them to normal star-forming galaxies at that cosmic epoch. The correlation between 24μm and radio luminosity (or lack thereof) will provide a stringent test on the hypothesis that 24μm emission is due to underlying SF.

Interstellar medium of radio-loud AGN

Local universe based evidence suggests radio-loud AGN are likely to reside in spheroidals (slow-rotating systems; Barišić et al., 2019). Yet, not all slow-rotating systems host radio-loud AGN. Employing the stellar kinematics information available from LEGA-C data-set I can identify slow-rotators among our quiescent galaxies, and characterize their interstellar medium through emission line diagnostics, attenuation curve properties and 24μm luminosity. This will enable me to conduct a cross comparison between slow-rotating non-AGN and radio-loud AGN, and allow me to quantify their dust content.

24μm excess and cold interstellar medium

It has been argued that 24μm excess could point to a presence of an underlying AGN, or even a short starburst activity (e.g. Huynh et al., 2010). Focusing on flat disk-like quiescent galaxies – which show no evidence of hosting a radio-loud AGN, I intend to compare the attenuation curve characteristics with the galaxy geometry. This will provide insight into the distribution of the dust content — thin disk vs. well mixed with the stellar body. Tracing the correlation between optical and 24μm luminosity will allow me to put constraints on the origin of dust in flat disk-like early-type galaxies.

As a future step, to provide more information on the cold interstellar medium content of a carefully selected sub-sample of flat disk-like quiescent z∼1 galaxies, I am planning to propose to observe their molecular gas content, and separately dust continuum with the Atacama Large (Sub/) Millimeter Array.

Chapter 6

First author publications

I. Barišić, A. L. Faisst, P. L. Capak, et al., Dust Properties of [CII] Detected z $\sim$ 5.5 Galaxies: New HST/WFC3 Near-IR Observations, The Astrophysical Journal, 845, 41

I. Barišić, A. van der Wel, R. Bezanson, et al., Stellar Dynamics and Star Formation Histories of z $\sim$ 1 Radio-loud Galaxies, The Astrophysical Journal, 847, 72
This work has been used in this thesis

I. Barišić, A. van der Wel, J. van Houdt, et al., An Absence of Radio-loud Active Galactic Nuclei in Geometrically Flat Quiescent Galaxies: Implications for Maintenance-mode Feedback Models, The Astrophysical Journal Letters, 872, L12
This work has been used in this thesis

I. Barišić, C. Pacifici, A. van der Wel, et al., Dust Attenuation Curves at z $\sim$ 0.8 from LEGA-C: Precise Costraints on the Slope and UV Bump Strength, submitted to the Astrophysical Journal
This work has been used in this thesis

Bibliography

Abazajian K. N., et al., 2009, *The seventh data release of the Sloan Digital Sky Survey*, The Astrophysical Journal Supplement Series, 182, 543

Athreya R. M., Kapahi V. K., 1998, *The redshift dependence of spectral index in powerful radio galaxies*, Journal of Astrophysics and Astronomy, 19, 63

Balogh M. L., Morris S. L., Yee H., Carlberg R., Ellingson E., 1999, *Differential galaxy evolution in cluster and field galaxies at z 0.3*, The Astrophysical Journal, 527, 54

Barisic I., et al., 2017a, *Dust Properties of C ii Detected z 5.5 Galaxies: New HST/WFC3 Near-IR Observations*, The Astrophysical Journal, 845, 41

Barišić I., et al., 2017b, *Stellar Dynamics and Star Formation Histories of z 1 Radio-loud Galaxies*, The Astrophysical Journal, 847, 72

Barišić I., et al., 2019, *An Absence of Radio-loud Active Galactic Nuclei in Geometrically Flat Quiescent Galaxies: Implications for Maintenance-mode Feedback Models*, The Astrophysical Journal Letters, 872, L12

Battisti A., Calzetti D., Chary R.-R., 2016, *Characterizing dust attenuation in local star-forming galaxies: Uv and optical reddening*, The Astrophysical Journal, 818, 13

Battisti A., Calzetti D., Chary R.-R., 2017, *Characterizing Dust Attenuation in Local Star Forming Galaxies: Inclination Effects and the 2175\AA\Feature*, arXiv preprint arXiv:1711.04814

Becker R. H., White R. L., Helfand D. J., 1995, *The FIRST survey: faint images of the radio sky at twenty centimeters*, The Astrophysical Journal, 450, 559

Beegle L. W., Wdowiak T. J., Robinson M. S., Cronin J. R., McGehee M. D., Clemett S. J., Gillette S., 1997, *Experimental Indication of a Naphthalene-Base Molecular Aggregate for the Carrier of the 2175 Å Interstellar Extinction Feature*, The Astrophysical Journal, 487, 976

Beifiori A., Courteau S., Corsini E., Zhu Y., 2012, *On the correlations between galaxy properties and supermassive black hole mass*, Monthly Notices of the Royal Astronomical Society, 419, 2497

Bell E. F., 2003, *Estimating star formation rates from infrared and radio luminosities: the origin of the radio-infrared correlation*, The Astrophysical Journal, 586, 794

Bell E. F., et al., 2004, *Nearly 5000 distant early-type galaxies in COMBO-17: a red sequence and its evolution since z˜ 1*, The Astrophysical Journal, 608, 752

Best P., Heckman T., 2012, *On the fundamental dichotomy in the local radio-AGN population: accretion, evolution and host galaxy properties*, Monthly Notices of the Royal Astronomical Society, 421, 1569

Best P., Kauffmann G., Heckman T., Brinchmann J., Charlot S., Ivezić Ž., White S., 2005, *The host galaxies of radio-loud active galactic nuclei: mass dependences, gas cooling and active galactic nuclei feedback*, Monthly Notices of the Royal Astronomical Society, 362, 25

Best P., Ker L., Simpson C., Rigby E., Sabater J., 2014, *The cosmic evolution of radio-AGN feedback to z= 1*, Monthly Notices of the Royal Astronomical Society, 445, 955

Blandford R. D., Znajek R. L., 1977, *Electromagnetic extraction of energy from Kerr black holes*, Monthly Notices of the Royal Astronomical Society, 179, 433

Blanton E. L., Sarazin C. L., McNamara B. R., Wise M. W., 2001, *Chandra observation of the radio source/X-ray gas interaction in the cooling flow cluster Abell 2052*, The Astrophysical Journal Letters, 558, L15

Blumenthal G. R., Faber S., Primack J. R., Rees M. J., 1984, *Formation of galaxies and large-scale structure with cold dark matter*, Nature, 311, 517

Boquien M., Burgarella D., Roehlly Y., Buat V., Ciesla L., Corre D., Inoue A., Salas H., 2019, *CIGALE: a python Code Investigating GALaxy Emission*, Astronomy & Astrophysics, 622, A103

Bourne N., et al., 2017, *Evolution of cosmic star formation in the SCUBA-2 Cosmology Legacy Survey*, Monthly Notices of the Royal Astronomical Society, 467, 1360

Bouwens R. J., et al., 2016, *ALMA spectroscopic survey in the Hubble Ultra Deep Field: the infrared excess of UV-selected z= 2–10 galaxies as a function of UV-continuum slope and stellar mass*, The Astrophysical Journal, 833, 72

Bower R., Benson A., Malbon R., Helly J., Frenk C., Baugh C., Cole S., Lacey C. G., 2006, *Breaking the hierarchy of galaxy formation*, Monthly Notices of the Royal Astronomical Society, 370, 645

Brinchmann J., Charlot S., White S., Tremonti C., Kauffmann G., Heckman T., Brinkmann J., 2004, *The physical properties of star-forming galaxies in the low-redshift Universe*, Monthly Notices of the Royal Astronomical Society, 351, 1151

Bruzual G., Charlot S., 2003, *Stellar population synthesis at the resolution of 2003*, Monthly Notices of the Royal Astronomical Society, 344, 1000

Bruzual A., et al., 1983, *Spectral evolution of galaxies. I-Early-type systems*, The Astrophysical Journal, 273, 105

Buat V., et al., 2012, *GOODS-Herschel: dust attenuation properties of UV selected high redshift galaxies*, Astronomy & Astrophysics, 545, A141

Burgarella D., Buat V., Iglesias-Paramo J., 2005, *Star formation and dust attenuation properties in galaxies from a statistical ultraviolet-to-far-infrared analysis*, Monthly Notices of the Royal Astronomical Society, 360, 1413

Calhau J., Sobral D., Stroe A., Best P., Smail I., Lehmer B., Harrison C., Thomson A., 2017, *The growth of typical star-forming galaxies and their supermassive black holes across cosmic time since z 2*, Monthly Notices of the Royal Astronomical Society, 464, 303

Calzetti D., 2001, *The dust opacity of star-forming galaxies*, Publications of the Astronomical Society of the Pacific, 113, 1449

Calzetti D., Kinney A. L., Storchi-Bergmann T., 1994, *Dust extinction of the stellar continua in starburst galaxies: The ultraviolet and optical extinction law*, The astrophysical journal. Chicago. Vol. 429, no. 2, pt. 1 (July 1994), p. 582-601

Calzetti D., Armus L., Bohlin R. C., Kinney A. L., Koornneef J., Storchi-Bergmann T., 2000, *The dust content and opacity of actively star-forming galaxies*, The Astrophysical Journal, 533, 682

Capak P., et al., 2015, *Galaxies at redshifts 5 to 6 with systematically low dust content and high [C II] emission*, Nature, 522, 455

Capetti A., Balmaverde B., 2006, *The host galaxy/AGN connection in nearby early-type galaxies-A new view of the origin of the radio-quiet/radio-loud dichotomy?*, Astronomy & Astrophysics, 453, 27

Cardelli J. A., Clayton G. C., Mathis J. S., 1989, *The relationship between infrared, optical, and ultraviolet extinction*, The Astrophysical Journal, 345, 245

Chabrier G., 2003, *Galactic Stellar and Substellar Initial Mass FunctionThe page charges for this Review were partially covered by a generous gift from a PASP supporter.*, Publications of the Astronomical Society of the Pacific, 115, 763

Chang Y.-Y., et al., 2013, *Structural Evolution of Early-type Galaxies to z= 2.5 in CANDELS*, The Astrophysical Journal, 773, 149

Chang Y.-Y., van der Wel A., da Cunha E., Rix H.-W., 2015, *Stellar Masses and Star Formation Rates for 1 m Galaxies From SDSS+ WISE*, The Astrophysical Journal Supplement Series, 219, 8

Charlot S., Fall S. M., 2000, *A simple model for the absorption of starlight by dust in galaxies*, The Astrophysical Journal, 539, 718

Charlot S., Longhetti M., 2001, *Nebular emission from star-forming galaxies*, Monthly Notices of the Royal Astronomical Society, 323, 887

Chevallard J., Charlot S., Wandelt B., Wild V., 2013, *Insights into the content and spatial distribution of dust from the integrated spectral properties of galaxies*, Monthly Notices of the Royal Astronomical Society, 432, 2061

Condon J., 1992, *Radio emission from normal galaxies*, Annual review of astronomy and astrophysics, 30, 575

Condon J. J., Cotton W., Greisen E., Yin Q., Perley R., Taylor G., Broderick J., 1998, *The NRAO VLA sky survey*, The Astronomical Journal, 115, 1693

Conroy C., Schiminovich D., Blanton M. R., 2010, *Dust attenuation in disk-dominated galaxies: evidence for the 2175 Å dust feature*, The Astrophysical Journal, 718, 184

Cortese L., et al., 2012, *The dust scaling relations of the Herschel Reference Survey*, Astronomy & Astrophysics, 540, A52

Croton D. J., et al., 2006, *The many lives of active galactic nuclei: cooling flows, black holes and the luminosities and colours of galaxies*, Monthly Notices of the Royal Astronomical Society, 365, 11

Cutri R., et al., 2013, *Explanatory supplement to the AllWISE data release products*, Explanatory Supplement to the AllWISE Data Release Products, by RM Cutri et al.

De Breuck C., Van Breugel W., Stanford S., Röttgering H., Miley G., Stern D., 2002, *Optical and near-infrared imaging of ultra-steep-spectrum radio sources: The Kz diagram of radio-selected and optically selected galaxies*, The Astronomical Journal, 123, 637

De Lucia G., Blaizot J., 2007, *The hierarchical formation of the brightest cluster galaxies*, Monthly Notices of the Royal Astronomical Society, 375, 2

De Ruiter H., Parma P., Capetti A., Fanti R., Morganti R., Santantonio L., 2005, *Are radio galaxies and quiescent galaxies different? Results from the analysis of HST brightness profiles*, Astronomy & Astrophysics, 439, 487

Delhaize J., et al., 2017, *VLA-COSMOS 3GHz Large Project: The infrared-radio correlation of star-forming galaxies and AGN to z\lesssim6, arXivpreprintarXiv* : 1703.09723

Di Matteo T., Springel V., Hernquist L., 2005, *Energy input from quasars regulates the growth and activity of black holes and their host galaxies*, Nature, 433, 604

Donoso E., Best P., Kauffmann G., 2009, *Evolution of the radio-loud galaxy population*, Monthly Notices of the Royal Astronomical Society, 392, 617

Draine B. T., 2010, *Physics of the interstellar and intergalactic medium*. Princeton University Press

Elbaz D., et al., 2007, *The reversal of the star formation-density relation in the distant universe*, Astronomy & Astrophysics, 468, 33

Faber S., et al., 2007, *Galaxy luminosity functions to z˜ 1 from DEEP2 and COMBO-17: implications for red galaxy formation*, The Astrophysical Journal, 665, 265

Fabian A., 2012, *Observational evidence of active galactic nuclei feedback*, Annual Review of Astronomy and Astrophysics, 50, 455

Faisst A. L., et al., 2017, *Are high-redshift galaxies hot? Temperature of z¿ 5 galaxies and implications for their dust properties*, The Astrophysical Journal, 847, 21

Fanaroff B., Riley J., 1974, *The morphology of extragalactic radio sources of high and low luminosity*, Monthly Notices of the Royal Astronomical Society, 167, 31P

Fanidakis N., Baugh C., Benson A., Bower R., Cole S., Done C., Frenk C., 2010, *Grand unification of AGN activity in the ΛCDM cosmology*, Monthly Notices of the Royal Astronomical Society, 410, 53

Fitzpatrick E., Massa D., 1986, *An analysis on the shapes of ultraviolet extinction curves. I-The 2175 A bump*, The Astrophysical Journal, 307, 286

Fitzpatrick E. L., Massa D., 1988, *An analysis of the shapes of ultraviolet extinction curves. II-The far-UV extinction*, The Astrophysical Journal, 328, 734

Fitzpatrick E. L., Massa D., 1990, *An analysis of the shapes of ultraviolet extinction curves. III-an atlas of ultraviolet extinction curves*, The Astrophysical Journal Supplement Series, 72, 163

Fontanot F., De Lucia G., Monaco P., Somerville R. S., Santini P., 2009, *The many manifestations of downsizing: hierarchical galaxy formation models confront observations*, Monthly Notices of the Royal Astronomical Society, 397, 1776

Fudamoto Y., et al., 2017, *The dust attenuation of star-forming galaxies at z 3 and beyond: New insights from ALMA observations*, Monthly Notices of the Royal Astronomical Society, 472, 483

Galliano F., Galametz M., Jones A. P., 2018, *The interstellar dust properties of nearby galaxies*, Annual Review of Astronomy and Astrophysics, 56, 673

Gebhardt K., et al., 2003, *Axisymmetric dynamical models of the central regions of galaxies*, The Astrophysical Journal, 583, 92

Gobat R., et al., 2018, *The unexpectedly large dust and gas content of quiescent galaxies at z¿ 1.4*, Nature Astronomy, 2, 239

Gordon K. D., Clayton G. C., Misselt K., Landolt A. U., Wolff M. J., 2003, *A quantitative comparison of the Small Magellanic Cloud, Large Magellanic Cloud, and Milky Way ultraviolet to near-infrared extinction curves*, The Astrophysical Journal, 594, 279

Gordon K. D., et al., 2016, *The panchromatic Hubble Andromeda treasury. XV. The BEAST: Bayesian extinction and stellar tool*, The Astrophysical Journal, 826, 104

Häring N., Rix H.-W., 2004, *On the black hole mass-bulge mass relation*, The Astrophysical Journal Letters, 604, L89

Heckman T. M., Best P. N., 2014a, *The coevolution of galaxies and supermassive black holes: insights from surveys of the contemporary universe*, Annual Review of Astronomy and Astrophysics, 52, 589

Heckman T. M., Best P. N., 2014b, *The coevolution of galaxies and supermassive black holes: insights from surveys of the contemporary universe*, Annual Review of Astronomy and Astrophysics, 52, 589

Heckman T. M., Kauffmann G., Brinchmann J., Charlot S., Tremonti C., White S. D., 2004, *Present-day growth of black holes and bulges: The Sloan Digital Sky Survey perspective*, The Astrophysical Journal, 613, 109

Hine R., Longair M., 1979, *Optical spectra of 3CR radio galaxies*, Monthly Notices of the Royal Astronomical Society, 188, 111

Hopkins P. F., Quataert E., Murray N., 2012, *Stellar feedback in galaxies and the origin of galaxy-scale winds*, Monthly Notices of the Royal Astronomical Society, 421, 3522

Hughes S. A., Blandford R. D., 2003, *Black hole mass and spin coevolution by mergers*, The Astrophysical Journal Letters, 585, L101

Huynh M. T., Gawiser E., Marchesini D., Brammer G., Guaita L., 2010, *MIPS 24 μm observations of the Hubble Deep Field South: Probing the IR-radio correlation of galaxies at z¿ 1*, The Astrophysical Journal, 723, 1110

Janssen R., Röttgering H., Best P., Brinchmann J., 2012, *The triggering probability of radio-loud AGN-A comparison of high and low excitation radio galaxies in hosts of different colors*, Astronomy & Astrophysics, 541, A62

Joblin C., Léger A., Martin P., 1992, *Contribution of polycyclic aromatic hydrocarbon molecules to the interstellar extinction curve*, The Astrophysical Journal, 393, L79

Jones A., Fanciullo L., Köhler M., Verstraete L., Guillet V., Bocchio M., Ysard N., 2013, *The evolution of amorphous hydrocarbons in the ISM: dust modelling from a new vantage point*, Astronomy & Astrophysics, 558, A62

Kauffmann G., et al., 2003a, *Stellar masses and star formation histories for 105 galaxies from the Sloan Digital Sky Survey*, Monthly Notices of the Royal Astronomical Society, 341, 33

Kauffmann G., et al., 2003b, *The host galaxies of active galactic nuclei*, Monthly Notices of the Royal Astronomical Society, 346, 1055

Kennicutt Jr R. C., 1998, *Star formation in galaxies along the Hubble sequence*, Annual Review of Astronomy and Astrophysics, 36, 189

Kennicutt Jr R. C., Evans N. J., 2012, *Star formation in the Milky Way and nearby galaxies*, Annual Review of Astronomy and Astrophysics, 50, 531

Kriek M., Conroy C., 2013, *The dust attenuation law in distant galaxies: evidence for variation with spectral type*, The Astrophysical Journal Letters, 775, L16

Laing R., 1994, in The Physics of Active Galaxies. p. 227

LeFevre O., et al., 2003, in Astronomical Telescopes and Instrumentation. pp 1670–1681

Ledlow M. J., Owen F. N., 1996, in , Extragalactic Radio Sources. Springer, pp 238–239

Madau P., Dickinson M., 2014, *Cosmic star-formation history*, Annual Review of Astronomy and Astrophysics, 52, 415

Magnelli B., et al., 2015, *The far-infrared/radio correlation and radio spectral index of galaxies in the SFR–M plane up to z˜ 2*, Astronomy & Astrophysics, 573, A45

Matthews T. A., Morgan W. W., Schmidt M., 1964, *A Discussion of Galaxies Indentified with Radio Sources.*, The Astrophysical Journal, 140, 35

McKinney J. C., Gammie C. F., 2004, *A measurement of the electromagnetic luminosity of a Kerr black hole*, The Astrophysical Journal, 611, 977

McNamara B., Nulsen P., 2007, *Heating hot atmospheres with active galactic nuclei*, Annu. Rev. Astron. Astrophys., 45, 117

Mo H., Van den Bosch F., White S., 2010, *Galaxy formation and evolution*. Cambridge University Press

Moustakas J., Kennicutt Jr R. C., Tremonti C. A., 2006, *Optical star formation rate indicators*, The Astrophysical Journal, 642, 775

Muzzin A., et al., 2013, *A public Ks-selected catalog in the COSMOS/ULTRAVISTA field: photometry, photometric redshifts, and stellar population parameters*, The Astrophysical Journal Supplement Series, 206, 8

Narayan R., Mahadevan R., Grindlay J. E., Popham R. G., Gammie C., 1998, *Advection-dominated accretion model of Sagittarius A*: evidence for a black hole at the Galactic center*, The Astrophysical Journal, 492, 554

Narayanan D., Conroy C., Davé R., Johnson B. D., Popping G., 2018, *A Theory for the Variation of Dust Attenuation Laws in Galaxies*, The Astrophysical Journal, 869, 70

Noeske K., et al., 2007, *Star formation in AEGIS field galaxies since z= 1.1: the dominance of gradually declining star formation, and the main sequence of star-forming galaxies*, The Astrophysical Journal Letters, 660, L43

Noll S., Burgarella D., Giovannoli E., Buat V., Marcillac D., Munoz-Mateos J., 2009, *Analysis of galaxy spectral energy distributions from far-UV to far-IR with CIGALE: studying a SINGS test sample*, Astronomy & Astrophysics, 507, 1793

Pacifici C., Charlot S., Blaizot J., Brinchmann J., 2012, *Relative merits of different types of rest-frame optical observations to constrain galaxy physical parameters*, Monthly Notices of the Royal Astronomical Society, 421, 2002

Pacifici C., Oh S., Oh K., Lee J., Sukyoung K. Y., 2016, *Timing the Evolution of Quiescent and Star-forming Local Galaxies*, The Astrophysical Journal, 824, 45

Parma P., Murgia M., Morganti R., Capetti A., De Ruiter H., Fanti R., 1998, *Radiative ages in a representative sample of low luminosity radio galaxies*, Arxiv preprint astro-ph/9812413

Patel S. G., Holden B. P., Kelson D. D., Franx M., van der Wel A., Illingworth G. D., 2012, *The UVJ Selection of Quiescent and Star-forming Galaxies: Separating Early-and Late-type Galaxies and Isolating Edge-on Spirals*, The Astrophysical Journal Letters, 748, L27

Peebles P., 1982, *Large-scale background temperature and mass fluctuations due to scale-invariant primeval perturbations*

Pierini D., Gordon K., Witt A., Madsen G., 2004, *Dust attenuation in late-type galaxies. I. Effects on bulge and disk components*, The Astrophysical Journal, 617, 1022

Pillepich A., et al., 2017, *Simulating galaxy formation with the IllustrisTNG model*, Monthly Notices of the Royal Astronomical Society, 473, 4077

Reddy N. A., Steidel C. C., Fadda D., Yan L., Pettini M., Shapley A. E., Erb D. K., Adelberger K. L., 2006, *Star formation and extinction in redshift z˜ 2 galaxies: Inferences from Spitzer MIPS observations*, The Astrophysical Journal, 644, 792

Reddy N. A., et al., 2015, *The MOSDEF survey: measurements of Balmer decrements and the dust attenuation curve at redshifts z 1.4–2.6*, The Astrophysical Journal, 806, 259

Reddy N. A., et al., 2018, *The HDUV survey: a revised assessment of the relationship between UV slope and dust attenuation for high-redshift galaxies*, The Astrophysical Journal, 853, 56

Rees G., et al., 2016, *Radio galaxies in ZFOURGE/NMBS: no difference in the properties of massive galaxies with and without radio-AGN out to z= 2.25*, Monthly Notices of the Royal Astronomical Society, 455, 2731

Rémy-Ruyer A., et al., 2014, *Gas-to-dust mass ratios in local galaxies over a 2 dex metallicity range*, Astronomy & Astrophysics, 563, A31

Rieke G. H., et al., 2004, *The multiband imaging photometer for Spitzer (MIPS)*, The Astrophysical Journal Supplement Series, 154, 25

Rodighiero G., et al., 2011, *The lesser role of starbursts in star formation at z= 2*, The Astrophysical Journal Letters, 739, L40

Salim S., Narayanan D., 2020, *The Dust Attenuation Law in Galaxies*, arXiv preprint arXiv:2001.03181

Salim S., et al., 2005, *New constraints on the star formation histories and dust attenuation of galaxies in the local Universe from GALEX*, The Astrophysical Journal Letters, 619, L39

Salim S., Boquien M., Lee J. C., 2018, *Dust Attenuation Curves in the Local Universe: Demographics and New Laws for Star-forming Galaxies and High-redshift Analogs*, The Astrophysical Journal, 859, 11

Sanders D., et al., 2007, *S-COSMOS: The Spitzer legacy survey of the Hubble Space Telescope ACS 2 deg2 COSMOS field I: survey strategy and first analysis*, The Astrophysical Journal Supplement Series, 172, 86

Savage B., 1975, *Ultraviolet photometry from the Orbiting Astronomical Observatory. XX-The ultraviolet extinction bump*, The Astrophysical Journal, 199, 92

Schaye J., et al., 2015, *The EAGLE project: simulating the evolution and assembly of galaxies and their environments*, Monthly Notices of the Royal Astronomical Society, 446, 521

Schinnerer E., et al., 2010, *The VLA-COSMOS Survey. IV. Deep Data and Joint Catalog*, The Astrophysical Journal Supplement Series, 188, 384

Scoville N., et al., 2007, *The cosmic evolution survey (COSMOS): overview*, The Astrophysical Journal Supplement Series, 172, 1

Scoville N., Faisst A., Capak P., Kakazu Y., Li G., Steinhardt C., 2015, *Dust Attenuation in High Redshift Galaxies:"Diamonds in the Sky"*, The Astrophysical Journal, 800, 108

Shakura N. I., Sunyaev R. A., 1973, *Black holes in binary systems. Observational appearance.*, Astronomy and Astrophysics, 24, 337

Sikora M., Stawarz Ł., Lasota J.-P., 2007, *Radio loudness of active galactic nuclei: observational facts and theoretical implications*, The Astrophysical Journal, 658, 815

Simpson C., Westoby P., Arumugam V., Ivison R., Hartley W., Almaini O., 2013, *The prevalence of AGN feedback in massive galaxies at z 1*, Monthly Notices of the Royal Astronomical Society, p. stt940

Smolčić V., et al., 2009, *Cosmic evolution of radio selected active galactic nuclei in the cosmos field*, The Astrophysical Journal, 696, 24

Smolcic V., et al., 2017, *The VLA-COSMOS 3 GHz Large Project: Continuum data and source catalog release*, arXiv preprint arXiv:1703.09713

Speagle J. S., Steinhardt C. L., Capak P. L., Silverman J. D., 2014, *A highly consistent framework for the evolution of the star-forming "main sequence" from z 0-6*, The Astrophysical Journal Supplement Series, 214, 15

Stebbins J., Huffer C. M., Whitford A. E., 1939, *Space Reddening in the Galaxy.*, The Astrophysical Journal, 90, 209

Stecher T. P., 1965, *Interstellar Ectinction in the Ultraviolet.*, The Astrophysical Journal, 142, 1683

Steglich M., Jäger C., Rouillé G., Huisken F., Mutschke H., Henning T., 2010, *Electronic spectroscopy of medium-sized polycyclic aromatic hydrocarbons: implications for the carriers of the 2175 Å uv bump*, The Astrophysical Journal Letters, 712, L16

Straatman C. M., et al., 2018, *The Large Early Galaxy Astrophysics Census (LEGA-C) Data Release 2: Dynamical and Stellar Population Properties of z 1 Galaxies in the COSMOS Field*, The Astrophysical Journal Supplement Series, 239, 27

Terrazas B. A., Bell E. F., Henriques B. M., White S. D., 2016, *The diversity of growth histories of Milky Way-mass galaxies*, Monthly Notices of the Royal Astronomical Society, 459, 1929

Terrazas B. A., Bell E. F., Woo J., Henriques B. M., 2017, *Supermassive black holes as the regulators of star formation in central galaxies*, The Astrophysical Journal, 844, 170

Tress M., et al., 2018, *SHARDS: Constraints on the dust attenuation law of star-forming galaxies at z 2*, Monthly Notices of the Royal Astronomical Society, 475, 2363

Van Den Bosch F. C., Aquino D., Yang X., Mo H., Pasquali A., McIntosh D. H., Weinmann S. M., Kang X., 2008, *The importance of satellite quenching for the build-up of the red sequence of present-day galaxies*, Monthly Notices of the Royal Astronomical Society, 387, 79

Van der Wel A., Bell E. F., Holden B. P., Skibba R. A., Rix H.-W., 2010, *The Physical Origins of the Morphology-Density Relation: Evidence for Gas Stripping from the Sloan Digital Sky Survey*, The Astrophysical Journal, 714, 1779

Vogelsberger M., et al., 2014, *Introducing the Illustris Project: Simulating the coevolution of dark and visible matter in the Universe*, Monthly Notices of the Royal Astronomical Society, 444, 1518

Wang W., et al., 2018, *Galaxy Inclination and the IRX– Relation: Effects on UV Star Formation Rate Measurements at Intermediate to High Redshifts*, The Astrophysical Journal, 869, 161

Weingartner J. C., Draine B. T., 2001, *Dust grain-size distributions and extinction in the milky way, large magellanic cloud, and small magellanic cloud*, The Astrophysical Journal, 548, 296

Werner N., Allen S., Simionescu A., 2012, *On the thermodynamic self-similarity of the nearest, most relaxed, giant ellipticals*, Monthly Notices of the Royal Astronomical Society, 425, 2731

Werner N., et al., 2014, *The origin of cold gas in giant elliptical galaxies and its role in fuelling radio-mode AGN feedback*, Monthly Notices of the Royal Astronomical Society, 439, 2291

Whitaker K. E., Kriek M., Van Dokkum P. G., Bezanson R., Brammer G., Franx M., Labbé I., 2012a, *A Large Population of Massive Compact Post-starburst Galaxies at zgt; 1: Implications for the Size Evolution and Quenching Mechanism of Quiescent Galaxies*, The Astrophysical Journal, 745, 179

Whitaker K. E., Van Dokkum P. G., Brammer G., Franx M., 2012b, *The Star Formation Mass Sequence Out to z= 2.5*, The Astrophysical Journal Letters, 754, L29

White S. D., Frenk C. S., 1991, *Galaxy formation through hierarchical clustering*, The Astrophysical Journal, 379, 52

White S. D., Rees M. J., 1978, *Core condensation in heavy halos: a two-stage theory for galaxy formation and clustering*, Monthly Notices of the Royal Astronomical Society, 183, 341

Wild V., Charlot S., Brinchmann J., Heckman T., Vince O., Pacifici C., Chevallard J., 2011, *Empirical determination of the shape of dust attenuation curves in star-forming galaxies*, Monthly Notices of the Royal Astronomical Society, 417, 1760

Williams W., Röttgering H., 2015, *Radio-AGN feedback: when the little ones were monsters*, Monthly Notices of the Royal Astronomical Society, 450, 1538

Willott C. J., Rawlings S., Jarvis M. J., Blundell K. M., 2003, *Near-infrared imaging and the K—z relation for radio galaxies in the 7C Redshift Survey*, Monthly Notices of the Royal Astronomical Society, 339, 173

Wilson A., Colbert E., 1995, in Bulletin of the American Astronomical Society. p. 830

Wu P.-F., et al., 2018, *Stellar Populations of over 1000 z 0.8 Galaxies from LEGA-C: Ages and Star Formation Histories from D n 4000 and Hδ*, The Astrophysical Journal, 855, 85

Yang X., Mo H., Van den Bosch F. C., Pasquali A., Li C., Barden M., 2007, *Galaxy groups in the SDSS DR4. I. The catalog and basic properties*, The Astrophysical Journal, 671, 153

York D. G., et al., 2000, *The sloan digital sky survey: Technical summary*, The Astronomical Journal, 120, 1579

da Cunha E., Charlot S., 2011, *MAGPHYS: Multi-wavelength Analysis of Galaxy Physical Properties*, Astrophysics Source Code Library

van den Bosch R. C., 2016, *Unification of the fundamental plane and super massive black hole masses*, The Astrophysical Journal, 831, 134

van der Wel A., et al., 2016, *The vlt lega-c spectroscopic survey: the physics of galaxies at a lookback time of 7 gyr*, The Astrophysical Journal Supplement Series, 223, 29

Acknowledgements

First and foremost I would like to express my gratitude to Arjen van der Wel for being my advisor during my PhD. I am grateful to you for all the knowledge I gained and I thank you for your kindness, patient guidance, support and encouragement.

To Fabian Walter, thank you for your time, support, helpful advice, and for all the valuable discussions.

I would like to extend my gratitude to N. Scoville, A. Faisst and P. Capak – thank you for your advice, useful critiques and continued support throughout the years.

Thank you to the members of the LEGA-C team, I am grateful for all the discussions we had.

Thank you to M. Novak for proofreading parts of my thesis, and to J. Delhaize for the language editing.

To my little brother, thank you for the illustrations!